ELECTRODEPOSITION OF LEAD CHALCOGENIDE THIN FILMS, SUPERLATTICES AND PHOTOVOLTAICS BY ELECTROCHEMICAL ATOMIC LAYER DEPOSITION (EC-ALD)

by

DHEGO BANGA

(Under the Direction of John L. Stickney)

ABSTRACT

This dissertation mainly presents how electrochemical atomic layer deposition (EC-ALD) was used to grow thin films and superlattices of lead chalcogenides and photovoltaics. EC-ALD is the electrochemical analog of atomic layer deposition. It is an electrodeposition technique based on the use of surface limited reactions known as under potential deposition (UPD). UPD is a phenomenon where an atomic layer is deposited on the second at a potential prior to its formal potential to form deposits with atomic level control. EC-ALD is carried out at room temperature, thus considerably reducing interdiffusion in layers of the deposits. EC-ALD has been used successfully to deposit compound semiconductors and metal nanofilms on metallic substrates such as Au, Cu and Pt. The goal of the research investigation was to optimize the deposition of Pb chalcogenides (PbSe, PbTe, and their subsequent superlattices) as they are of interest for their optical and electronic properties, which make them useful in thermoelectric device structures, infrared sensors and in photovoltaics. The formation of PbTe/CdTe superlattices was also pursued as PbTe, being an excellent material for IR laser can be improved by the insertion of a barrier material that has a sufficient electrical and optical confinement such as CdTe. The low lattice mismatch of 0.3 % between PbTe and CdTe could also promote the superlattice growth by electrochemical ALD. Studies on the electrodeposition of $CuInSe_2$ (CIS) and $CuIn_{1-x}Ga_xSe_2$ (CIGS) photovoltaic cells were undertaken and will also be reported as these materials are one of the promising thin film candidates for the advancement of photovoltaic solar cell technology due to their high conversion efficiency.

INDEX WORDS: Electrochemical atomic layer deposition, Underpotential deposition, Quantum confinement, Thin films, Superlattices, Photovoltaics, Cyclic voltammetry, EPMA, XRD, AFM, STM, FTIR spectrophotometer

ELECTRODEPOSITION OF LEAD CHALCOGENIDE THIN FILMS, SUPERLATTICES AND PHOTOVOLTAICS BY ELECTROCHEMICAL ATOMIC LAYER DEPOSITION (EC-ALD)

by

DHEGO BANGA

B.S. Columbia College, Columbia, MO, 1999

A Dissertation Submitted to the Graduate Faculty of The University of Georgia in Partial Fulfillment of the Requirements for the Degree

DOCTOR OF PHILOSOPHY

ATHENS, GEORGIA

2009

ELECTRODEPOSITION OF LEAD CHALCOGENIDE THIN FILMS, SUPERLATTICES AND PHOTOVOLTAICS BY ELECTROCHEMICAL ATOMIC LAYER DEPOSITION (EC-ALD)

by

DHEGO BANGA

Major Professor:	John L. Stickney
Committee:	I. Jonathan Amster Marcus D. Lay

Electronic Version Approved:

Maureen Grasso
Dean of the Graduate School
The University of Georgia
December 2009

DEDICATION

I dedicate this work to my Dad, Jean Dhego Dido (1932-2007). Though you have past away, your advice and words of wisdom lived on in me. Without your unconditional love and support, I would have never been where I am today. Thank you for instilling in me the sense of hard work, perseverance and learning. To my Mother, Marcelline Dhenza Ngave, thank you for the love and words of encouragement. To my Wife, Neema, thank you for your unwavering support. Without your help, this work would not have been possible. To my daughter Olivia and son Jean-Christophe, you are the reason I hung in there. To my sisters (Kave, Mamy and Vingi) and brothers (Innoncent, Lina, Sai, Patrick, Eric and Johnny), thank you for your support and prayers.

ACKNOWLEDGEMENTS

First and foremost, thank you God for the strength, perseverance, courage and patience that You gave me during the course of this work. I will forever be thankful.

I would like to thank my supervisor, Dr. Stickney, for his guidance during the course of my Ph.D. studies. I would like to also thank my committee members Dr. Amster and Dr. Lay.

Special thanks go to the following present and past group members: Dr. Raman Vaidyanathan, Dr. Ken Mathe, Dr. Madhivanan Muthuvel, Dr. Venkatram Venkatasamy, Dr. Youn-Geun Kim, Dr. Jay Kim, Dr. Chandru Thambidurai, Nagarajan Jarayaju, Xuehai Liang, Daniel Gebregziabiher, Leah Sheridan and Brian Perdue.

To those that I forgot to mention, believe me, it was not intentional.

TABLE OF CONTENTS

Page

CHAPTER

LIST OF TABLES

Page

LIST OF FIGURES

CHAPTER 1

INTRODUCTION

Recent years have seen an explosive interest in nanotechnology, as it is actively pursued by scientists from different fields. The intensive research in nanotechnology has shown promise or has resulted in various breakthroughs that have a huge impact on or will change the direction of technological advances in a wide range of applications, ranging from producing lighter and stronger materials, increasing the storage capacity of recording media or magnetic tapes, allowing the manufacture of nanostructured drug delivery devices to the body's circulatory systems and contributing to increasing light conversion efficiencies in photovoltaic materials. As particles get smaller, changes in their electronic structure, conductivity, reactivity, melting temperature and mechanical properties have been observed. These changes in properties as particles get smaller have been the main reason behind the growing interest in nanotechnology as properties can be engineered [1-2]. As the electronics industry embraces nanotechnology, submicrometer trenches [3-4] and patterned substrates [5] are becoming standard features. However, conformal coatings of trenches and patterned substrates are becoming more difficult to achieve the smaller these features become. How does one coat minuscule trenches and patterned substrates with atomic level control?

Epitaxial growth of thin films can be achieved using the electrochemical analog of atomic layer deposition known as the electrochemical atomic layer deposition (EC-ALD) [6], which was used in all of the work reported in this dissertation. Epitaxial growth of an element on a substrate is due to the surface limited reaction known as underpotential deposition (UPD), a phenomenon where an atomic layer of one element deposits on the second at a potential prior to that needed to form bulk deposits [7-9]. Electrochemical ALD is performed at room temperature and atmospheric pressure and no annealing is required for crystal structure of the grown material to become visible in the X-ray diffraction pattern. EC-ALD has control over deposition at atomic scale as one atomic layer is deposited at a time, whereas in the other known deposition methods such as chemical vapor deposition (CVD), molecular beam epitaxy (MBE) and others, thin film deposition requires the substrate to be maintained at high temperature. Moreover, in most of these deposition processes, annealing after deposition is required to obtain a well ordered surface.

Lead chalcogenides have widely been studied for their importance in applications, in crystalline and polycrystalline forms, as detectors of IR radiation, IR resistors, thermoelectric devices and more recently as IR emitters and solar control coatings [10]. They are IV-VI compound semiconductors that are known for their narrow bandgap (E_g) values, large Bohr radii, and small and relatively equal electron and hole masses compared to III-V or II-VI compound semiconductors which result in larger confinement effect for nanostructures [11-12]. Lead chalcogenides reported in this dissertation include PbSe thin films in chapter 2, PbTe thin films in chapter 3, PbSe/PbTe superlattices in chapter 4, and PbTe/CdTe superlattices in chapter 5.

The general concern associated with global warming, due the emission of greenhouse gases during the production of primary power by conventional means, and the volatile price of fuels have all contributed and lead to the interest in renewable energy source. Known technologies of renewable energy sources include wind, fuel cells, solar cells, geothermal, biofuels, etc. The most appealing of them all is the solar energy conversion as the energy source is readily available [13-14]. $CuInSe_2$ and $CuIn_{1-x}Ga_xSe_2$ (CIGS) are well known advanced absorber materials for thin film solar cells due to their large optical absorption coefficient and direct bandgap (E_g) values. Conversion efficiency of up to 19.9 % has been reported in multilayer of CIGS-based devices [15-19]. $CuInSe_2$ and $CuIn_{1-x}Ga_xSe_2$ grown using electrochemical atomic layer deposition will be reported in chapter 7 and 8 respectively.

X-ray diffraction (XRD), electron probe microanalysis (EPMA), scanning tunneling microscopy (STM), atomic force microscopy (AFM) and FTIR spectrometer were used for the characterization of the deposits grown in this dissertation.

References

1. Long, R. and N.J. English, *Band gap engineering of (N, Ta)-codoped TiO2: A first-principles calculation.* Chemical Physics Letters, 2009. **478**(4-6): p. 175-179.
2. Mondal, R., et al., *Molecular design for improved photovoltaic efficiency: band gap and absorption coefficient engineering.* Journal of Materials Chemistry, 2009. **19**(39): p. 7195-7197.
3. Lee, C.H., et al., *Superconformal Electrodeposition of Co and Co-Fe Alloys Using 2-Mercapto-5-benzimidazolesulfonic Acid.* Journal of the Electrochemical Society, 2009. **156**(8): p. D301-D309.
4. Moffat, T.P., et al., *Electrodeposition of Cu on Ru barrier layers for damascene processing.* Journal of the Electrochemical Society, 2006. **153**(1): p. C37-C50.
5. Moffat, T.P. and H. Yang, *Patterned Metal Electrodeposition using an alkanethiolate mask.* JECS, 1995. **142**(11): p. L220-L222.
6. Stickney, J.L., et al., *Electrodeposition of compound semiconductors by electrochemical atomic layer epitaxy (EC-ALE).* Encyclopedia of Electrochemistry, 2003. **1**: p. 513-560.
7. Kolb, D.M. and H. Gerisher, *Further aspects concerning the correlation between underpotential depsoition and work function defferences.* SS, 1975. **51**: p. 323.
8. Kolb, D.M., Przasnys.M, and Gerische.H, *Underpotential Deposition of Metals and Work Function Differences.* Journal of Electroanalytical Chemistry, 1974. **54**(1): p. 25-38.
9. Magnussen, O.M. and R.J. Behm, *Structure and growth in metal epitaxy on low-index Au surfaces - a comparison between solid vertical bar electrolyte and solid vertical bar vacuum interfaces.* Journal of Electroanalytical Chemistry, 1999. **467**(1-2): p. 258-269.

10. Kumar, S., et al., *Studies on thin films of lead chalcogenides.* Current Applied Physics, 2005. **5**(6): p. 561-566.

11. Wise, F.W., *Lead salt quantum dots: the limit of strong quantum confinement.* acr, 2000. **2000**(33): p. 773-780.

12. Banga, D.O., et al., *Formation of PbTe nanofilms by electrochemical atomic layer deposition (ALD).* Electrochimica Acta, 2008. **53**(23): p. 6988-6994.

13. Lewis, N.S., *Renewable energy.* Chemical & Engineering News, 2001. **79**(13): p. 278-278.

14. Lewis, N.S. and D.G. Nocera, *Powering the planet: Chemical challenges in solar energy utilization.* Proceedings of the National Academy of Sciences of the United States of America, 2006. **103**(43): p. 15729-15735.

15. Bhattacharya, R. and E. al., *Electrodeposition of CuIn1-xGaxSe2 Materialsfor Solar Cells*. 2001, NREL. p. 1-55.

16. Bhattacharya, R.N. and K. Ramanathan, *Cu(In,Ga)Se2 thin film solar cells with buffer layer alternative to CdS.* Solar Energy, 2004. **77**(6): p. 679-683.

17. Chaure, N.B., A.P. Samantilleke, and I.M. Dharmadasa, *The effects of inclusion of iodine in CdTe thin films on material properties and solar cell performance.* Solar Energy Materials and Solar Cells, 2003. **77**(3): p. 303-317.

18. Ramanathan, K., et al., *Properties of 19.2% efficiency ZnO/CdS/CuInGaSe2 thin-film solar cells.* Progress in Photovoltaics, 2003. **11**(4): p. 225-230.

19. Ingrid, R., et al., *Short Communication: Accelerated Publication 19·9%-efficient ZnO/CdS/CuInGaSe2 solar cell with 81·2% fill factor.* Progress in Photovoltaics: Research and Applications, 2008. **16**(3): p. 235-239.

CHAPTER 2

OPTIMIZATION OF PBSE NANOFILMS FORMATION BY ELECTROCHEMICAL ATOMIC LAYER DEPOSITION (EC-ALD)[1]

---

[1] Banga, D., et al., ECS Transactions 19:245 (2009)
Reprinted here with permission of publisher.

Abstract

Optimization studies of lead selenide (PbSe) nanofilm formation using electrochemical atomic layer deposition (ALD) are reported here. IV-VI compounds semiconductors, such as the lead chalcogenides (PbSe, PbTe and PbS), have narrow band gaps and crystallize in the cubic rock salt structure. They are of interest for their optical and electronic properties, which make them useful in thermoelectric device structures, infrared sensors, and photovoltaics. PbSe has the narrowest band gap of the lead chalcogenides, 0.26 eV at room temperature. PbSe deposits were formed using an ALD cycle on Au substrates, one atomic layer at a time, from separate solutions, containing Pb or Se ions. Single atomic layers were formed using surface limited reactions, referred to as underpotential deposition (UPD). UPD is a phenomenon where an atomic layer of one element deposits on a second at a potential prior to that needed to form that element in a bulk form. The deposition cycle consisted of the alternated UPD of Se and Pb. In the optimized process, Se and Pb deposition potentials were ramped up from -0.3 V and -0.25 V respectively to -0.04 V over the first 20 cycles, and then held constant for the remaining cycles. Coverages near one monolayer in each cycle were indicated by the coulometry for the reduction of both Se and Pb. Electron probe microanalysis (EPMA) indicated a uniform and stoichiometric deposit, with a Se/Pb ratio of 1.02. X-ray diffraction patterns showed peaks matching the rock salt structure, with a preferential (200) orientation for the as formed deposits. Infrared reflection absorption measurements of the PbSe films formed with 100, 200, 250 and 300 cycles indicated strong quantum confinement. STM suggested conformal film growth on the Au on glass substrate.

Introduction

The interest in lead chalcogenides (PbS, PbSe and PbTe) and their alloys stems from their importance in applications, in crystalline and polycrystalline forms, as detectors of IR radiation, IR resistors, thermoelectric devices and more recently as IR emitters and solar control coatings[1]. Lead chalcogenides exhibit quite unique properties relative to other semiconductors such as the positive temperature coefficients (dE_g/dT) of the minimum energy gap E_g, the narrow direct band gap which decreases with hydrostatic pressure and increases with temperature and the large dielectric constants[1]. IV-VI compound semiconductors have small and relatively equal electron and hole masses compared to III-V or II-VI compound semiconductors which result in larger confinement effects for nanostructures, that is they have a large Bohr radius[2-3]. The Bohr radius of PbSe is ~ 46 nm, suggesting that strong quantum confinement effects should still be evident when confining dimensions are as large 50 nm [4-5]. In the present report, very strong band gap shifts, from 0.26 eV, are reported for nanofilms of PbSe.

Other methods used to grow PbSe thin films have included molecular beam epitaxy (6-8), chemical vapor deposition [6], sonochemistry [7], sonoelectrochemistry [8], microwave heating [9], codeposition (4, 13-20) and electrochemical atomic layer deposition (ALD) [3] also known as electrochemical atomic layer epitaxy (EC-ALE) [10].

Extensive work on the growth of compound semiconductor and metal nanofilms have been carried out by the Author's group and others using electrochemical atomic layer deposition (ALD)[11-28]. Electrochemical ALD makes use of underpotential deposition (UPD) [11, 29-33], a phenomenon where an atomic layer of one element deposits on a second, at a potential prior to that needed to form the element in bulk form. The result is a surface limited reaction: deposition limited by the surface area of the deposit. The basis of the electrochemical ALD consists of forming compound monolayers using UPD in a sequence, referred to here as a cycle, which can be repeated as many times as needed to form more compound monolayers. In ALD, materials can be grown layer by layer with atomic level control [10].

Electrochemical ALD has been used successfully to grow various compounds such as CdTe [34-35], CdS [13, 36], ZnSe [37], ZnS [36], CdS / HgS superlattices [38], PbS [39], PbSe [3], PbTe [11], PbSe / PbTe superlattices [23], GaAs [40-41], InAs (50-52), InSb [42] and superlattices of InAs / InSb [42]. In this report, which is an extension of previous work on PbSe deposition by this group[3], attempts to optimize the formation PbSe nanofilms on Au on glass and Au on mica substrates will be presented. The first new cycles involved reductive deposition of both Se and Pb at constant potentials for the duration of the deposition process. The second new ALD cycles involved the inclusion of a Se reductive stripping step, at a controlled potential to strip off excess Se, while both Se and Pb deposition potentials were maintained constant throughout the deposition process. The last new ALD cycle involved ramping positively both Se and Pb potentials over the first 20 cycles, before holding them constant for the remaining cycles.

Experimental

An automated thin layer flow electrodeposition system described previously (Electrochemical ALD L.C.)(42, 47, 53) consisting of a series of solution reservoirs, computer controlled pumps, valves, a thin layer electrochemical flow cell and a potentiostat was used in this study to grow thin films of PbSe. Minor changes were made to the reference electrode compartment and the auxiliary electrode. A simple O-ring was used to hold the reference electrode instead of the Teflon compression fitting, providing a better seal, and a Au wire embedded into the Plexiglas flow cell was used as the auxiliary electrode, instead of the ITO glass slide, which has proven more durable. The electrochemical flow cell was designed to promote laminar flow. The working electrode was Au on glass, the auxiliary was a Au wire, and the reference electrode was Ag/AgCl (3M NaCl) (Bioanalytical systems, Inc., West Lafayette, IN). The cell volume was about 0.3 mL and solutions were pumped at 50 mL min^{-1}. The system was contained within a nitrogen purged Plexiglas box to reduce the influence of oxygen during electrodeposition.

Substrates used in the study consisted of 300 nm thick vapor deposited gold on glass microscope slides. Prior to insertion into the vapor deposition chamber, the glass slides were cleaned in HF, and rinsed with copious amounts of deionized water from a Nanopure water filtration system (Barnstead, Dubuque, IA), fed from the house distilled water system. Deposition began with 3 nm of Ti, as an adhesion layer, followed by 300 nm of Au deposition at around 250 ^{o}C. The glass slides were then annealed in the deposition chamber at 400 ^{o}C for 12 hours, while the pressure was maintained at 10^{-6} Torr.

Reagent grade or better chemicals and deionized water were used to prepare the solutions. Three different solutions were used in this study. The lead solution consisted of 0.5

mM $Pb(ClO_4)_2$ (Alfa Aesar, Ward Hill, MA), pH 3, with 0.1 M $NaClO_4$ (Fischer Scientific, Pittsburgh, PA) as the supporting electrolyte. The selenium solution was made of 0.5 mM SeO_2 (Alfa Aesar, Ward Hill, MA), pH 5, buffered with 50.0 mM sodium acetate and 0.1 M $NaClO_4$ (Fischer Scientific, Pittsburgh, PA) as the supporting electrolyte. A pH 3 blank solution of 0.1 M $NaClO_4$ (Fischer Scientific, Pittsburgh, PA) was used as well. NaOH and $HClO_4$ (Fischer Scientific, Pittsburgh, PA) were used to adjust the pH values of all the solutions in this study.

The electrochemical ALD cycle program used to grow PbSe consisted of the following: the Se solution was flushed in to the cell for 2 s at the chosen potential, and then held quiescent for 15 s for deposition. The blank solution was then flushed through the cell at the same potential for 3 s, to rinse out excess $HSeO_3^-$ ions. The Pb solution was then flushed through the cell for 2 s at the Pb deposition potential, and held quiescent for 15 s for deposition. Blank solution was again flushed through the cell for 3 s to rinse out excess Pb^{2+} ions from the cell. This process was referred to as one cycle, and was repeated 100 times to form each of the deposits described in this paper.

Microanalyses (EPMA) of the samples were performed with a Joel JXA-8600 electron probe. Glancing angle X-ray diffraction patterns were obtained on a Scintag PAD V diffractometer, equipped with a 6” long set of Soller slits on the detector to improve resolution in the asymmetric diffraction configuration. Absorption measurements were performed using a variable angle reflection rig in conjunction with a Bruker 66v FTIR spectrometer equipped with a Si detector. STM measurements were taken with a Princeton Research Instruments Nanoscope.

Results and Discussions

Figures 1 and 2 display the cyclic voltammograms for the deposition of Se and Pb on the Au on glass substrates; which were used to determine initial deposition potentials for the ALD cycle. Many studies of the electrochemical deposition of both Se and Pb have been carried out by this and other groups (3, 24, 32, 44, 47, 54-62). From previous studies by this group, Se deposition is known to be kinetically slow [43-45]. Four CVs of Au in the Se solution, each to an increasingly lower potential and each to just past a different reduction feature, are shown in Figure 1. Distinct reduction features were observed at 0.6 V, 0.1 V, and -0.25 V, with a sharp increase in reduction current at -0.45 V, corresponding Se reduction to selenide and hydrogen evolution (Fig. 1(b)). The first reductive feature, around 0.6 V, was reduction of small amounts of Au oxide, formed at the most positive potentials. Previous studies of Se deposition (57, 59, 60) showed that selenite reduction did not result in deposition at an underpotential, as suggested by the term UPD. However, if UPD is considered to denote formation of a surface limited amount, then the reduction peak at -0.05 V (an overpotential) could be considered UPD. The peak occurs at an overpotential because of the slow kinetics for $HSeO_3^-$ reduction. The reductive features (Figure 1a) at -0.05 V display all the characteristics of surface limited deposition, except that it occurs at an overpotential, since the formal potential for $HSeO_3^-$/Se appears to be 0.4 V. When the scan was reversed at -0.3 V (Figure 1a), the only oxidative feature occurs at around 0.6 V, positive of the formal potential, and as the more negative the scan (-0.025 V to -0.3 V), the larger the 0.6 V peaks becomes. It is felt by these authors that all this reduction (to -0.3) is associated with surface limited deposition (Figure 1a). When the scan was reversed at much more negative potentials as (Figure 1b), a new oxidative feature was evident, just positive of 0.4 V, apparently the oxidation of bulk Se. It is known from other studies that near -0.5 V, a different process begins, reduction of Se to selenide (Se^{2-}), a soluble species which diffuses away. So there are really three processes contributing to the increase in reduction near -0.5 V, bulk Se formation, selenide formation, and hydrogen evolution. The clear difference between bulk Se and UPD, evident in Figure 1, prompted use of -0.3 V for Se atomic layer deposition, which is well positive of the potential corresponding to bulk Se formation (-0.45 V). Some bulk Se will still deposit at -0.3 V, given that the formal potential is 0.4 V, but the kinetics appear slow enough that if little time is given for deposition, some small fraction of a monolayer of bulk at most will form.

Figure 2 depicts Au CVs in the Pb^{2+} solution. A slowly increasing reduction current was observed as the negative going scan (started at 0.25 V) progressed, then producing a characteristic Pb^{2+} reduction peak (reversible) at -0.25 V, reminiscent of Pb UPD on a Au(111) electrode [46-52]. The sharp increase in current negative of -0.45 V, and displaying hysteresis suggesting nucleation and growth, corresponds to bulk Pb deposition. In the corresponding positive going scan, there was a small sharp peak for bulk Pb oxidation at -0.47 V, as well as a large broad peak around -0.38 V, suggesting oxidation of Pb from a Pb/Au alloy [53]. Based on the features in Figure 2, -0.25 V was selected for use as the starting potential for Pb atomic layer formation in the ALD cycle.

From the CVs for Se and Pb, the ALD cycle shown in Figure 3 was devised. The initial step was filling the cell with the $HSeO_3^+$ solution for 2 s, followed by depositing Se for 15 s with no flow and then rinsing the cell with blank for 3 s, all at -0.3 V. This was followed by filling for 2 s with the Pb^{2+} solution, depositing Pb for 15 s with no flow, and then rinsing the cell for 3 s, all at -0.25 V. Each cycle was intended to form a compound monolayer or single compound bilayers of PbSe on (2 x 2) cm^2 electrode surface.

Figure 4 displays the charges in monolayers (ML), where a monolayer is defined as one depositing atom for each surface atom, or $1.35X10^{15}$ atoms/cm^2, assuming the geometric area of the substrate is composed of Au(111), hexagonal surface of fcc Au. The substrate will not be completely (111), and there will be some roughening relative to an atomically flat surface. However, such numbers give a relative idea of the amounts of depositing elements. During the first cycle, the Pb deposition was much larger than expected. Previous studies of the II-VI compound CdTe suggested that after deposition of a chalcogenides layer on Au, the first metal deposition results in deposition both on top of the chalcogenide and below it, as the Cd has a strong affinity for the Au surface. If such a process is at work here, after one cycle of deposition (Figure 3), there should be an atomic layer of Pb on the Au, then Se, followed by another layer of Pb.

It is notable that the coverages for the first 3 cycles are below 1 ML. On the other hand, the coverages increase dramatically up to 2 ML, about twice the amount needed to form one compound bi-layer. It has been observed by this group that more than the amount needed to form a compound bi-layer is generally too much, as excess deposition suggests bulk formation, and it is not clear if bulk can be converted quantitatively into the desired compound. Thus when more than that needed to form the bi-layer is deposited; it is probable that surface roughening will result. From Figure 4, it is clear that too much is being deposited, although it starts out reasonably, over the first 20 cycles the coverages increase to about 2 times too much. This particular trend was also observed for the formation of PbTe using electrochemical ALD [11].

An explanation suggested for these changes (3, 70, 71) was that there was a drop of some of the applied potential across a growing space charge layer (SCL), or Schottky barrier, between the Au electrode and the growing semiconductor thin film. It seems, however, unrealistic that a space charge layer fully developed after only 20 ALD cycles [54]. Reasons for the changes in coverage as the cycle number increased are not yet understood, though it may have to do with deposition and growth kinetics, as similar behavior is frequently observed for gas phase ALD studies [55-57]. Deposits formed under the conditions described above appeared overgrown and roughened, when inspected using optical microscope, as expected based on the excess deposited amounts. Given the voltammetries shown in Figures 1 and 2, the chosen potentials should have worked. However, such choices were based on deposition on Au surfaces, not on deposition on the compound.

Se electrodeposition is generally kinetically slow (57, 59, 60). The kinetics for PbSe might be as well, beginning slowly, and increasing as more facets of the compound are formed, possibly explaining the overgrowth observed above. Au on glass or mica substrates , such as used in this experiment, are polycrystalline surface with steps and defects on and between 50 nm clusters, with only small Au (111) terraces; as shown in Figure 5. The energetics for deposition on such defect sites and terraces may be slower then for deposition on atomically flat Au(111) planes. Furthermore the lattice mismatch between the substrate, say Au(111), and the PbSe deposit will increase dislocations and defects as the deposit grows. As the defects grow, the surface area increases, and the amounts deposited increase. The Se/Pb ratios for these deposits were 1.1 from EPMA analysis, indicating an excess of Se in the deposit, which may also increase the deposit roughness.

Another ALD cycle was devised to circumvent the excessive Se deposition observed with increasing cycle number, when the Se and Pb potentials were held constant. An extra step, designed to reduce excess Se to a soluble selenide species (22, 76), was added to the cycle as shown in Figure 6. The ALD cycle started with rinsing the Se solution into the cell for 2 s, where it was held static for 15 s of Se deposition, both at -0.3 V. The cell was then flushed with blank solution for 3 s at -0.45 V. After that, the Pb solution was flushed into the cell for 2 s and held without flow for 15 s for deposition, all at -0.35 V. This was followed by another blank rinse for

3 s at -0.45 V, referred to here are the Se reductive stripping step. The inclusion of the extra Se stripping step at a much more negative potential was intended to remove excess Se, as at this potential bulk Se was expected to reduce to HSe^-, a soluble species which diffused away, leaving only a Se atomic layer. Figure 7 shows the current time traces for three ALD cycles of PbSe, where current for Se reductive stripping is clearly depicted. However, the deposit grown using this cycle appeared thin, suggesting that too much Se was removed during the stripped step, leaving little Se to react with the Pb ions. EPMA of the deposit suggested only ¼ of the amount expected, around 6 atomic % of both Se and Pb which resulted in atomic ratio of ~ 1. Upon inspection under the microscope, the deposits appeared too thin for 100 cycle-run.

A third ALD cycle was then devised where the potentials were shifted positive from cycle to cycle, for the first 20 cycles, before constant potentials were applied for the remaining cycles. The use of a sequence of potential shift for the first 10 to 20 cycles has been use in previous studies to grow compounds such as PbSe [3], CdTe [35], InAs [42], and others , in order to achieve constant cycle to cycle growth and stoichiometry ratio of 1.0. Other than in the case of PbTe [11] where the potential shift for Te was positive for the first 20 cycles, the potential shifts have been negative. A series of experiments were carried out using different functional forms for calculating the sequence of positive shifts of both Se and Pb potentials, in order to optimize this process. Figure 8 shows the potential steps selected for the first 20 ALD cycles, which resulted in the most consistent deposited amounts. For that deposit, the Se potential began at -0.3 V, while the Pb potential started at -0.25 V, and both were stepped as in Figure 8, over 20 cycles, to a “steady state” value of -0.04 V, which was used for all subsequent cycles. A set of current time traces using this ALD cycle is shown in Figure 9. Figure 10 shows the coverages in compound ML, from coulometry, for all 100 cycles, formed by stepping the potential positive for the first 20 cycles. There was some scatter for the first couple cycles, but for the rest of the run, the coverages were essentially equal, and just under one compound ML a cycle. In general, it is better for a cycle to be low than to be high. More than a compound ML in a cycle is likely to result in roughening of the deposit, while less will only result in a slower deposit, but not harm the quality. Stepping the potentials avoided the gradient in coverage observed over the first 20 cycles seen in Figure 4, where the same potentials were used for the whole deposit. No significant increase in coverage or charge was observed when both Se and Pb deposition times were increased from 15 to 30 s, confirming the surface limited nature of the chosen potentials for Se and Pb, as was observed for PbTe [11]. EPMA results for the 100 cycles PbSe deposit formed using ramps for Se and Pb potentials, from -0.3 V and -0.25 V respectively to -0.04 V, are shown in Table 1. The deposit was homogeneous from inlet to outlet, and the Se/Pb ratio was within a couple % of 1.

Figure 11 displays the glancing angle (1^o from the sample plane) X-ray diffraction patterns of a 100 cycle PbSe deposit, formed with potential steps for both Se and Pb, from -0.3 V and -0.25 V to -0.04 V. The sample was not annealed. As expected, peaks for the rock salt structure were for the (111), (200), (220), (311), (222), (400), (331) and (420) planes of PbSe [JCPDS 20-0494], along with polycrystalline Au substrate peaks, were clearly evident in the X-ray diffraction pattern. The X-ray diffraction pattern exhibited a preferential (200) peak. No elemental peaks for Se or Pb were evident in the XRD pattern.

Figure 12 displays a series of absorption spectra for PbSe electrodeposited nanofilms formed with different numbers of cycles, where both the Se and Pb potentials were stepped positively from -0.3 V and -0.25 V to -0.04 V over the first 20 cycles. Bulk PbSe has a direct bandgap of 0.26 eV. The band gaps of the nanofilms formed in this report, however, were strongly blue shifted, as expected given that their thicknesses were similar to the Bohr radius for PbSe (~ 46 nm). When samples with different cycle numbers (100, 200, 250 and 300 cycles) were deposited, the extent of the blue shift resulting was clearly evident as attested by Figure 12. Despite the large value of PbSe bandgap of around 0.26, the blue shifts of 0.7, 0.46, 0.38 and 0.36 eV were observed for 100, 200, 250 and 250 cycles respectively. A considerable amount in spectrum of the 100 cycle deposit attesting that its absorption is blue shifted out of the spectrometer's range.

A PbSe nanofilm formed by stepping the potentials for both Se and Pb from -0.3 V and -0.25 V, respectively, to -0.04 V was grown on a template stripped Au (TSG) substrate ref. The TSG was formed by taking a Au film deposited on mica, and covering it with epoxy. The mica was then defoliated, leaving the Au film on the epoxy, and with the surface, previously in contact with the ultra flat mica surface, exposed. EPMA analysis of the sample indicated a similar composition to that grown on Au on glass. Figure 13 displays STM images of a 100 cycle deposit formed on Au on mica substrate, which showed 80 nm, approximately hexagonal terraces, unlike those displayed in Figure 5. In both cases (Figures 5 & 13), three different spots were measured, resulting in similar images. Roughness (RMS) values of around 4.0 nm were observed for both the Au surface before and the PbSe deposit surface, suggesting the PbSe films formed using electrochemical ALD did not result in a rougher deposit. However, the terraces shown in Figure 13 were more hexagonal and flatter than the TSG substrate used, indicating that the ALD PbSe films showed improved crystallinity in Figure 13, relative to the Au substrate, where the crystallites were more rounded. In addition, the grain size of the PbSe film in Figure 13 appears relatively larger, compared with the bare gold (Figure 5). The X-ray diffraction pattern of the PbSe grown on Au on mica is displayed in Figure 14. The rocksalt structure of

PbSe is once again evident in the pattern for the as formed deposit, given the peaks for the (200), (111), (220) and (311) reflections. There was little indication of the Au substrate, besides a small (111) peak since a glancing angle of 0.1^{o} was used for this pattern. As it was the case for the ALD cycle PbSe film grown on Au on glass, no elemental peaks for either Se or Pb were present in the XRD pattern attesting to the quality of the deposit.

Conclusion

This paper presented various electrochemical ALD cycle methods of which the one containing the ramps of both Se and Pb for the first 20 cycles resulted in the optimal and successful growth of smooth epitaxial PbSe films on both Au on glass and Au on mica substrates after the inspection under the microscope. Coulometry and charges confirmed coverage of near or below a ML/cycle. Quantum confinement effects were visible in the samples grown at 300 cycles or less as observed from the absorption spectra. EPMA results confirmed that the deposits were homogeneous and stoichiometric. XRD revealed the films had a rocksalt structure and a preferential (200) orientation in deposits on both Au on glass and Au on mica substrates. STM images of PbSe samples showed clusters of improved crystallinity and similar roughness to the ones seen on Au on glass.

Acknowledgements

Support from the National Science Foundation is gratefully acknowledged.

References

1. Kumar, S., et al., *Studies on thin films of lead chalcogenides.* Current Applied Physics, 2005. **5**(6): p. 561-566.
2. Allan, G. and C. Delerue, *Confinement effects in PbSe quantum wells and nanocrystals.* Physical Review B, 2004. **70**(24).
3. Vaidyanathan, R., J.L. Stickney, and U. Happek, *Quantum confinement in PbSe thin films electrodeposited by electrochemical atomic layer epitaxy (EC-ALE).* Electrochimica Acta, 2004. **49**(8): p. 1321-1326.
4. Hens, Z., et al., *Effect of quantum confinement on the dielectric function of PbSe.* Physical Review Letters, 2004. **92**(2).
5. Wise, F.W., *Lead salt quantum dots: the limit of strong quantum confinement.* acr, 2000. **2000**(33): p. 773-780.
6. Bierman, M.J., Y.K.A. Lau, and S. Jin, *Hyperbranched PbS and PbSe nanowires and the effect of hydrogen gas on their synthesis.* Nano Letters, 2007. **7**(9): p. 2907-2912.
7. Li, B., et al., *Sonochemical synthesis of silver, copper and lead selenides.* Ultrasonics Sonochemistry, 1999. **6**(4): p. 217-220.
8. Zhu, J.J., et al., *A novel method for the preparation of lead selenide: Pulse sonoelectrochemical synthesis of lead selenide nanoparticles.* Chemistry of Materials, 2000. **12**(1): p. 143-147.
9. Zhu, J.J., et al., *Microwave assisted preparation of CdSe, PbSe, and Cu2-xSe nanoparticles.* Journal of Physical Chemistry B, 2000. **104**(31): p. 7344-7347.
10. Stickney, J.L., et al., *Electrodeposition of compound semiconductors by electrochemical atomic layer epitaxy (EC-ALE).* Encyclopedia of Electrochemistry, 2003. **1**: p. 513-560.

11. Banga, D.O., et al., *Formation of PbTe nanofilms by electrochemical atomic layer deposition (ALD).* Electrochimica Acta, 2008. **53**(23): p. 6988-6994.

12. Colletti, L., et al., *FORMATION OF II-VI COMPOUNDS USING ECALE.* Abstracts of Papers of the American Chemical Society, 1994. **208**: p. 131-COLL.

13. Colletti, L.P., B.H. Flowers, Jr., and J.L. Stickney, *Formation of thin films of CdTe, CdSe, and CdS by electrochemical atomic layer epitaxy.* Journal of the Electrochemical Society, 1998. **145**(5): p. 1442-1449.

14. Goetting, L.B., et al., *THE USE OF IODINE AS A SURFACE-TREATMENT FOR AU SINGLE-CRYSTALS USED IN THE ECALE DEPOSITION OF CDTE.* Abstracts of Papers of the American Chemical Society, 1994. **208**: p. 115-COLL.

15. Goetting, L.B., et al., *Preparation of Au single crystals for studies of the ECALE deposition of CdTe.* Electrochimica Acta, 1995. **40**(1): p. 143-158.

16. Huang, B.M., et al., *Preliminary Studies of the Use of On Automated Flow-Cell Electrodeposition System For the Formation of Cdte Thin-Films By Electrochemical Atomic Layer Epitaxy.* Journal of the Electrochemical Society, 1995. **142**(9): p. 3007.

17. Huang, B.M., L.B. Goetting, and J.L. Stickney, *Preparation of the 1st atomic layer of Te in the ECALE deposition of CdTe.* Abstracts of Papers of the American Chemical Society, 1994. **208**: p. 134-COLL.

18. Lister, T.E., R.D. Herrick, and J.L. Stickney, *Studies of ECALE deposition of CdSe on the low-index planes of gold.* Abstracts of Papers of the American Chemical Society, 1994. **208**: p. 128-COLL.

19. Lister, T.E. and J.L. Stickney. *Formation of the first monolayer of CdSe on Au(111) by electrochemical ALE*. 1996.

20. Lister, T.E. and J.L. Stickney, *Atomic level studies of Se electrodeposition on Au(111) and Au(110).* JPC, 1997. **in press**.

21. Loglio, F., et al., *Ternary CdxZn1-xSe deposited on Ag (111) by ECALE: Electrochemical and EXAFS characterization.* Electrochimica Acta, 2008. **53**(23): p. 6978-6987.

22. Stickney, J.L., *II-VI compound semiconductor thin film electrodeposition by ECALE.* Abstracts of Papers of the American Chemical Society, 1995. **210**: p. 297-INOR.

23. Vaidyanathan, R., et al., *Preliminary studies in the electrodeposition of PbSe/PbTe superlattice thin films via electrochemical atomic layer deposition (ALD).* Langmuir, 2006. **22**(25): p. 10590-10595.

24. Yang, J.Y., et al., *Formation and characterization of Sb2Te3 nanofilms on Pt by electrochemical atomic layer epitaxy.* Journal of Physical Chemistry B, 2006. **110**(10): p. 4599-4604.

25. Zhang, X., X.Z. Shi, and C.M. Wang, *Optimization of electrochemical aspects for epitaxial depositing nanoscale ZnSe thin films.* Journal of Solid State Electrochemistry, 2009. **13**(3): p. 469-475.

26. Zhu, W., et al., *Electrochemical atom-by-atom growth of highly uniform thin sheets of thermoelectric bismuth telluride via the route of ECALE.* Journal of Electroanalytical Chemistry, 2008. **614**(1-2): p. 41-48.

27. Zhu, W., et al., *Growth of bismuth telluride thin film on Pt by electrochemical atomic layer epitaxy.* Transactions of Nonferrous Metals Society of China, 2005. **15**(2): p. 404-409.

28. Zhu, W., et al., *Development of growth cycle for antimony telluride film on Au(111) disk by electrochemical atomic layer epitaxy.* Electrochimica Acta, 2008. **53**(10): p. 3579-3586.

29. Gewirth, A.A. and B.K. Niece, *Electrochemical applications of in situ scanning probe microscopy.* Chem. Rev., 1997. **97**: p. 1129-1162.

30. Kolb, D.M. and H. Gerischer, *Further Aspects Concerning Correlation between Underpotential Deposition and Work Function Differences.* 1975. **51**(1): p. 323-327.

31. Kolb, D.M., Przasnys.M, and Gerische.H, *Underpotential Deposition of Metals and Work Function Differences.* Journal of Electroanalytical Chemistry, 1974. **54**(1): p. 25-38.

32. Magnussen, O.M. and R.J. Behm, *Structure and growth in metal epitaxy on low-index Au surfaces - a comparison between solid vertical bar electrolyte and solid vertical bar vacuum interfaces.* Journal of Electroanalytical Chemistry, 1999. **467**(1-2): p. 258-269.

33. Moller, F., O.M. Magnussen, and R.J. Behm, *Cucl Adlayer Formation and Cl Induced Surface Alloying - an in-Situ Stm Study on Cu Underpotential Deposition on Au(110) Electrode Surfaces.* Electrochimica Acta, 1995. **40**(10): p. 1259-1265.

34. Venkatasamy, V., et al., *Optimization of CdTe nanofilm formation by electrochemical atomic layer epitaxy (EC-ALE).* Journal of Applied Electrochemistry, 2006. **36**(11): p. 1223-1229.

35. Flowers, B.H., et al., *Atomic layer epitaxy of CdTe using an automated electrochemical thin-layer flow deposition reactor.* Journal of Electroanalytical Chemistry, 2002. **524-525**: p. 273-285.

36. Innocenti, M., et al., *CdS and ZnS deposition on Ag(111) by electrochemical atomic layer epitaxy.* Journal of the Electrochemical Society, 2001. **148**(5): p. C357-C362.

37. Pezzatini, G., et al., *Formation of ZnSe on Ag(111) by electrochemical atomic layer epitaxy.* Journal of Electroanalytical Chemistry, 1999. **475**(2): p. 164-170.

38. Gichuhi, A., B.E. Boone, and C. Shannon, *Electrosynthesized CdS/HgS heterojunctions.* Langmuir, 1999. **15**(3): p. 763-766.

39. Oznuluer, T., et al., *Electrochemical atom-by-atom growth of PbS by modified ECALE method.* Chemistry of Materials, 2005. **17**(5): p. 935-937.

40. Villegas, I. and J.L. Stickney, *Preliminary studies of gallium arsenide deposition on gold (100), (110), and (111) surfaces by electrochemical atomic layer epitaxy.* Journal of the Electrochemical Society, 1992. **139**(3): p. 686-94.

41. Villegas, I. and J.L. Stickney, *Gallium arsenide deposition on the (100) and (110) planes of gold by electrochemical atomic layer epitaxy: a low-energy electron diffraction, Auger electron spectroscopy, and scanning tunneling microscopy study.* Journal of Vacuum Science & Technology, A: Vacuum, Surfaces, and Films, 1992. **10**(5): p. 3032-8.

42. Wade, T.L., et al., *Electrochemical Formation of a III-V Compound Semiconductor Superlattice: InAs/InSb.* JEC, 2001. **500**: p. 322-332.

43. Huang, B.M., T.E. Lister, and J.L. Stickney, *Se adlattices formed on Au (100), studies by LEED, AES, STM and electrochemistry.* Surface Science, 1997. **392**(1-3): p. 27.

44. Lister, T.E., et al., *Electrochemical Formation of Se Atomic Layers On Au(100).* Journal of Vacuum Science & Technology B, 1995. **13**(3): p. 1268.

45. Lister, T.E. and J.L. Stickney, *Atomic level studies of selenium electrodeposition on gold (111) and gold (110).* Journal of Physical Chemistry, 1996. **100**(50): p. 19568-19576.

46. Bondarenko, A.S., et al., *Potentiodynamic electrochemical impedance spectroscopy of lead upd on polycrystalline gold and on selenium atomic underlayer.* Electrochemistry Communications, 2005. **7**(6): p. 631-636.

47. Chang, B.Y., E. Ahn, and S.M. Park, *Real-Time Staircase Cyclic Voltammetry Fourier Transform Electrochemical Impedance Spectroscopic Studies on Underpotential Deposition of Lead on Gold.* Journal of Physical Chemistry C, 2008. **112**(43): p. 16902-16909.

48. Conway, B.E. and J.C. Chacha, *Effects of temperature on the states of Pb adatoms underpotentially deposited from various solvents on Au : entropies of adatom states.* Journal of New Materials for Electrochemical Systems, 2004. **7**(3): p. 231-240.

49. Dimitrov, N., R. Vasilic, and N. Vasiljevic, *A Kinetic Model for Redox Replacement of UPD Layers.* Electrochemical and Solid-State Letters, 2007. **10**(7): p. D79-D83.

50. Kim, Y.G., et al., *Pb deposition on I-coated Au(111). UHV-EC and EC-STM studies.* Langmuir, 2007. **23**(5): p. 2539-2545.

51. Seo, M. and M. Yamazaki, *Changes in Surface Stress of Gold Electrode during Underpotential Deposition of Pb.* Journal of the Electrochemical Society, 2004. **151**(8): p. E276-E281.

52. Stafford, G.R. and U. Bertocci, *In situ stress and nanogravimetric measurements during underpotential deposition of pb on (111)-textured au.* Journal of Physical Chemistry C, 2007. **111**(47): p. 17580-17586.

53. Green, M.P. and K.J. Hanson, *Alloy formation in an electrodeposited monolayer.* Surface Science, 1991. **259**(3): p. L743-L749.

54. Sze, S.M., *Physics of Semiconductor Devices*. 2nd ed. 1981, New York: john Wiley & Sons.

55. Elam, J.W., et al., *Nucleation and growth during tungsten atomic layer deposition on SiO2 surfaces.* Thin Solid Films, 2001. **386**(1): p. 41-52.

56. Elam, J.W., et al., *Atomic layer deposition of palladium films on Al2O3 surfaces.* Thin Solid Films, 2006. **515**(4): p. 1664-1673.

57. Fabreguette, F.H., et al., *Quartz crystal microbalance study of tungsten atomic layer deposition using WF6 and Si2H6.* Thin Solid Films, 2005. **488**(1-2): p. 103-110.

Table 1. Electron Probe Microanalysis (EPMA) Data of 100 ALD cycle PbSe film formed when both Se and Pb potentials were positively increased from -0.3 V and -0.25 V to steady state -0.04 V. Electrode area: 4 cm^2.

PbSe Sample	Se Atomic %	Pb Atomic %	Se / Pb Ratio
Inlet	**18.78**	**18.06**	**1.04**
Middle	**20.03**	**19.86**	**1.01**
Outlet	**20.27**	**19.94**	**1.02**

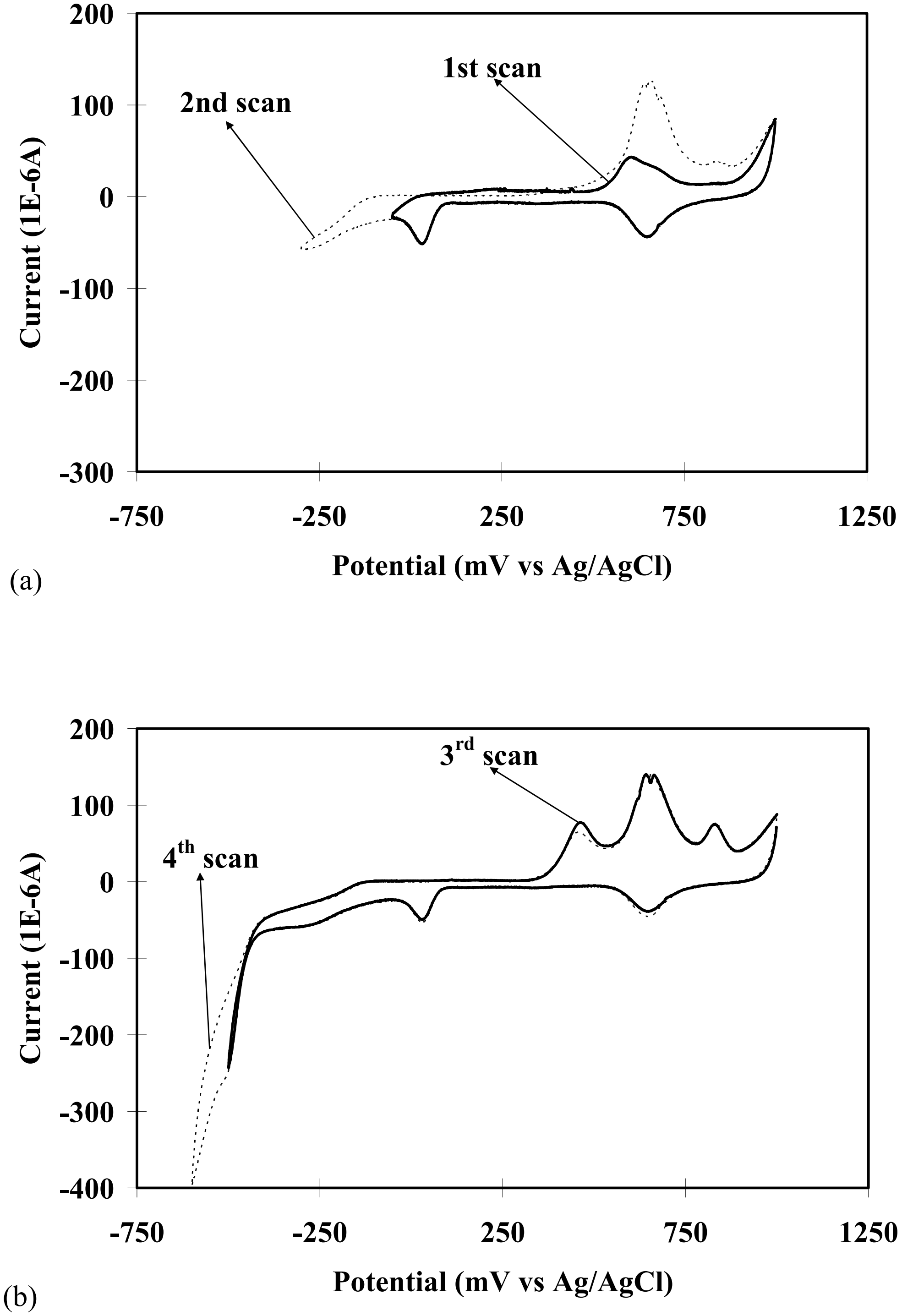

Figure 2.1: Cyclic voltammograms (a) and (b) of Au electrode in 0.5 mM $HSeO_3^+$ to successive decreasing potentials, pH 5, (electrode area: 4 cm^2, scan rate: 10 mV s^{-1}).

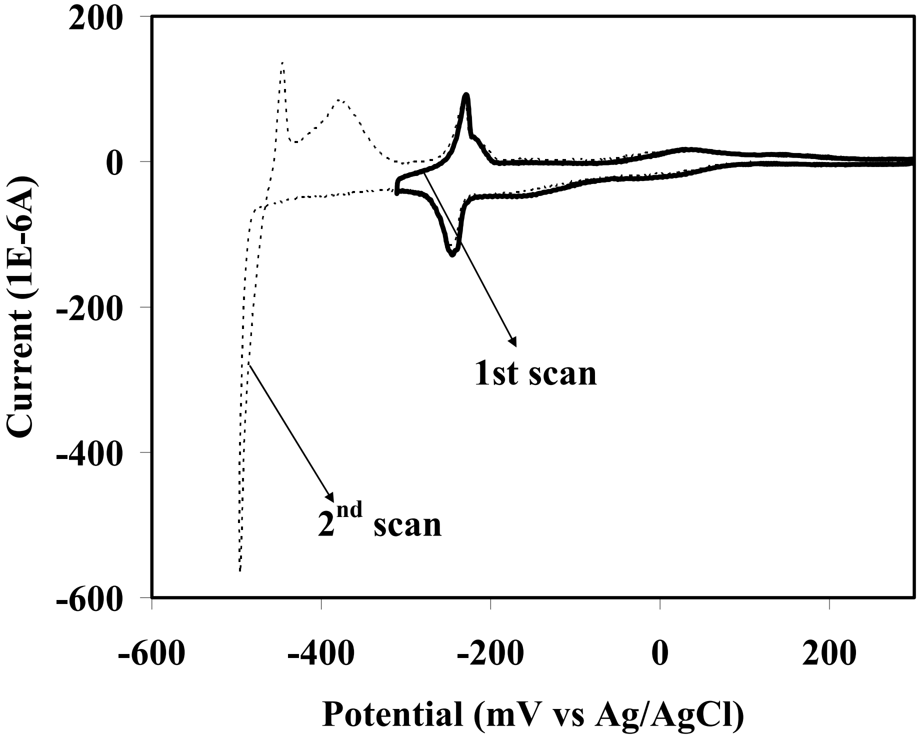

Figure 2.2: Cyclic voltammogram of Au electrode in 0.5 mM Pb^{2+}, pH 3, (electrode area: 4 cm^2, scan rate: 10 mV s^{-1}).

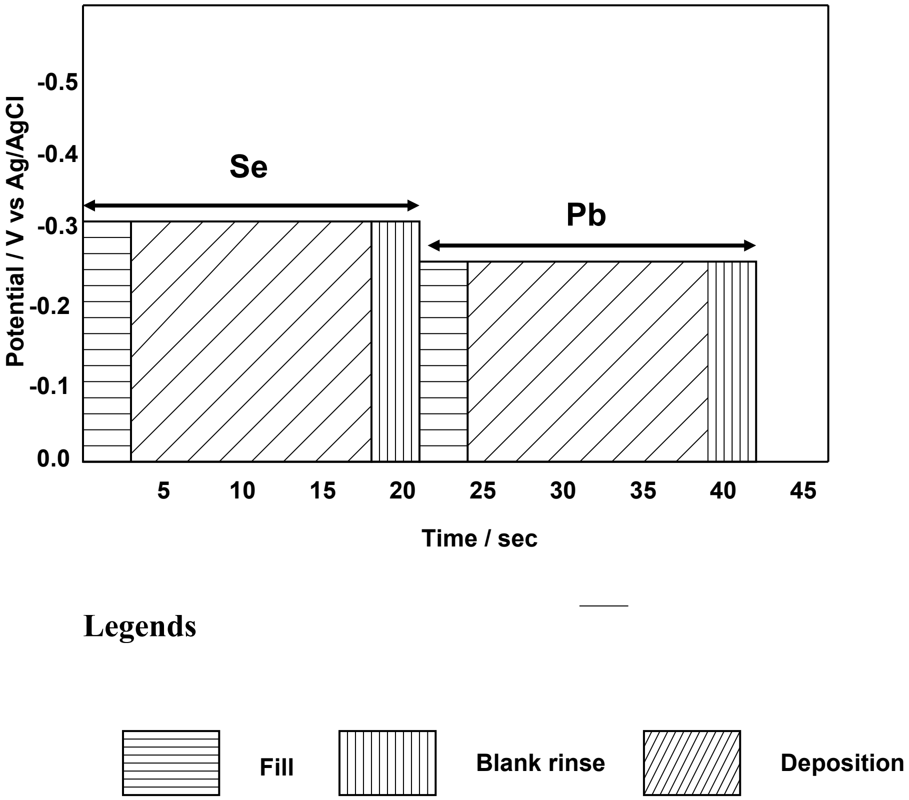

Figure 2.3: PbSe ALD deposition program with both Se and Pb potentials held constant at -0.3 and -0.25 V respectively.

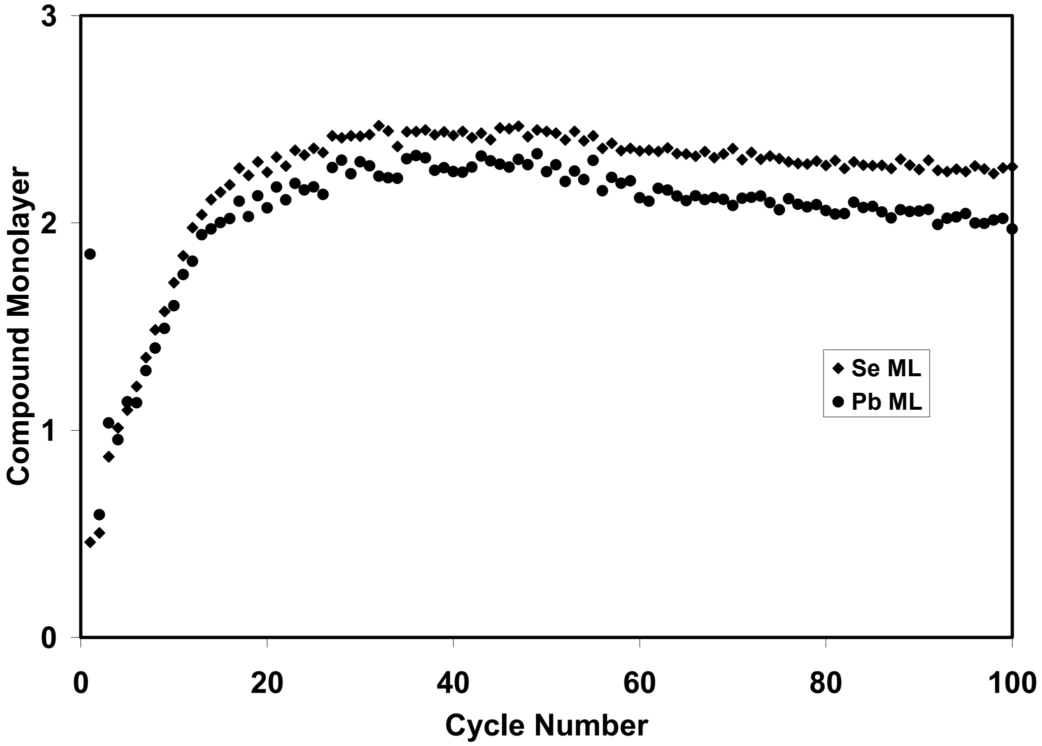

Figure 2.4: Deposition currents (coverage) of 100 ALD cycles of PbSe with both Se and Pb potentials held constant at -0.3 V and -0.25 V respectively. Electrode area: 4 cm^2.

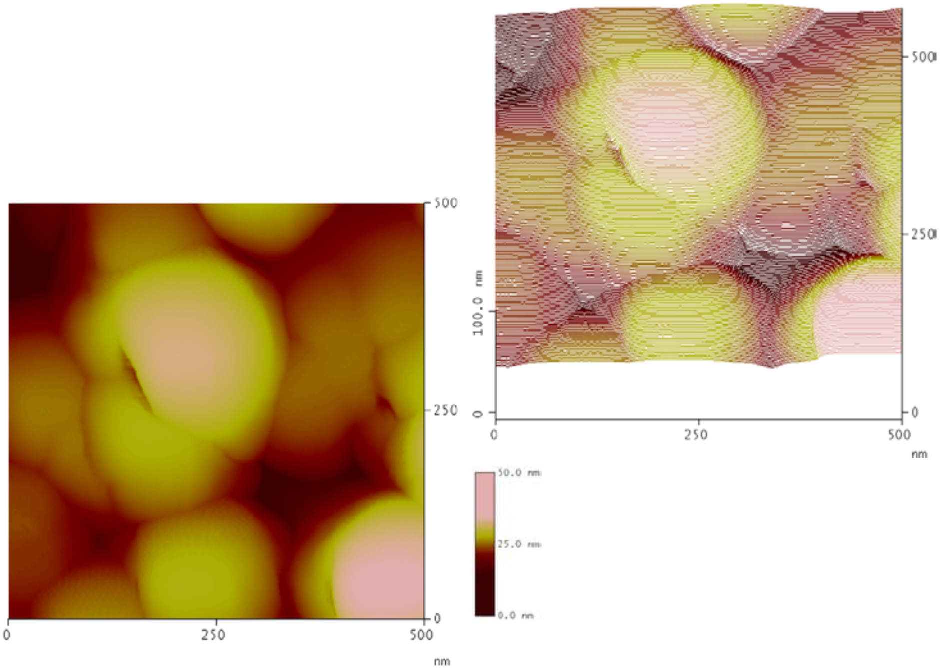

Figure 2.5: STM image of template stripped Au (500 nm^2 image). Electrode area: 4 cm^2.

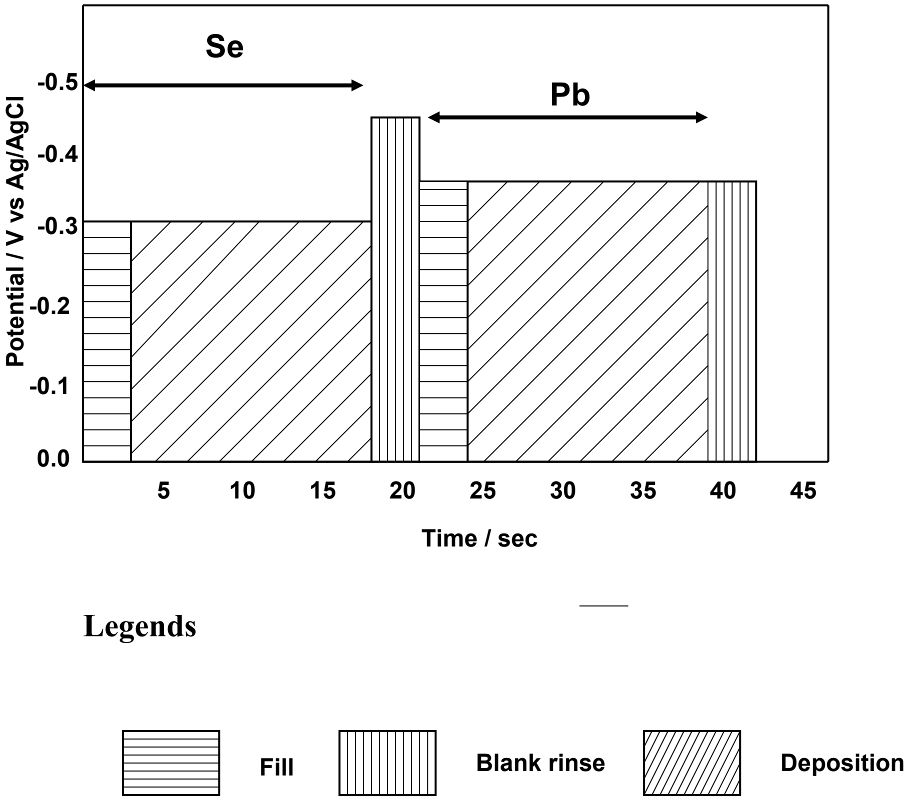

Figure 2.6: PbSe ALD deposition program with both Se and Pb potentials held constant including a Se reductive stripping step.

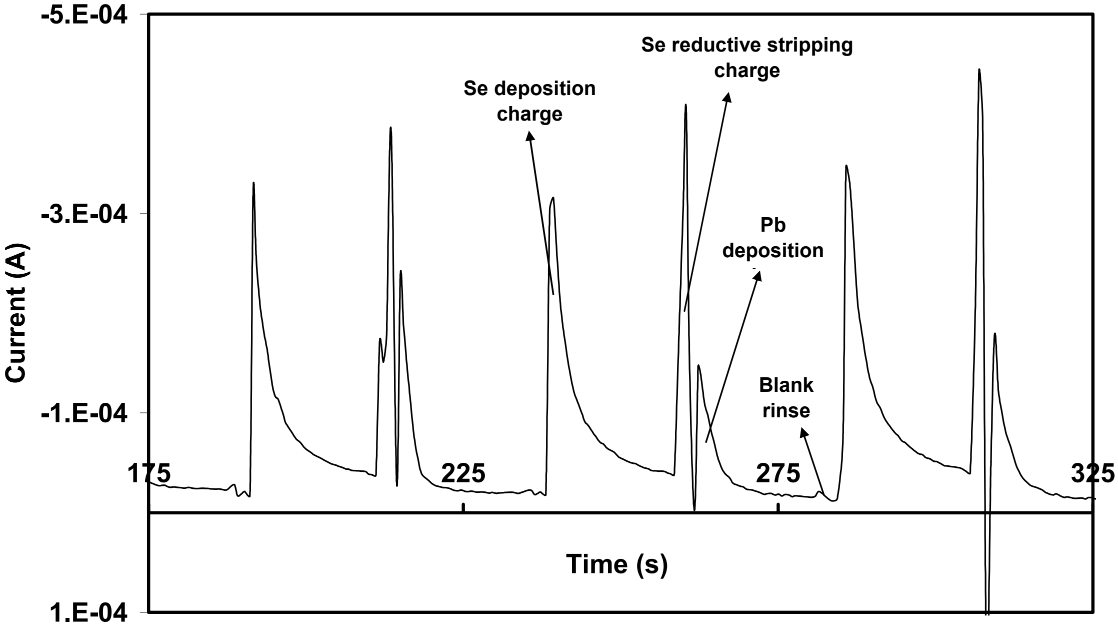

Figure 2.7: Current time traces of 100 cycles of PbSe formed by electrochemical ALD with the inclusion of the Se reductive stripping step. Electrode area: 4 cm^2.

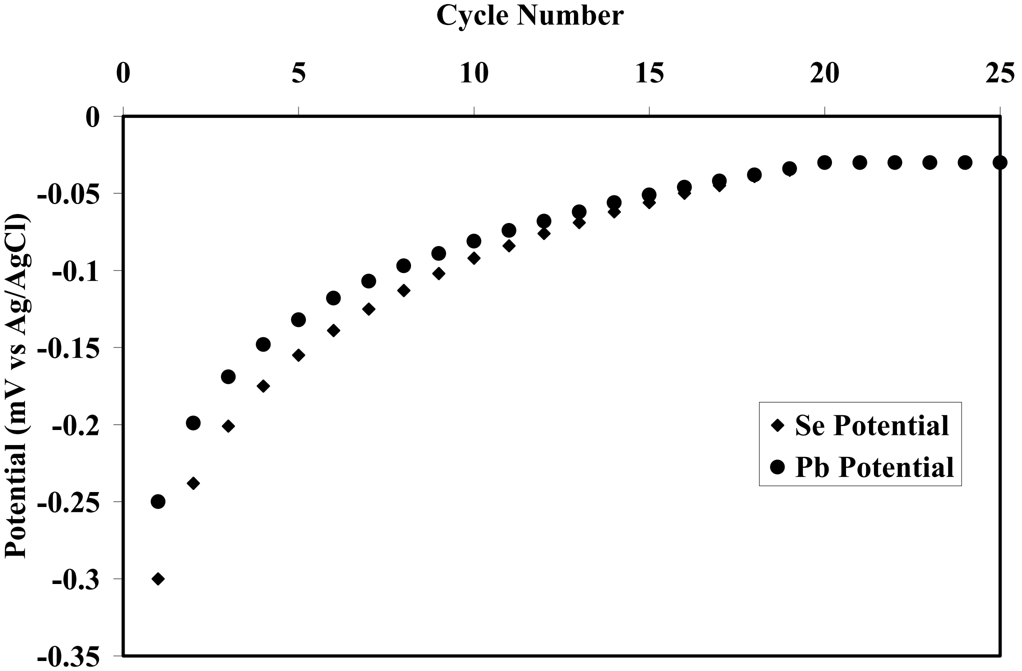

Figure 2.8: PbSe ALD cycle showing Se and Pb deposition potentials being shifted positive from -0.3 V and -0.25 V respectively to the steady state -0.04V. Electrode area: 4 cm^2.

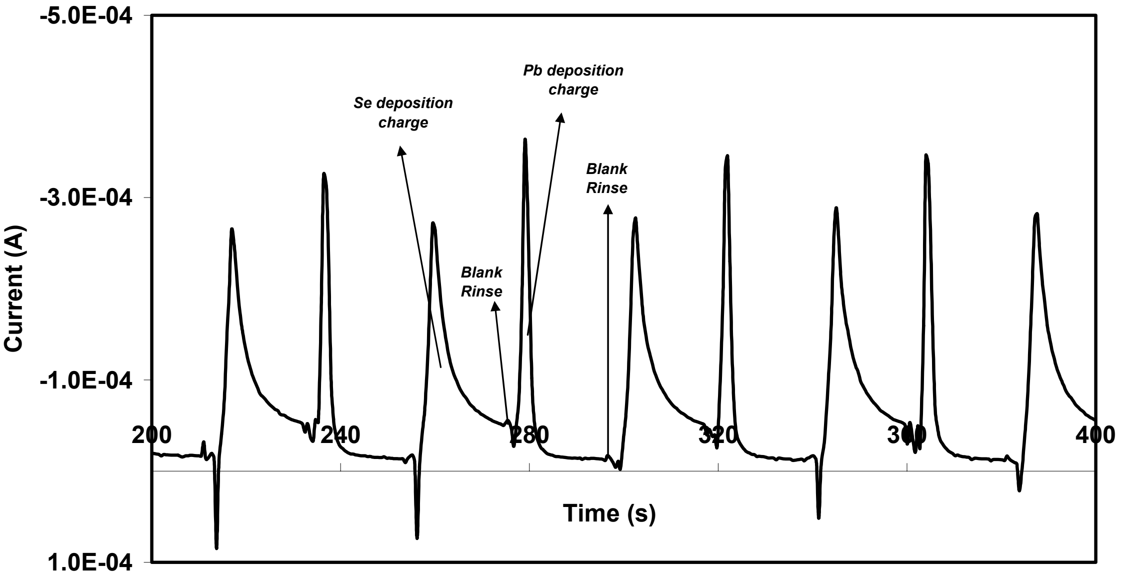

Figure 2.9: Current time traces of 100 cycles of PbSe formed when Se and Pb potentials were positively shifted from -0.3 V and -0.25 V respectively to the steady state -0.04 V. Electrode area: 4 cm^2.

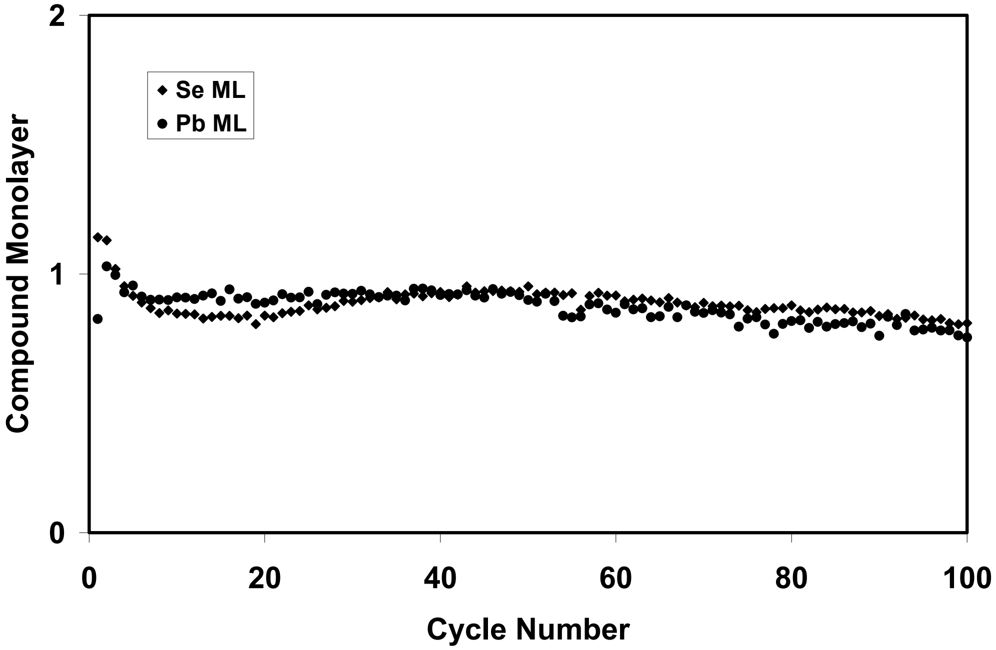

Figure 2.10: Deposition currents (coverage) of 100 ALD cycles of PbSe formed when both Se and Pb potentials were positively shifted from -0.3 V and -0.25 V respectively to -0.04 V. Electrode area: 4 cm^2.

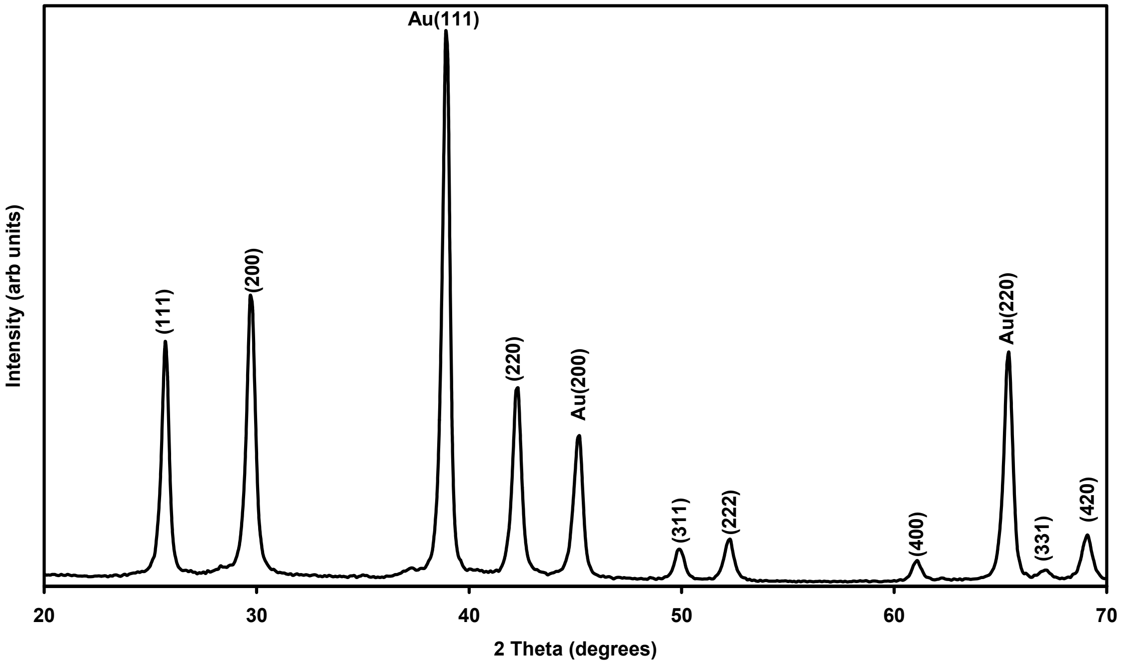

Figure 2.11: X-ray diffraction of 100 ALD cycles of PbSe thin film formed when both Se and Pb potentials were positively shifted from -0.3 V and -0.25 V respectively to -0.04 V. Angle of incidence is 1°, Cu Kα source. Electrode area: 4 cm^2.

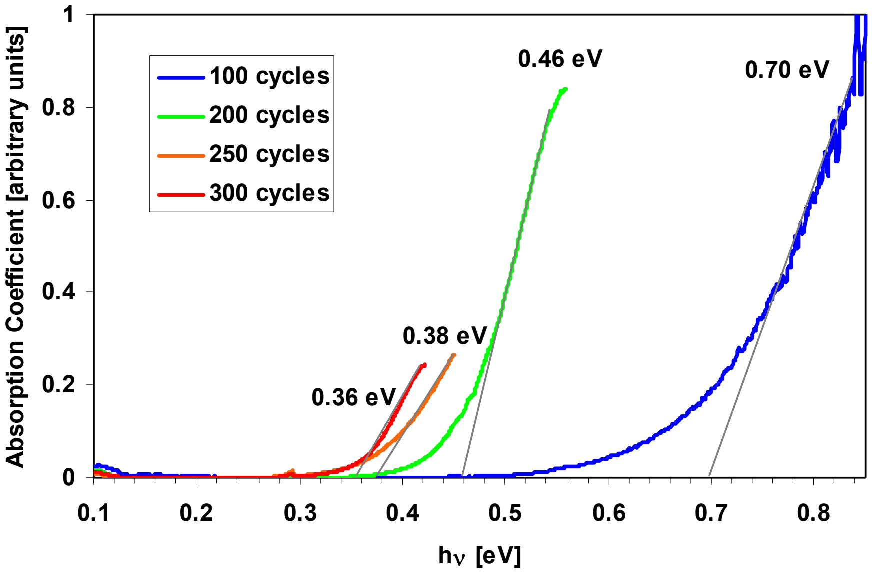

Figure 2.12: Absorption spectra of a) 100 ALD cycle, b) 200 ALD cycles, c) 250 ALD cycles and d) 300 ALD cycles of PbSe thin films formed when both Se and Pb potentials were positively shifted from -0.3 V and -0.25 V respectively to -0.04 V. Electrode area: 4 cm^2.

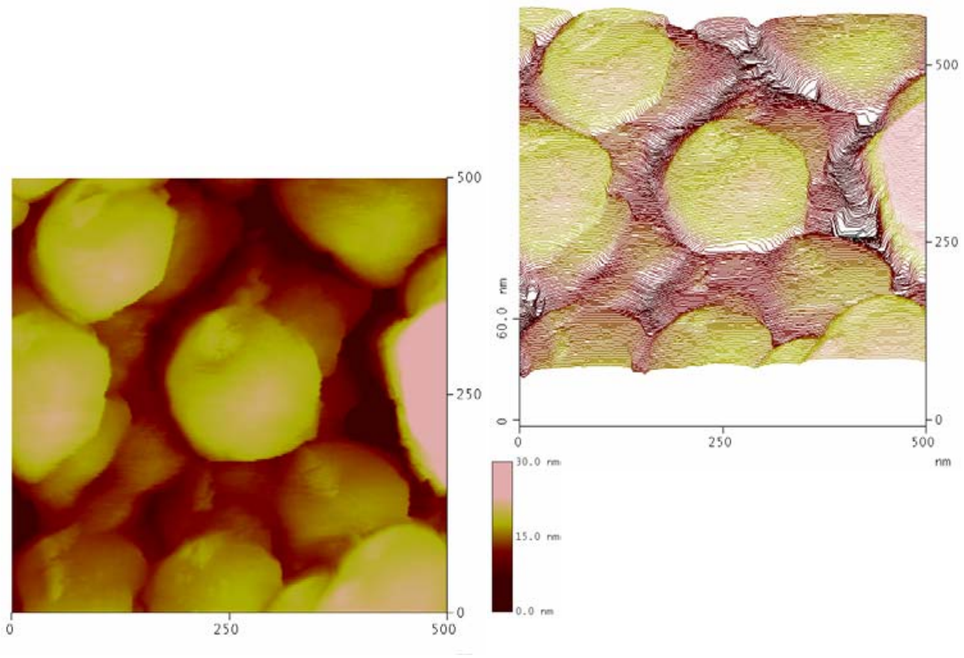

Figure 2.13: STM image (500 nm^2 image) of 100 ALD cycles of PbSe thin film on template stripped Au formed when both Se and Pb potentials were positively shifted from -0.3 V and -0.25 V respectively to -0.04 V. Electrode area: 4 cm^2.

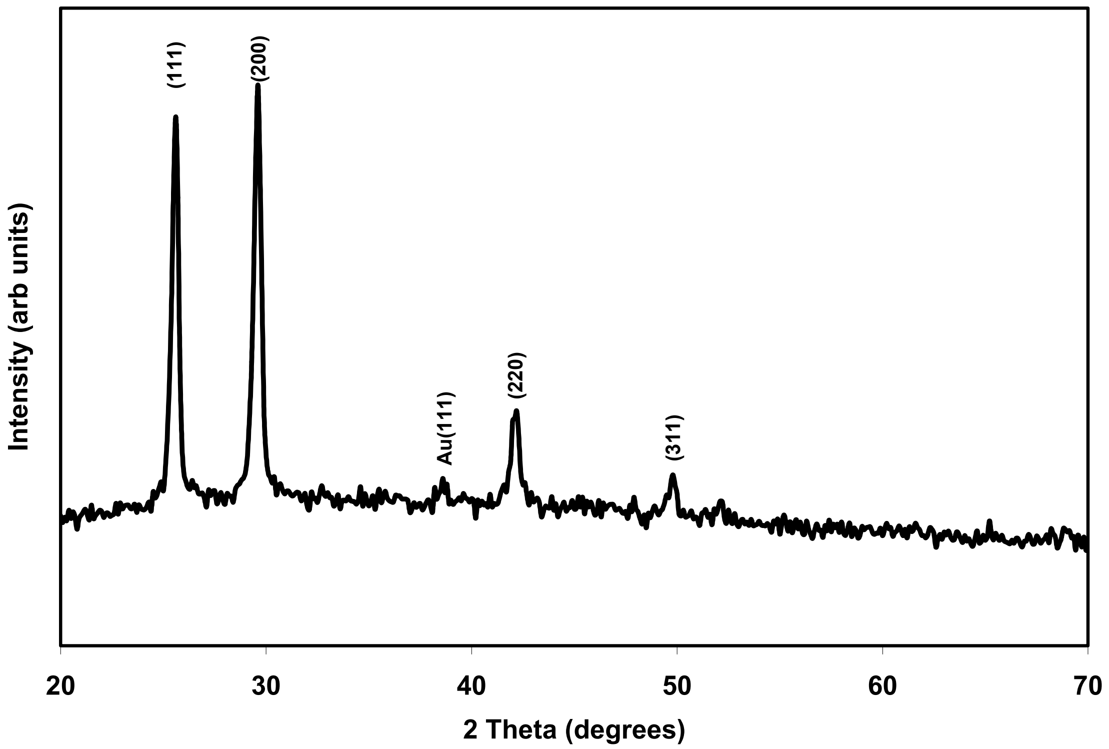

Figure 2.14: X-ray diffraction of 100 ALD cycles of PbSe thin film on Au on Mica formed when both Se and Pb potentials were positively shifted from -0.3 V and -0.25 V respectively to -0.04 V. Angle of incidence is 0.1°, Cu Kα source. Electrode area: 4 cm^2.

CHAPTER 3

FORMATION OF PbTe NANOFILMS BY ELECTROCHEMICAL ATOMIC LAYER DEPOSITION (EC-ALD)[2]

---

[2] Banga, D., et al., Electrochimica Acta 53:6988 (2008)
Reprinted here with permission of publisher.

Abstract

This article describes optimization of a cycle for the deposition of lead telluride (PbTe) nanofilms using electrochemical Atomic Layer Deposition (ALD). PbTe is of interest for the formation of thermoelectric device structures. Deposits were formed using an ALD cycle on Au substrates, one atomic layer at a time, from separate solutions, containing Pb^{+2} or $HTeO_2^+$ ions. Single atomic layers were formed using surface limited reactions, referred to as underpotential deposition (UPD), so the deposition cycle consisted of alternating UPD of Te and Pb. The Pb deposition potential was maintained at -0.35 V throughout the 100 cycle-runs, while the Te deposition potential was ramped up from -0.55 V to -0.40 V over the first 20 cycles and then held constant for the remaining ALD cycles. Coulometry for the reduction of both Te and Pb indicated coverages near one monolayer, each cycle. Electron probe microanalysis (EPMA) indicated a uniform and stoichiometric deposit, with a Te/Pb ratio of 1.01. X-ray diffraction measurement showed that the thin films had the rock salt structure, with a preferential (200) orientation for the as formed deposits. No annealing was used. Infrared reflection absorption measurements of PbTe films formed with 50, 65, and 100 cycles indicated strong quantum confinement.

Introduction

The search for more efficient thermoelectric materials has increased in recent years, in order to save energy and for microchip cooling. Compounds such as PbTe, PbSe, Sb_2Te_3, and Bi_2Te_3 are well known thermoelectric materials, presently under study by a number of groups around the world [1-3]. Thermoelectric materials are characterized by their dimensionless figure of merit (ZT) [1], where T is the absolute temperature and Z is a material's coefficient defined by the equation $Z = \alpha^2 / (\rho\lambda)$, where α is the Seebeck coefficient, ρ the electric conductivity and λ the thermal conductivity. The higher the figure of merit of a material, the more efficiently it can generate electricity from heat. PbTe is an important thermoelectric material [4-14] due to its high figure of merit, good chemical stability, low vapor pressure and high melting point (~ 900 K). PbTe is IV-VI compound semiconductor, with the rock salt structure and a narrow bandgap (Eg = 0.29 eV). In addition to thermoelectric applications, PbTe has been used for infrared detectors and photovoltaics [15-17]. With a large Bohr radius (a_o) (50 nm), relatively large PbTe nanostructures tend to exhibit quantum confinement effects [18]. Optical, mechanical and magnetic properties of semiconductors with large Bohr radii can change when dimensions are less than its Bohr radius, the result of electron confinement. IV-VI compound semiconductors have small and equal electron and hole masses, compared to III-V or II-VI compound semiconductors, enabling large confinement energies to be equally split between carriers, so they tend to exhibit greater confinement effects [18]. The band gap values of the quantum confined materials are frequently larger than the bulk materials, 0.2 – 0.3 eV for the Pb chalcogenides. It has also been proposed that ZT for nanostructure materials, formed as superlattices, quantum wells and or quantum wires may dramatically increase the figure of merit over the corresponding bulk materials, increasing the electronic density of the states that occurs in ideal two and one-dimensional systems [19-20].

Other techniques previously used to grow PbTe thin films have included molecular beam epitaxy [21-22], chemical vapor deposition [23-24], pulsed laser deposition [25-26] and hot-wall epitaxy [15]. One of the major drawbacks of these techniques is the use of high temperatures for the growth of films which results in heat-induced interdiffusion [27] of elements in adjacent structure layers, which can degrade deposit quality. Electrodeposition is therefore an appealing technique for the formation of complex compound semiconductor structures, as it can be performed at or near room temperature, minimizing interdiffusion. The most notable electrodeposition techniques include precipitation [28], codeposition [29-30], two stage [31] and atomic layer deposition (ALD) [32-34], also known as electrochemical atomic layer epitaxy (EC-ALE).

The Author's group and others have worked extensively on the growth of compound semiconductor nanofilms, and more recently on the growth of metal nanofilms using electrochemical atomic layer deposition (ALD) [3, 33-45]. Electrochemical ALD makes use of underpotential deposition (UPD) [46-49], a phenomena where an atomic layer of one element deposits on a second, at a potential prior to that needed to form bulk deposits. The result is a surface limited reaction, deposition limited by the surface area of the deposit. By forming compound monolayers using UPD in a sequence, referred to here as a cycle, which can be repeated to form more compound monolayers, materials can be grown layer by layer with atomic level control, the basis of the electrochemical ALD.

Numerous compounds that have been successfully formed by electrochemical ALD, include II-VI compounds such as CdTe [50-57], CdS [35, 58], ZnSe [59], ZnS [58] and CdS/HgS superlattices [60] , IV-VI compounds such as PbS [61], PbSe [43] and superlattice of PbSe/PbTe [33], as well as III-V compounds such as GaAs [62-63], InAs [64-65], InSb [66] and superlattices of InAs/InSb [66]. This paper will focus on the optimization of an electrochemical ALD cycle used for the growth of PbTe nanofilms on Au on glass substrates.

Experimental

Thin films of PbTe were grown in this study using an automated thin layer flow electrodeposition system consisting of a series of solution reservoirs, computer controlled pumps, valves, a thin layer electrochemical flow cell and a potentiostat. Most of the hardware used has been described previously [51], with minor changes made to the reference compartment and the auxiliary electrode. A simple O-ring was used to hold the reference electrode instead of the Teflon compression fitting, providing a better seal, and a Au wire embedded into the Plexiglas flow cell was used as the auxiliary electrode, instead of the ITO glass slide, which has proven more durable. The electrochemical flow cell was designed to promote laminar flow. The working electrode was Au on glass, the auxiliary was a Au wire, and the reference electrode was Ag/AgCl (3M NaCl) (Bioanalytical systems, Inc., West Lafayette, IN). The cell volume was about 0.3 mL and solutions were pumped at 50 mL min^{-1}. The system was contained within a nitrogen purged Plexiglas box to reduce the influence of oxygen during electrodeposition.

Substrates used in the study consisted of 300 nm thick vapor deposited gold on glass microscope slides. Prior to insertion into the vapor deposition chamber, the glass slides were cleaned in HF, and rinsed with copious amounts of deionized water from a Nanopure water filtration system (Barnstead, Dubuque, IA), fed from the house distilled water system. Deposition began with 3 nm of Ti, an adhesion layer, then 300 nm of Au deposition at around

250 °C. The glass slides were then annealed in the deposition chamber at 400 °C for 12 hours, while the pressure was maintained at 10^{-6} Torr.

Solutions were prepared using reagent grade or better chemicals and deionized water. Three different solutions were used in this study. The lead solution consisted of 0.5 mM $Pb(ClO_4)_2$ (Alfa Aesar, Ward Hill, MA), pH 3, with 0.1 M $NaClO_4$ (Fischer Scientific, Pittsburgh, PA) as the supporting electrolyte. The tellurium solution was made of 0.5 mM TeO_2 (Alfa Aesar, Ward Hill, MA), pH 9.2, buffered with 50.0 mM sodium borate and 0.1 M $NaClO_4$ (Fischer Scientific, Pittsburgh, PA) as the supporting electrolyte. A pH 3 blank solution of 0.1 M $NaClO_4$ (Fischer Scientific, Pittsburgh, PA) was used as well. The pH values of all the solutions were adjusted with $HClO_4$ and NaOH (Fischer Scientific, Pittsburgh, PA).

The electrochemical ALD cycle program used to form PbTe consisted of the following: the Te solution was flushed in to the cell for 2 s at the chosen potential, and then held quiescent for 15 s for deposition. The blank solution was then flushed through the cell at the same potential for 3 s, to rinse out excess $HTeO_2^+$ ions. The Pb solution was then flushed through the cell for 2 s at the Pb potential, and held quiescent for 15 s for deposition. Blank solution was again flushed through the cell for 3 s to rinse out excess Pb^{2+} ions from the cell. This process was referred to as one cycle, and was repeated 100 times to form each of the deposits described in this paper.

A Joel JXA-8600 electron probe was used for electron probe microanalysis (EPMA). Glancing angle X-ray diffraction patterns were obtained on a Scintag PAD V diffractometer, equipped with a 6" long set of Soller slits on the detector to improve resolution in the asymmetric diffraction configuration. Absorption measurements were performed using a variable angle reflection rig in conjunction with a Bruker 66v FTIR spectrometer equipped with a Si detector.

Results and Discussions

Cyclic voltammograms of deposition of each element on the Au on glass substrates (Figures 1 and 2) were used to determine an initial set of UPD potentials for the cycle. Both Te and Pb deposition have been extensively studied by this group and others [54, 67-70]. Previous studies showed that Te deposition is kinetically slow and dependent on the pH. The peaks for Te UPD and stripping tend to shift in a linear fashion to more negative potentials the more basic the solution [54].

Figure 1 shows four cyclic voltammograms, each to an increasingly lower potential, each to just past a different reduction feature. Three distinct reduction peaks were observed at -0.170 V, -0.4 V and -0.6 V, with a sharp increase in reduction current at -0.70 V, corresponding to bulk Te deposition (Figure 1(b)). It was assumed that the formal potential was probably about -0.1 V in that system, thus each of the three reduction peaks occur at overpotential. Experience has shown, as do the CV curves in Figure 1, that each of the three reduction peaks was some sort of surface limited deposition. The term UPD suggests that surface limited deposition should occur at potentials prior to the formal potential for deposition of the element, and that is obviously not the case for Te. The reason for this behavior involves the slow kinetics for $HTeO_2^+$ reduction. The definition of UPD used here is that it corresponds to the surface limited deposition of an element at potentials prior to bulk deposition. Since bulk deposition becomes prominent at around -0.6 V as seen in Figure 1(b), each of the three reduction peaks could and is referred to as a UPD process in this paper. Looking at the subsequent oxidation scans in Figure 1(b), it is clear that bulk oxidation of Te starts around -0.05 V, with a peak near 0.05 V. On the other hand, if the potential was reversed before significant bulk deposition as in Figure 1(a), all stripping of the surface limited Te deposits, Te UPD, occurred positive of 0.1 V, clearly differentiating it from bulk stripping, and showing that the use of -0.55 V does not result in a detectable amount of bulk Te stripping (Figure 1(a)).

The Pb scan in Figure 2 started at 0.25 V, and displayed a slowly increasing current during the negative going scan, with a sharp spike at -0.25 V, reminiscent of Pb UPD on a Au(111) electrode [71]. Bulk Pb deposition began near -0.45 V. In the corresponding positive going scan, there was a small sharp oxidation peak for bulk Pb at -0.47 V, as well as a large broad peak around -0.38 V, evidently also for bulk Pb. Why it was shifted to higher potentials than the initial sharp spike was not clear, but suggests some minor passivation. The sharp UPD stripping peak at about -0.25 V shows the reversibility of the Pb UPD on the (111) facets of the Au on glass substrate.

Based on the cyclic voltammograms in Figures 1 and 2, UPD potentials of -0.55 V for Te and -0.35 V for Pb were identified as possible starting points for the deposition of PbTe. The initial cycle thus involved a 2 s filling with the $HTeO_2^+$ solution, and deposition for 15 s at -0.55 V. The cell was then rinsed with blank for 3 s, at the same potential, then a 2 s filling with the Pb^{2+} solution and a 15 s deposition at -0.35 V. The Pb^{2+} ions were then rinsed from the cell with blank for 3 sec at -0.35 V. This cycle was intended to form one monolayer of the IV-VI semiconductor PbTe, and was repeated to form PbTe films. One compound monolayer refers to deposition of a single compound bilayer, one atomic layer of Te and one of Pb, with the 200 orientation. After about 8 cycles, this program resulted in more than a single compound monolayer per cycle as shown in Figure 3. That is, initially a little over 1.0 ML/cycle were deposited, but this gradually increased over the first 30 cycles to 1.9 ML/cycle, at which point it remained steady.

Experience with electrochemical ALD programs for many compounds has shown that deposition rates significantly more than a ML/cycle tend to result in roughening of the deposit, while better morphology was obtained when the deposition rate was near a ML/cycle or less. Deposition of more than needed to form a compound monolayer can result in an excess, that may not completely react with the next atomic layer, and thus result in non stoichiometric deposits, and production of islands. These islands and incompletely reacted deposits accumulate from cycle to cycle producing a rougher deposit.

This raises the question of why more than that needed to form a single compound monolayer would be deposited at an under potential to begin with? The single compound monolayer is a cartoon, used to think about the ALD process. In actuality, the amount deposited is controlled by the potential, if the system reaches equilibrium. The coverage will correspond to what was stable on the surface at the chosen potential. The cartoon suggests that only that which reacts one to one with the other element will deposit. However, as the surface is not a single crystal plane, but a polycrystalline Au surface with 40 nm clusters (with a number of small Au (111) terraces); there were lots of defects and steps. The energetics of deposition on such defect sites should be different than for deposition on a Au (111) plane. In addition, there will be a lattice mismatch between the substrate and the deposit, which will increase dislocations and defects as the deposit grows above the critical thickness. Further, there may be conditions where a different compound, with a different crystal structure, or even a different stoichiometry, might form. For these reasons, it is advantageous to form deposits near or below a compound monolayer/cycle.

During optimization of an ALD cycle, it is thus desirable to keep the deposition rate low and constant. Past experience, using constant deposition potentials throughout the electrochemical ALD run in the formation of CdTe, resulted in a decrease in deposition rate (ML/cycle), with increasing numbers of cycles, for the first 10 to 20 cycles [51]. The present study (Figure 3) was the first encounter by this group of a tendency for the ML/cycle to increase with cycle number, when constant deposition potentials were used.

Reasons for changes in the ML/cycle are not yet clear. Figure 3 may simply result from choosing deposition potentials based on the thermodynamics for Pb and Te depositions on the Au substrate, and then expecting the same energetics for atomic layer formation on the growing compound film. However, why it takes 30 cycles to change completely (Figure 3) is not clear. It may be a result of nucleation and growth kinetics. It does not appear that 3D nucleation is occurring, but each layer probably involves some form of 2D nucleation and growth. The kinetics for this process may be slowed initially, and get faster as the film improves in quality. Te deposition is a function of slow kinetics as Figure 1 displays, with all the deposits forming at overpotential. It is probable that the kinetics for Te deposition will be a function of the surface structure and composition. Thus the overpotential required for Te deposition on Au should be different from that on CdTe and that on PbTe. In addition, as noted above, the Au on glass films used here have a significant defect density. As the films form, the nature of the surface may change significantly over the first 30 cycles, as the PbTe surface morphology establishes itself. Recent STM studies, by this group, of ALD grown films suggest that the deposit roughness can be lower than the substrate. There may be a kind of self healing process resulting from the ALD. With increasing numbers of cycles, the deposit facets increase in size and quality, and the kinetics for Te deposition may improve, requiring a lower overpotential for deposition of the same atomic layer.

An alternative justification for these changes with cycle, suggested by this group and others [1, 3] involves dropping some of the applied potential across a growing space charge layer (SCL), or Schottky barrier, between the Au electrode and the growing semiconductor thin film. However, given how thin the films are by the point where steady state is achieved, it is unrealistic to think that a space charge layer has been fully developed [72].

The first attempts to improve the PbTe coverage from cycle to cycle involved continuing to use constant potentials, but shifting them positive. Increasing the Te potential from -0.55 V to -0.4V dropped the overall coverage; while the variations in ML/cycle continued during the first 20 cycles. On the other hand, using -0.35 V for Te deposition resulted in a more inhomogeneous deposit and a Te/Pb ratio closer to 1.1. Shifting the Pb potential from -0.35 to -0.30 V resulted in some variation in coverage across the deposit, and a Te/Pb ratio of 1.04. In each case, using constant potentials resulted in an initially low value for the ML/cycle, which then increased over the first 20 cycle, before reaching steady state values of ML/cycle, as in Figure 3.

Previous studies have shown that using a sequence of potential shifts for the first 10-20 cycles can work to achieve constant cycle to cycle growth, with a stoichiometry ratio of 1.0. So far, as mentioned above, the shifts used in the deposition of other compounds such as PbSe, CdTe, Bi_2Te_3, InSb and InAs have been negative [1, 3, 43, 51, 65-66] in order to increase the amounts deposited. The present case (Figure 1) was the first where positive shifts were required. To investigate this process, a number of deposits were run using different functional forms for a sequence of shifts in the deposition potentials. Figure 4 represents a successful sequence for the growth of PbTe, where the Pb potential was maintained at -0.35 V, and the potential for Te was increased from -0.55V, asymptotically approaching the steady state value of -0.4 V over the first 20 cycles. After 20 cycles, the steady state potential was maintained at -0.4 V for the remainder of the 100 cycle run (Figure 4). Figure 5 shows nearly constant charges for the whole 100 cycle run. In addition, the coulometry suggests that essentially one compound monolayer was formed with each cycle. Increasing deposition times for both Te and Pb from 15 to 60 s displayed no significant increase in charge or coverage determined using EPMA, attesting to the surface limited nature of the potentials chosen for each element.

The data in Figure 5 was the result of integration of current time traces, such as those shown in Figure 6. Such current time traces are important to an understanding of the deposition process. It is clear from Figure 6 that there was more charge for deposition of Te than Pb, as expected since Te is reduced from a tellurite precursor, a four electron process ($HTeO_2^+ + 3H^+ + 4e^- \rightarrow Te_{UPD} + 2H_2O$), while Pb^{2+} reduction is a two electron process ($Pb^{2+} + 2e^- \rightarrow Pb_{UPD}$). Rinsing the reactant solutions into the cell was accompanied by a large current spike, as the majority of the atomic layer was deposited, and some charging current could also contribute when the potential is made more negative. In addition, rinsing with the blank solution shows up as short sections with little current. From the ratio of Te/Pb using EPMA, the overall stoichiometry was essentially 1.0, even though the charges may not exactly match from graphs like Figure 6. Discrepancies can arise due to the presence of small amounts of side reactions, such as hydrogen evolution or oxygen reduction. Although the current time traces, or the charges obtained for them, help in following the deposition process, the overall stoichiometry of the resulting deposits are best determined using an independent analytical method such as EPMA or by dissolving the deposit and using ICP-MS etc. Table I shows the atomic % obtained with EPMA, relative to the composition of the film. That is, as the deposits are very thin, a significant atomic % of the Au substrate was recorded as well. However, as the Te and Pb are assumed to be homogeneously distributed on top of the Au, the ratio of the Te to Pb atomic percentages should be a direct measure of the deposit stoichiometry. Three points on the deposit were investigated, near the inlet, middle and outlet. The coverages look to be very similar, essentially 20 % for both Te and Pb at each position. In addition, the ratio was 1.0 at each point.

Figure 7 shows the glancing angle (1^o from the sample plane) X-ray diffraction patterns of a 100 cycle PbTe deposit. The rock salt structure peaks for the (200), (111), (222), (400) and (311) planes of PbTe [JCPDS 20-0494], along with polycrystalline Au substrate peaks are clearly evident in the X-ray diffraction pattern. The X-ray diffraction pattern showed a strong (200) preference. The absence of elemental peaks for Te and Pb was another indicator of deposit quality. It is important to note that no annealing was used. Therefore, this was an as deposited film.

PbTe is a direct bandgap semiconductor (0.29 eV), and so has a large absorption coefficient. Thus, even though the deposits were formed with only 100 cycles, they were easily visible as shinny gray films (Figure 8). The band gap is in the infrared (0.29 eV) and thus would be expected to absorb at all visible wavelengths. However, for very thin deposits, quantum confinement effects are at work, and result in a blue shift of the band gap. As noted in the introduction, the Bohr radius of PbTe is quite large, and thus such effects are clearly evident for the nanofilms formed in this study. The result is the appearance of a sequence of vivid colors as the deposit becomes thicker. Also, at the edges of the deposits, a rainbow of color is always observed, as the thickness of the deposit ramps up over a distance of about 0.1 mm. One of the reasons for these colors is that the band gap is shifted well into the visible. The appearance of colored films initially is a clear indication that compound films are being formed, rather than metallic films. In addition, variations in the color indicate variations in deposit thickness across the deposit. The deposits formed in these studies were very homogenous upon visual inspection, in agreement with the EPMA results shown in Table 2. As an indication of the extent of the blue shift that results from quantum confinement, a series of absorption spectra were obtained in the IR for deposits formed with different numbers of cycles (50, 65 and 100 cycles). Quantum confinement is clearly evident in Figure 9 by the blue shifted absorption values of all the three deposits. Although PbTe has a band gap value of 0.29 eV, the 50, 65 and 100 cycle deposits had band gap values shifted to 1, 0.9 and 0.7 eV respectively. The 50 cycle deposit shows considerable noise in the spectrum as its absorption is blue shifted out of the spectrometer's range.

Conclusion

Electrochemical ALD was successfully used to form smooth epitaxial PbTe thin films as confirmed by optical microscopy and visual inspection of the deposit. EPMA results confirmed that the deposit was homogeneous and stoichiometric as expected from the current time traces. XRD revealed the films had a preferential (200) orientation. Strong quantum confinement effects were also observed in the PbTe deposits grown with 100 cycles or less, as evident from the absorption spectra.

Acknowledgements

Support from the National Science Foundation is gratefully acknowledged.

References

1. Zhu, W., et al., *Optimization of the formation of bismuth telluride thin film by using ECALE.* Journal of Electroanalytical Chemistry, 2005. 585(1): p. 83-88.
2. Zhu, W., et al., *Growth of bismuth telluride thin film on Pt by electrochemical atomic layer epitaxy.* Transactions of Nonferrous Metals Society of China, 2005. 15(2): p. 404-409.
3. Yang, J.Y., et al., *Formation and characterization of Sb2Te3 nanofilms on Pt by electrochemical atomic layer epitaxy*. Journal of Physical Chemistry B, 2006. 110(10): p. 4599-4604.
4. Beyer, H., et al., *PbTe based superlattice structures with high thermoelectric efficiency.* Appl. Phys. Lett., 2002. 80(7): p. 1216-1218.
5. Broido, D.A. and T.L. Reinecke, *Thermoelectric power factor in superlattice systems*. Appl. Phys. Lett., 2000. 77(5): p. 705-707.
6. Broido, D.A. and T.L. Reinecke, *Theory of thermoelectric power factor in quantum well and quantum wire superlattices*. Phys. Rev. B, 2001. 6404(4): p. 45324.
7. Dresselhaus, M.S., et al., *Quantum wells and quantum wires for potential thermoelectric applications.* Semiconductors and Semimetals, 2001. 71(Recent Trends in Thermoelectric Materials Research III): p. 1-121.
8. Harman, T.C., et al., *Thermoelectric quantum-dot superlattices with high ZT*. 2000. 29(1): p. L1-L4.
9. Harman, T.C., et al., *Quantum dot superlattice thermoelectric materials and devices.* Science, 2002. 297(5590): p. 2229-2232.

10. Orihashi, M., et al., *Carrier concentration dependence of thermal conductivity of iodine-doped n-type PbTe.* Mater. Trans. JIM, 2000. 41(10): p. 1282-1286.

11. Rogacheva, E.I., et al., *Effect of oxidation on the thermoelectric properties of PbTe and PbS epitaxial films.* Appl. Phys. Lett., 2001. 78(12): p. 1661-1663.

12. Yoneda, S., et al., *Grain size effect on thermoelectric properties of PbTe prepared by spark plasma sintering*. Mater. Trans. JIM, 2001. 42(2): p. 329-335.

13. Zhu, P.W., et al., *Thermoelectric properties of PbTe prepared at high pressure and high temperature*. J. Phys.-Condes. Matter, 2002. 14(44): p. 11185-11188.

14. Boschetti, C., et al., *Molecular beam epitaxial growth of PbTe and PbSnTe on Si(100) substrates for heterojunction infrared detectors*. 2001. 42(2): p. 91-99.

15. Rudakov, V.I. and I.M. Smirnov, *Forming PbTe on Si-substrates for IR sensor*s. Journal De Physique Iv, 2002. 12(PR3): p. 75-78.

16. Ugai, Y.A., et al., *Electrical properties of thin PbTe films on Si substrates*. Inorg. Mater., 2000. 36(5): p. 449-453.

17. Zimin, D., K. Alchalabi, and H. Zogg, *Heteroepitaxial PbTe-on-Si pn-junction IR-sensors: correlations between material and device properties.* Physica E, 2002. 13(2-4): p. 1220-1223.

18. Wise, F.W., *Lead salt quantum dots: the limit of strong quantum confinement*. acr, 2000. 2000(33): p. 773-780.

19. Dresselhaus, M.S., *Thermoelectric figure of merit of a one-dimensional conductor*. Physical Review, 1993. - 47(- 24): p. 634.

20. Khitun, A., et al., *Enhancement of the thermoelectric figure of merit of Si1-xGex quantum wires due to spatial confinement of acoustic phonons*. Physica E: Low-dimensional Systems and Nanostructures, 2000. 8(1): p. 13-18.

21. Wu, H.Z., et al., *Observation of phonon modes in epitaxial PbTe films grown by molecular beam epitaxy*. Journal of Applied Physics, 2007. 101(10).

22. Barros, A.S., et al., *Characterization of PbTe p-n(+) junction grown by molecular beam epitaxy*. Brazilian Journal of Physics, 2004. 34(2B): p. 641-643.

23. Zhang, B., J. He, and T.M. Tritt, *Size-selective high-yield growth of lead telluride (PbTe) nanocrystals using a chemical vapor deposition technique*. Applied Physics Letters, 2006. 88(4).

24. Ferreira, S.O., et al., *AFM characterization of PbTe quantum dots grown by molecular beam epitaxy under Volmer-Weber mode*. J. Cryst. Growth, 2001. 231(1-2): p. 121-128.

25. Dauscher, A., et al., *Temperature-dependant growth of PbTe pulsed laser deposited films on various substrates*. Thin Solid Films, 2006. 497(1-2): p. 170-176.

26. Jacquot, A., et al., *Pulsed laser deposition of PbTe films on glass substrates*. Appl. Phys. A-Mater. Sci. Process., 1999. 69: p. S613-S615.

27. Belyansky, M.P., A.M. Gaskov, and A.V. Strelkov, *Chalcogen Interdiffusion in PbSe/PbTe Heterostructures*. 1992. 15(1): p. 78-81.

28. Scanlon, W.W., *Precipitation of Te and Pb in PbTe Crystals*. Physical Review, 1962. 126(2): p. 509-&.

29. Ivanova, Y.A., D.K. Ivanou, and E.A. Streltsov, *Electrochemical deposition of PbTe onto n-Si(100) wafers*. 2007. 9(4): p. 599-604.

30. Saloniemi, H., et al., *PbTe electrodeposition studied by combined electrochemncial quartz crystal microbalance and cyclic voltammetry*. JEC, 2000. 482: p. 139-148.

31. Li, W.-J. and K.-L. Hsueh, *Study of electrodeposition of bismuth telluride by voltammetric methods and in-situ electrochemical quartz crystal microbalance method*. Thin Solid Films, 2007. 515(20-21): p. 7847-7854.

32. Kim, J.Y., Y.-G. Kim, and J.L. Stickney, *Copper Nanofilm Formation by Electrochemical Atomic Layer Deposition. Ultrahigh-Vacuum Electrochemical and In Situ STM Studies.* Journal of the Electrochemical Society, 2007. 154(4): p. D260-D266.

33. Vaidyanathan, R., et al., *Preliminary studies in the electrodeposition of PbSe/PbTe superlattice thin films via electrochemical atomic layer deposition (ALD).* Langmuir, 2006. 22(25): p. 10590-10595.

34. Venkatasamy, V., et al., *Studies of Hg(1-x)CdxTe Formation by Electrochemical Atomic Layer Deposition and Investigations into Bandgap Engineering*. Journal of the Electrochemical Society, 2007. 154(8): p. H720-H725.

35. Colletti, L.P., B.H. Flowers, Jr., and J.L. Stickney, *Formation of thin films of CdTe, CdSe, and CdS by electrochemical atomic layer epitaxy*. Journal of the Electrochemical Society, 1998. 145(5): p. 1442-1449.

36. Kim, J.Y., Y.-G. Kim, and J.L. Stickney, *Copper Nanofilm Formation by Electrochemical Atomic Layer Deposition*. Journal of the Electrochemical Society, 2007. 154(4): p. D260-D266.

37. Kim, Y.-S., et al., *Electrochemical deposition of copper and ruthenium on titanium.* Electrochimica Acta, 2006. 51(25): p. 5445-5451.

38. Lister, T.E., L.P. Colletti, and J.L. Stickney, *Electrochemical formation of CdSe monolayers on the low index planes of Au*. Israel Journal of Chemistry, 1997. 37(2-3): p. 287.

39. Muthuvel, M. and J.L. Stickney, *Surface chemistry of InP(100) after wet and Electrochemical etching: Is digital etching possible?* J. Electrochem. Soc., 2006. 153(1): p. C67-C73.

40. Oznuluer, T. and U. Demir, *Formation of Bi2S3 thin films on Au(111) by electrochemical atomic layer epitaxy: kinetics of structural changes in the initial monolayers*. Journal of Electroanalytical Chemistry, 2002. 529(1): p. 34-42.

41. Salvietti, E., et al., *Patterned growth of US by combined electrochemical atomic layer epitaxy and microcontact printing techniques*. Electrochimica Acta, 2007. 52(19): p. 6034-6040.

42. Stickney, J.L., *Electrochemical atomic layer epitaxy*. Electroanalytical Chemistry, 1999. 21: p. 75-209.

43. Vaidyanathan, R., J.L. Stickney, and U. Happek, *Quantum confinement in PbSe thin films electrodeposited by electrochemical atomic layer epitaxy (EC-ALE)*. Electrochimica Acta, 2004. 49(8): p. 1321-1326.

44. Venkatasamy, V., et al., *Optimization of CdTe nanofilm formation by electrochemical atomic layer epitaxy (EC-ALE)*. Journal of Applied Electrochemistry, 2006. 36(11): p. 1223-1229.

45. Villegas, I. and P. Napolitano, *Development of a continuous-flow system for the growth of compound semiconductor thin films via electrochemical atomic layer epitaxy*. Journal of the Electrochemical Society, 1999. 146(1): p. 117.

46. Kolb, D.M., *Physical and Electrochemical Properties of Metal Monolayers on Metallic Substrates, in Advances in Electrochemistry and Electrochemical Engineering*, H. Gerischer and C.W. Tobias, Editors. 1978, John Wiley: New York. p. 125.

47. Gewirth, A.A. and B.K. Niece, *Electrochemical applications of in situ scanning probe microscopy*. Chem. Rev., 1997. 97: p. 1129-1162.

48. Magnussen, O.M. and R.J. Behm, *Structure and growth in metal epitaxy on low-index Au surfaces - a comparison between solid vertical bar electrolyte and solid vertical bar vacuum interfaces*. Journal of Electroanalytical Chemistry, 1999. 467(1-2): p. 258-269.

49. Moller, F.A., O.M. Magnussen, and R.J. Behm, *In-situ stm studies of cu underpotential deposition on au(100) in the presence of sulfate and chloride anions*. Physical Review B-Condensed Matter, 1995. 51(4): p. 2484-2490.

50. Colletti, L.P. and J.L. Stickney, *Optimization of the growth of CdTe thin films formed by electrochemical atomic layer epitaxy in an automated deposition system.* Journal of the Electrochemical Society, 1998. 145(10): p. 3594.

51. Flowers, J., Billy H., et al., *Atomic layer epitaxy of CdTe using an automated electrochemical thin-layer flow deposition reactor*. Journal of Electroanalytical Chemistry, 2002. 524-525: p. 273-285.

52. Forni, F., et al., *Electrochemical aspects of CdTe growth on the face (111) of silver by ECALE*. Electrochimica Acta, 2000. 45(20): p. 3225-3231.

53. Hayden, B.E. and I.S. Nandhakumar, In situ STM study of CdTe ECALE bilayers on gold. Journal of Physical Chemistry B, 1998. 102(25): p. 4897.

54. Lay, M.D. and J.L. Stickney, *EC-STM Studies of Te and CdTe Atomic Layer Formation from a Basic Te Solution*. Journal of the Electrochemical Society, 2004. 151(6): p. C431-C435.

55. Muthuvel, M. and J.L. Stickney, *CdTe Electrodeposition on InP(100) via Electrochemical Atomic Layer Epitaxy (EC-ALE): Studies Using UHV-EC*. Langmuir, 2006. 22(12): p. 5504-5508.

56. Varazo, K., et al., *Formation of the first monolayers of CdTe on Au(111) by electrochemical atomic layer epitaxy (EC-ALE): studied by LEED, Auger, XPS, and in-situ STM*. Journal of Electroanalytical Chemistry, 2002. 522(1): p. 104-114.

57. Venkatasamy, V., et al., *Formation of Hg(1-x)CdxTe (MCT) by electrochemical atomic layer epitaxy (EC-ALE)*. ECS Transactions, 2006. 3(5, State-of-the-Art Program on Compound Semiconductors 45 (SOTAPOCS 45) and Wide Bandgap Semiconductor Materials and Devices 7): p. 95-110.

58. Innocenti, M., et al., *CdS and ZnS deposition on Ag(111) by electrochemical atomic layer epitaxy*. Journal of the Electrochemical Society, 2001. 148(5): p. C357-C362.

59. Pezzatini, G., et al., *Formation of ZnSe on Ag(111) by electrochemical atomic layer epitaxy.* Journal of Electroanalytical Chemistry, 1999. 475(2): p. 164-170.

60. Gichuhi, A., B.E. Boone, and C. Shannon, *Electrosynthesized CdS/HgS heterojunctions.* Langmuir, 1999. 15(3): p. 763-766.

61. Oznuluer, T., et al., *Electrochemical atom-by-atom growth of PbS by modified ECALE method.* Chemistry of Materials, 2005. 17(5): p. 935-937.

62. Villegas, I. and J.L. Stickney, *Preliminary studies of gallium arsenide deposition on gold (100), (110), and (111) surfaces by electrochemical atomic layer epitaxy*. Journal of the Electrochemical Society, 1992. 139(3): p. 686-94.

63. Villegas, I. and J.L. Stickney, *Gallium arsenide deposition on the (100) and (110) planes of gold by electrochemical atomic layer epitaxy: a low-energy electron diffraction, Auger electron spectroscopy, and scanning tunneling microscopy study*. Journal of Vacuum Science & Technology, A: Vacuum, Surfaces, and Films, 1992. 10(5): p. 3032-8.

64. Innocenti, M., et al., *Electrochemical behavior of As on silver single crystals and experimental conditions for InAs growth by ECALE*. Journal of Electroanalytical Chemistry, 2001. 514(1-2): p. 75-82.

65. Wade, T.L., et al., *Electrodeposition of InAs*. Electrochemical and Solid-State Letters, 1999. 2(12): p. 616-618.

66. Wade, T.L., et al., *Electrochemical Formation of a III-V Compound Semiconductor Superlattice: InAs/InSb*. JEC, 2001. 500: p. 322-332.

67. Kim, J.Y. and J.L. Stickney, *Electrodeposition of a Tellurium atomic layer on a n-GaAs(100) substrate*. ECS Transactions, 2007. 11(5, State-of-the-Art Program on Compound Semiconductors 47 (SOTAPOCS 47)-and-Wide-Bandgap Semiconductor Materials and Devices 8): p. 145-151.

68. Nicic, I., et al., *Underpotential Deposition of Te Monolayers on Au Surfaces from Perchloric Acid Solution Studied by Chronocoulometry and EQCM*. Journal of Physical Chemistry B, 2002. 106(47): p. 12247-12252.

69. Seo, M. and M. Yamazaki, *Changes in Surface Stress of Gold Electrode during Underpotential Deposition of Pb*. Journal of the Electrochemical Society, 2004. 151(8): p. E276-E281.

70. Zhu, W., et al., *Electrochemical characterization of the underpotential deposition of tellurium on Au electrode*. Electrochimica Acta, 2007. 52(11): p. 3660-3666.

71. Kim, Y.G., et al., *Pb deposition on I-coated Au(111). UHV-EC and EC-STM studies.* Langmuir, 2007. 23(5): p. 2539-2545.

72. Sze, S.M., *Physics of Semiconductor Devices*. 2nd ed. 1981, New York: john Wiley & Sons.

Table 2: Electron Probe Microanalysis (EPMA) Result of 100 cycles of PbTe formed by electrochemical ALD.

PbTe Sample	**Te Atomic %**	**Pb Atomic %**	**Te / Pb Ratio**
Inlet	**17.78**	**17.43**	**1.02**
Middle	**18.03**	**17.68**	**1.01**
Outlet	**18.27**	**17.91**	**1.02**

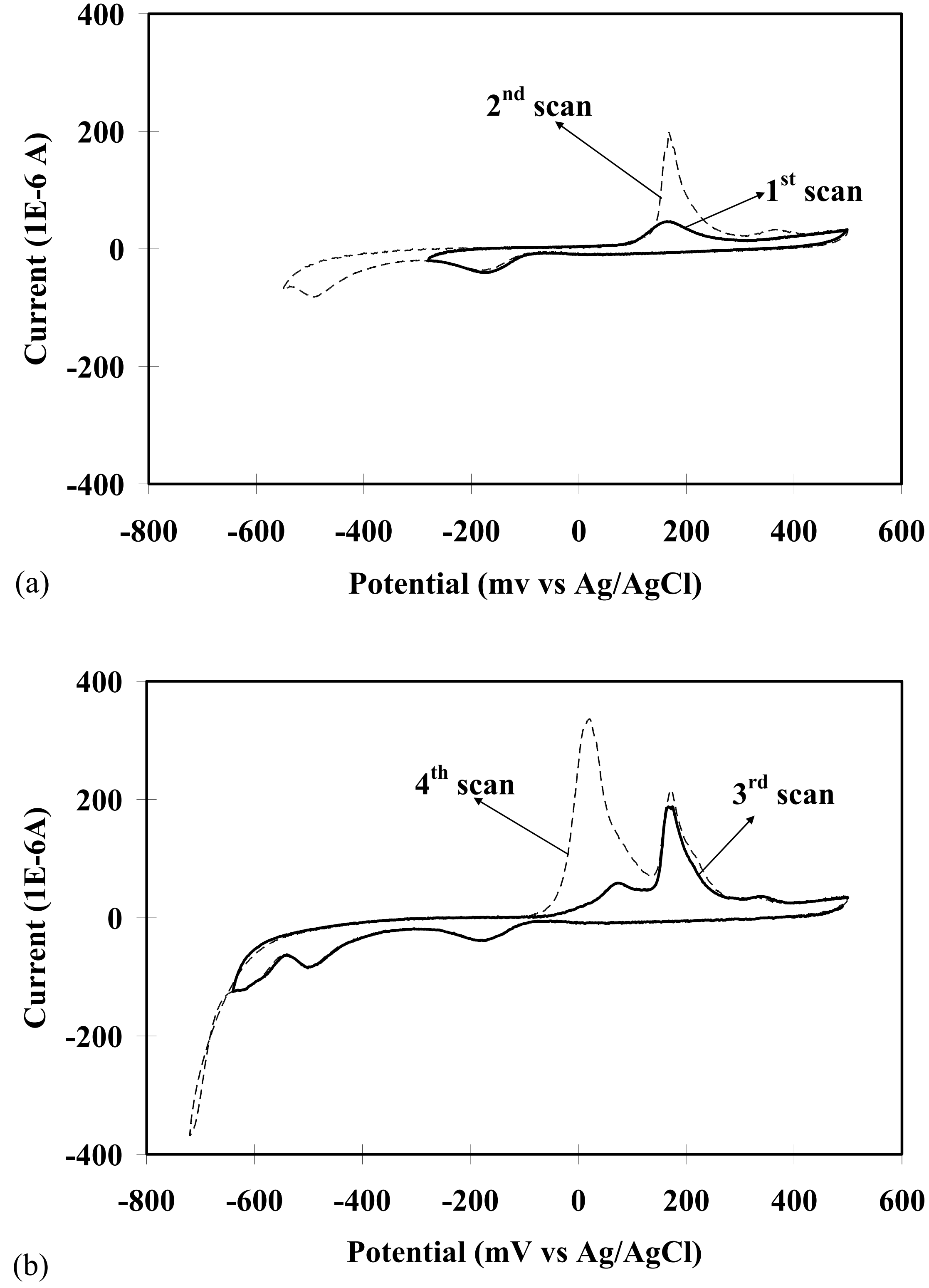

Figure 3.1: Cyclic voltammograms (a) and (b) of Au electrode in 0.5 mM $HTeO_2^+$ to successive decreasing potentials, pH 9.2, (electrode area: 4 cm^2, scan rate: 10 mV s^{-1}).

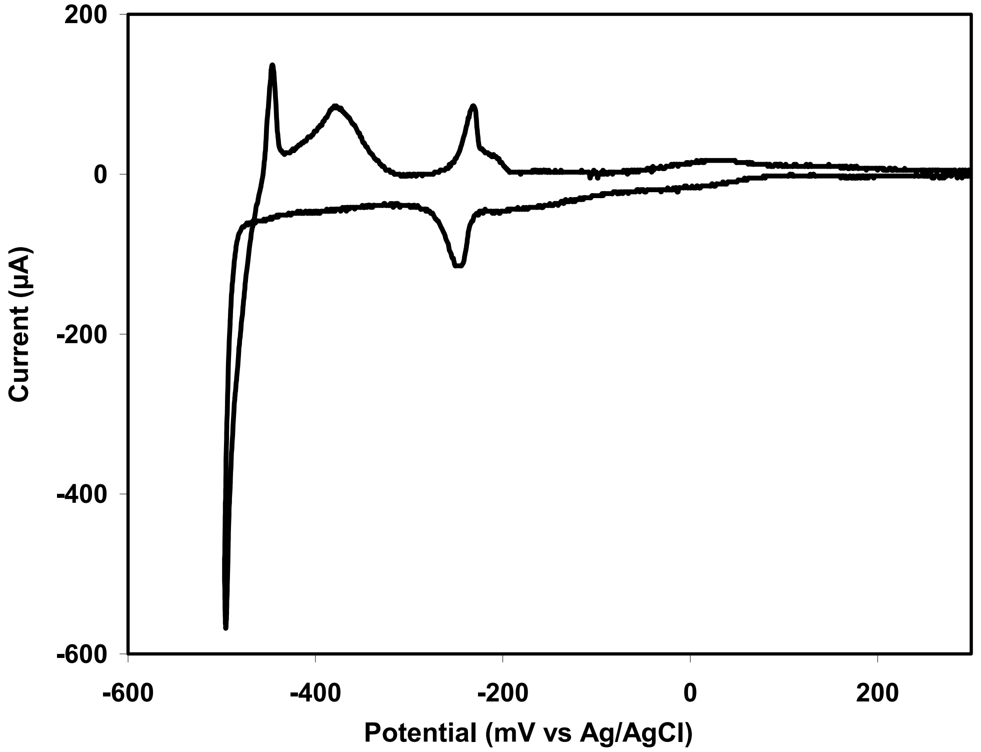

Figure 3.2: Cyclic voltammogram of Au electrode in 0.5 mM Pb^{2+}, pH 3, (electrode area: 4 cm^2, scan rate: 10 mV s^{-1}).

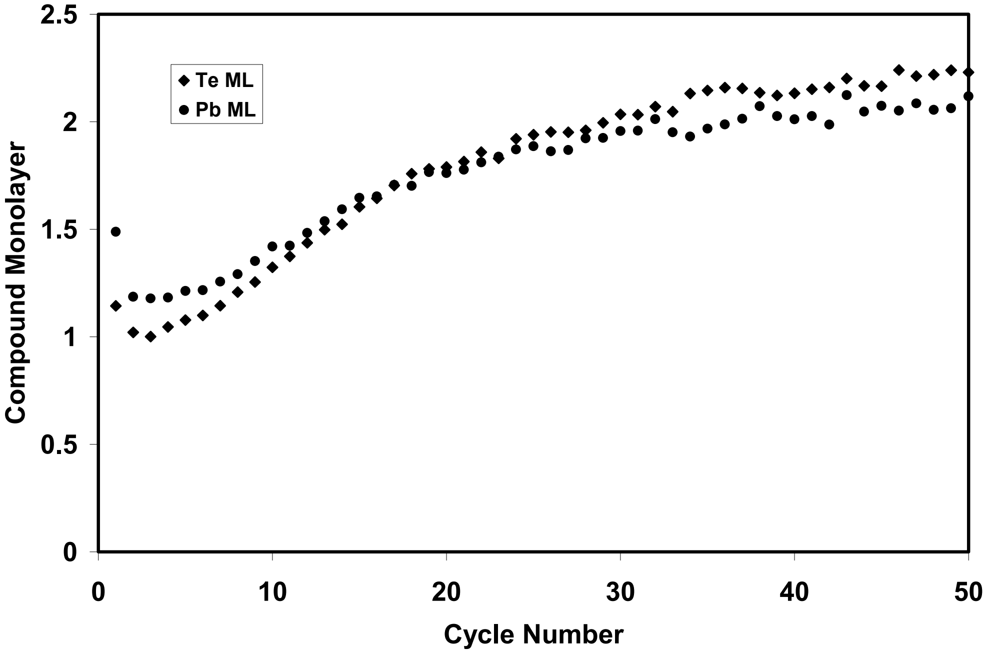

Figure 3.3: Deposition currents (coverage) of 50 cycles of PbTe formed by electrochemical ALD without potential ramp with both Te and Pb held constant at -0.55 V and -0.4 V respectively.

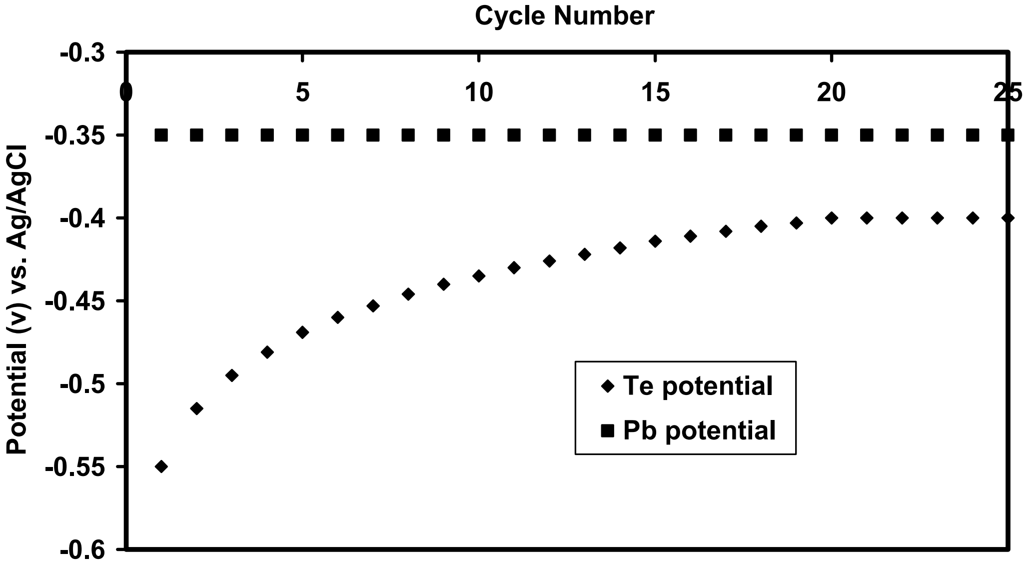

Figure 3.4: Te and Pb deposition potentials vs. cycle number for PbTe formation by electrochemical ALD showing Te potential ramp.

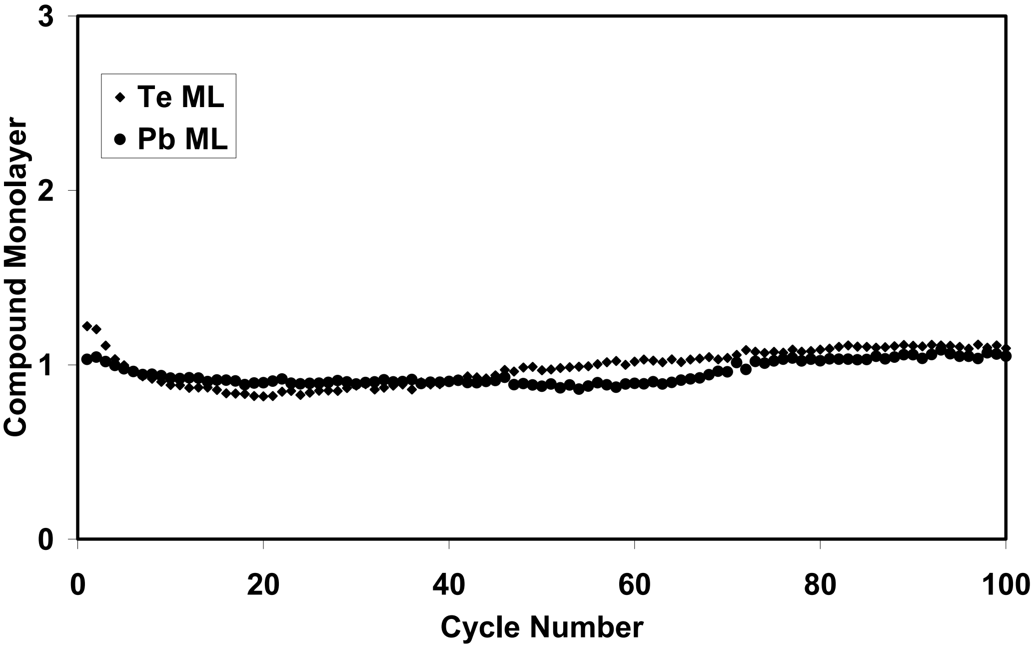

Figure 3.5: Deposition currents (coverage) of 100 cycles of PbTe formed by electrochemical ALD with Te potential ramp from -0.55 V to -0.40 V and a constant Pb potential held at -0.35 V.

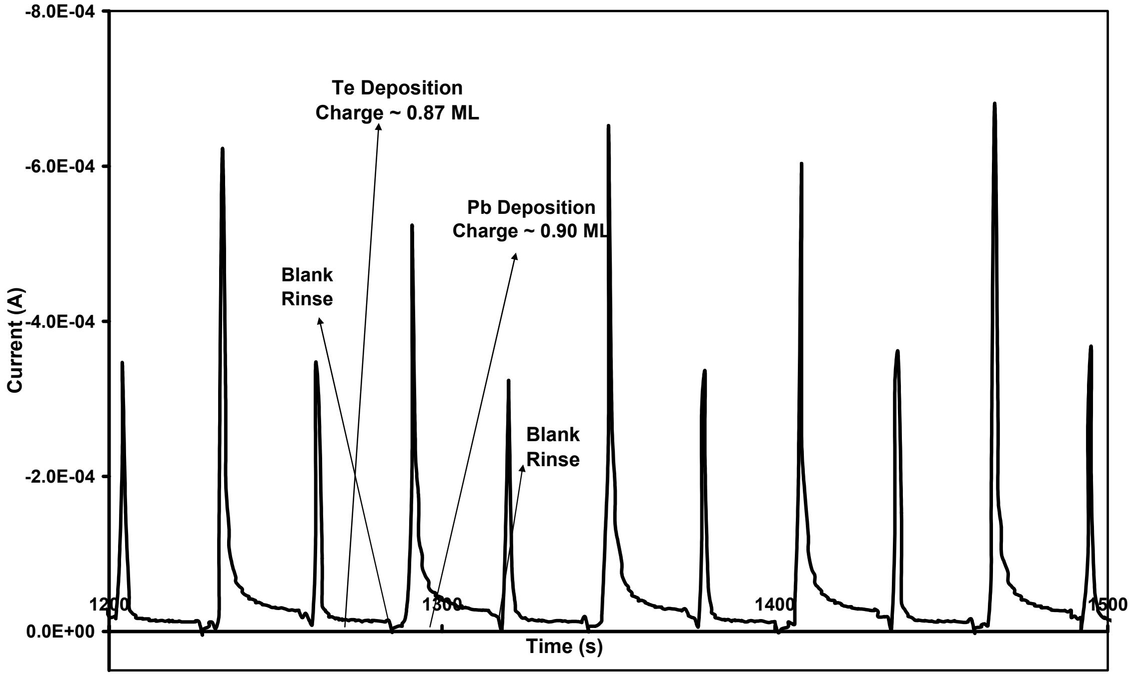

Figure 3.6: Current time traces of 100 cycles of PbTe formed by electrochemical ALD with Te potential ramp from -0.55 V to -0.40 V and a constant Pb potential held at -0.35 V.

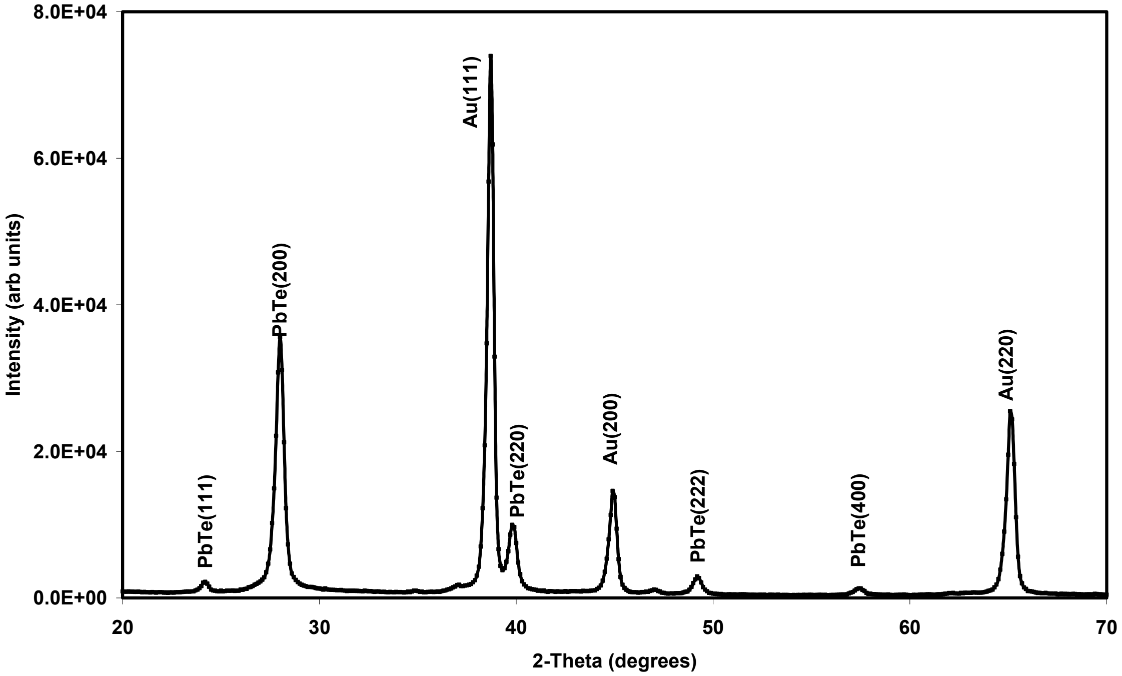

Figure 3.7: X-ray diffraction of 100 cycle electrodeposited PbTe thin film. Angle of incidence is 1°, Cu Kα source.

Figure 3.8: Picture of 100 cycles of PbTe formed by Electrochemical ALD with Te potential ramp from -0.55 V to -0.40 V and a constant Pb potential held at -0.35 V.

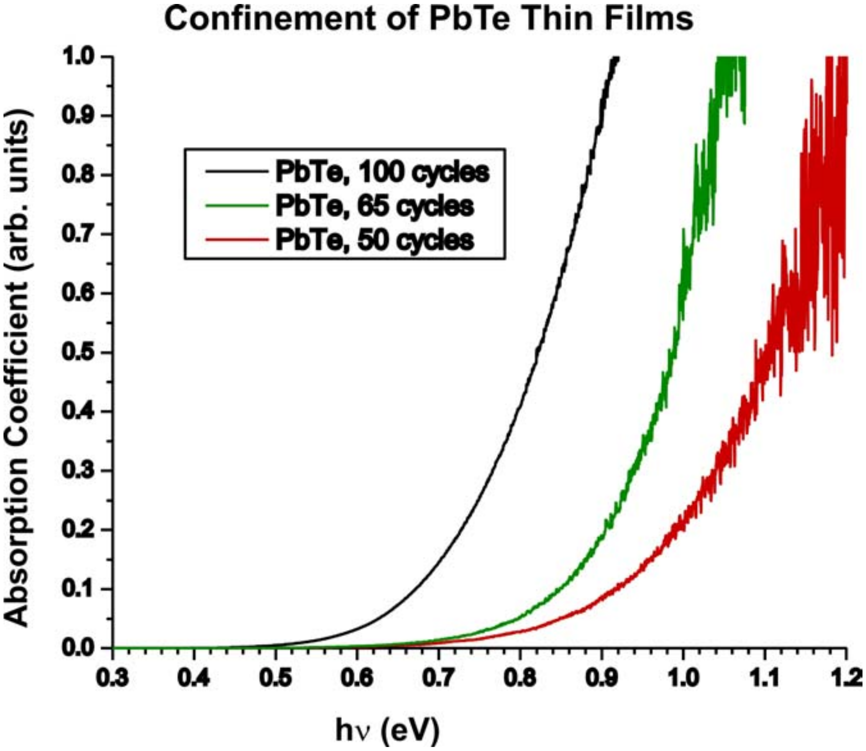

Figure 3.9: Absorption spectra of a) 50 cycle, b) 65 cycle and c) 100 cycle electrodeposited PbTe thin films.

CHAPTER 4

FURTHER STUDIES IN THE ELECTRODEPOSITION OF PbSe/PbTe SUPERLATTICES VIA ELECTROCHEMICAL ATOMIC LAYER DEPOSITION (EC-ALD)[3]

---

[3] Banga, D., et al. To be submitted to Langmuir.

Abstract

This paper reports on further investigation of the formation of PbSe/PbTe superlattices consisting of samples of equal (4:4 superlattice) and unequal (3:15 superlattice) numbers of cycles of PbSe and PbTe within periods using electrochemical atomic layer deposition (ALD). In this case, the superlattices are made by the sequential electrodeposition of Pb, Se and Te atomic layers to form compound monolayers of PbSe and PbTe atomic layers on gold substrates. The period is then repeated as many times as desired to form the superlattice. Deposition potentials for the cycles for PbSe and PbTe of the superlattices are determined from individual studies of their ALD formation. The potential ranges and the current time traces for the deposition cycles of PbSe and PbTe is presented. The coverage based on the deposition charges of each compound of the superlattice in both cases is found to average more or less one monolayer. Adjusting the number of cycles in a superlattice period results in changes in the X-ray diffraction pattern of the superlattice adjacent to (111) peak as will be evidenced by the changes in the positions of the satellite peaks of the (111) Bragg's peak. Deposits are found to be stoichiometric, as determined by the electron probe micro analysis. In addition, the ratio of PbSe and PbTe cycles follows the relative numbers of cycles. Scanning tunneling microscope (STM) indicates that the superlattice thin films are essentially conformal with the Au substrates.

Introduction

Superlattices are examples of nano-structured materials that are defined by their periods, the combined thickness of the two nanofilms to create a new material with a new unit cell [1-2]. The interest in the formation of superlattices stems from the ability to grow artificially nano-structured unit cells produced from two different materials such as compound semiconductors with different bandgaps. In addition, the ability to vary the thickness of the period of a superlattice by changing the number of cycles of the compound semiconductors results in new optical and electronic properties in the superlattices [2]. Another reason behind the interest in superlattices is their enhanced mechanical properties, as they are known to have higher mechanical hardness or tensile strength compared to their alloys [3].

Esaki and Tsu [4] were the first pioneers in the growth of superlattices. Since then, superlattices of various combinations of compound semiconductors have been grown by various methods such as molecular beam epitaxy (MBE) [5], thermal evaporation [6], chemical synthesis [7], codeposition [3] and electrochemical atomic layer deposition (ALD) [1, 8]. Electrochemical ALD has been the method of choice in our group and others [8-11] because it is performed at room temperature and atmospheric pressure, thus limiting interdiffusion in layers of the superlattices. In addition, no annealing has so far been required for the crystal structure of the electrochemical ALD grown thin films to become visible in the X-ray diffraction pattern. As its name entails, the electrochemical atomic layer deposition (ALD) is the electrochemical analog of atomic layer deposition (ALD); a deposition method based on the formation of nanofilms an atomic layer at a time, using surface limited reactions known as underpotential deposition (UPD), a phenomenon where an atomic layer is deposited on the second at a potential prior to that needed to form bulk deposits [12-16].

PbSe and PbTe, well known for their large Bohr radii and the resulting quantum confinement implications, are IV – VI compound semiconductors that are vastly used for their optical and electronic properties in thermoelectric device structures [17-19], infrared sensors [20] and in photovoltaic [21]. We had previously reported preliminary results of the formation of 4:4 and 6:6 PbSe/PbTe superlattices [1] where the presence of satellite peaks were evident in the X-ray diffraction spectra of the formed superlattices although the individual cycles of PbSe and PbTe were not fully optimized. Steady state potentials of -0.3 v for Pb, -0.3 V for Se and -0.4 V for Te were then used for the ALD cycles of the superlattices. However, it was evident during the optimization studies of PbSe [22] and PbTe [23], that the steady potentials chosen for the formation of the superlattice [1] resulted in coverage higher than a monolayer per cycle as the number of the cycles increased. It was then discovered that in order to grow more or less one monolayer during every cycle of the deposition process, ramping the initial few ALD cycles in both PbSe and PbTe was needed [22-23]. In both cases, current time traces were used to determine the coverage during each cycle, which amounted to more or less a monolayer. This paper will report on the superlattices obtained from ALD cycles where ramping of the potentials of Pb, Se and Te are used.

Experimental

An automated thin layer flow electrodeposition system consisting of a series of solution reservoirs, computer controlled pumps, valves, a thin layer electrochemical flow cell and a potentiostat was used in this study to grow PbSe/PbTe superlattices. The reference electrode, Ag/AgCl (3M NaCl) (Bioanalytical systems, Inc., West Lafayette, IN), was held by a simple O-ring and the auxiliary electrode was a Au wire embedded into the Plexiglas flow cell. The electrochemical flow cell was designed to promote laminar flow. The cell volume was about 0.3

mL and solutions were pumped at 50 mL min^{-1}. The system was contained within a nitrogen purged Plexiglas box to reduce the influence of oxygen during electrodeposition.

Substrates used in the study consisted of 300 nm thick vapor deposited gold on glass microscope slides. Prior to insertion into the vapor deposition chamber, the glass slides were cleaned in HF, and rinsed with copious amounts of deionized water from a Nanopure water filtration system (Barnstead, Dubuque, IA), fed from the house distilled water system. Deposition began with 3 nm of Ti, as an adhesion layer, followed by 300 nm of Au deposition at around 250 ^{o}C. The glass slides were then annealed in the deposition chamber at 400 ^{o}C for 12 hours, while the pressure was maintained at 10^{-6} Torr.

Reagent grade or better chemicals and deionized water were used to prepare the three different solutions used in this study. The lead solution consisted of 0.5 mM $Pb(ClO_4)_2$ (Alfa Aesar, Ward Hill, MA), pH 3, with 0.1 M $NaClO_4$ (Fischer Scientific, Pittsburgh, PA) as the supporting electrolyte. The selenium solution was made of 0.5 mM SeO_2 (Alfa Aesar, Ward Hill, MA), pH 5, buffered with 50.0 mM sodium acetate and 0.1 M $NaClO_4$ (Fischer Scientific, Pittsburgh, PA) as the supporting electrolyte. The tellurium solution was made of 0.5 mM TeO_2 (Alfa Aesar, Ward Hill, MA), pH 9.2, buffered with 50.0 mM sodium borate and 0.1 M $NaClO_4$ (Fischer Scientific, Pittsburgh, PA) as the supporting electrolyte. A pH 3 blank solution of 0.1 M $NaClO_4$ (Fischer Scientific, Pittsburgh, PA) was used as well. NaOH and $HClO_4$ (Fischer Scientific, Pittsburgh, PA) were used to adjust the pH values of all the solutions in this study.

The electrochemical ALD cycle program used to grow PbSe consisted of the following: the Se solution was flushed in to the cell for 2 s at the chosen potential, and then held quiescent for 15 s for deposition. The blank solution was then flushed through the cell at the same potential for 3 s, to rinse out excess $HSeO_3^-$ ions. The Pb solution was then flushed through the cell for 2 s at the Pb deposition potential, and held quiescent for 15 s for deposition. Blank solution was again flushed through the cell for 3 s to rinse out excess Pb^{2+} ions from the cell. This process was referred to as one cycle, and was repeated as many times as needed to form PbSe cycles of the superlattices described in this paper. Whereas the electrochemical ALD cycle program used to form PbTe consisted of the following: the Te solution was flushed in to the cell for 2 s at the chosen potential, and then held quiescent for 15 s for deposition. The blank solution was then flushed through the cell at the same potential for 3 s, to rinse out excess $HTeO_2^+$ ions. The Pb solution was then flushed through the cell for 2 s at the Pb potential, and held quiescent for 15 s for deposition. Blank solution was again flushed through the cell for 3 s to rinse out excess Pb^{2+} ions from the cell. This process was referred to as one cycle, and was repeated as many times as needed to form PbTe cycles of the superlattices described in this report. The deposition area of Au electrode used in the experiments described in this paper was 4 cm^2.

Microanalyses (EPMA) of the samples were performed with a Joel JXA-8600 electron probe. Glancing angle X-ray diffraction patterns were obtained on a Scintag PAD V diffractometer, equipped with a 6” long set of Soller slits on the detector to improve resolution in the asymmetric diffraction configuration. STM measurements were taken with a Princeton Research Instruments Nanoscope.

Results and Discussions

Cyclic voltammograms of Au on glass electrodes were run in the solutions of Se, Te and Pb prior to devising the ALD program of the superlattices. Figure 1 depicts the cyclic voltammogram for the deposition of Se on the Au on glass substrate. Distinct reduction features are visible at 0.6 V, 0.1 V and -0.25 V, with a sharp increase in reduction current at -0.45 V which corresponds to Se reduction to selenide and hydrogen evolution. We had previously demonstrated [22] that only the oxidative feature at 0.6 V, positive of the formal potential, was present when the scan was reversed at potential values between -0.025 V and -0.3 V. When the scan was reversed at potential values more negative than -0.3 V, the oxidative feature just positive of 0.4 V appeared. Selenium deposition is known to be kinetically slow [24-26]. Because of the slow kinetics, the reductive peaks occurring from 0.1 V to -0.3 V exhibit characteristics of surface limited deposition although they appear negative of the formal potential 0.4 V of HSO_3^-/Se. The oxidative peak at 0.4 V could be attributed to the oxidation of bulk Se. Based on previous Se studies, the increase in reductive spike around -0.5 V is due to a combination of the following three different processes: bulk Se deposition, hydrogen evolution and Se reduction to Se^{-2}, a soluble species [24, 26-27].

Figure 2 shows the cyclic voltammogram of Au on glass electrode in Te solution. As was the case for Se in Figure 1, all the reductive features observed at -0.17 V, -0.40 V and -0.60 V attributed to Te occur at over potential, as they appear negative of the formal potential of around -0.05 V. Once again, the reason for this behavior is attributed to the slow kinetics of $HTeO_2^+$ reduction to Te, a known behavior in chalcogenides [24, 26-29]. In our previous publication [23], we showed that when the scan was reversed all the way up to -0.55 V, the only oxidative feature present was positive of 0.10 V and displayed all the characteristics of surface limited deposition. Whereas a new oxidative feature corresponding to bulk oxidation of Te is observed at around -0.05 V with a peak near 0.05V, when the scan was reversed at potentials negative of -0.55 V, thus clearly differentiating it from the stripping of the surface limited Te seen positive of 0.10 V. The sharp increase observed around -0.70 V could be attributed to hydrogen evolution, more bulk Te deposition and the reduction of Te to Te^{2-}, a soluble species as the bulk Te oxidative peak at -0.05 V became larger when the scan was reversed from -0.7 V, whereas the surface limited Te peak positive of 0.10 V stayed the same.

Figure 3 represents the cyclic voltammogram of Au on glass electrode in Pb^{2+} solution. Two major reductive features at around -0.25 V and -0.47 V are observed as the scan is reversed at -0.50 V, while three distinct oxidative peaks are evident at -0.45 V, -0.38 V and -0.22 V. The negative going scan starting at 0.25 V with a peak at -0.25 V is characteristic of the reversible Pb^{2+} UPD on Au electrode as reported elsewhere [30-34]. The reduction peak at -0.47 V is attributed to bulk Pb deposition as its corresponding oxidative peak at -0.45 V and a hysteresis suggesting nucleation and growth are visible in Figure 3. The broad oxidative peak observed in the positive going scan at -0.38 V is due to Pb oxidation from Pb/Au alloy [35].

As was the case for the ALD cycle deposition program of PbTe [23] and PbSe [22], using constant UPD potentials of the elements to grow the superlattices resulted in coverage of more than a monolayer per cycle for each element. In this case, surface roughening occurred as the resulting deposits appeared overgrown and not homogeneous when inspected using the optical microscope. The charges due to the deposition of Se, Te and Pb appeared all to increase from cycle to cycle within each period of the superlattice. The reasons for the increased charges have so far been attributed to a drop of some of the applied potentials across a growing space charge layer or Schottky barrier between Au electrode and the growing superlattice [36-37]. It may also be due to deposition and growth kinetics as similar trends have been frequently observed in gas phase ALD studies [38-39].

4:4 Superlattice. In our preliminary work [1], steady-state potentials of -0.3 V for Pb, -0.3 V for Se, and -0.4 V for Te were used to grow a 81 period-superlattice made of 4 PbSe and 4 PbTe cycles formed on an initial prelayer of 10 atomic layers of PbSe. Since then, extensive optimization studies of individual thin films of PbSe [22] and PbTe [23] were carried out. It was discovered that potential ramping of the first few ALD cycles was required prior to steady-state potentials in both cases in order for the coverage of more or less a monolayer per cycle to be maintained throughout the deposition time. For the optimized PbSe, -0.3 V and -0.25 V were chosen as initial potentials for Se and Pb respectively and were both stepped over 20 cycles to a steady state value of -0.04 V, which was used for the remaining cycles of the deposit. This program resulted in the most consistent, stoichiometric and homogeneous PbSe deposits. In case of PbTe, a successful sequence for the growth of PbTe was obtained when the Pb potential was maintained at -0.35 V throughout the deposition time, whereas the potential for the deposition of Te was stepped from -0.55 V to -0.40 V over the first 20 cycles and maintained at -0.40 V for the remainder of the 100 cycle-runs.

Based on the cyclic voltammograms in Figures 1 to 3, and the optimization studies of PbSe and PbTe thin films mentioned in the previous paragraph, various experiments consisting of potential ramping were attempted for the growth of 4PbSe/4PbTe superlattices. To minimize the stress between the superlattice and the polycrystalline Au electrode due to the lattice mismatch, a prelayer consisting of 20 cycles of PbSe was first grown on the Au electrode based on the optimized ALD program of PbSe prior to the superlattice growth. Figures 4 and 5 depict the successful deposition potential ranges of PbSe and PbTe cycles respectively within the period of the superlattice. For PbSe cycles, the initial potential of -0.15 V for both Pb and Se was ramped up over 4 cycles to -0.13 V and -0.12 V for Se and Pb respectively. For PbTe cycles, Te initial potential of -0.38 V was ramped down over 4 cycles to -0.40 V, whereas Pb potential was ramped over 4 cycles from -0.33 V to -0.35 V. This superlattice ALD program resulted in the desired coverage of near one monolayer (ML) / cycle as shown in Figures 6, 7, 8, and 9 depicting the coverage in compound ML from coulometry of the individual cycles of PbSe and PbTe within a period and all 15 periods of the superlattice. In these figures, charges are displayed in monolayers (ML), where a monolayer is defined as one depositing atom, or $1.35X10^{15}$ atoms/cm^2, assuming the geometric area of the substrate is composed of Au(111), hexagonal surface of the fcc Au. Although our Au substrate is not (111) single crystal, some roughening is expected as compared to the atomically flat (111) surface. However since our substrate is predominantly Au(111), such numbers provide an estimation of the relative amounts of the depositing elements. Figure 7 depicting the ML coverage of PbSe cycles of the 5th period, both Pb and Se coverage were essentially constant at around one ML/cycle. Similar trends were observed for PbSe cycles of the other periods of the superlattices as proven by the average coverage of PbSe cycles of all the 15 periods of superlattice observed in Figure 6 which clearly shows the coverage of around one ML/period all throughout the superlattice deposition run. Figure 9 shows the compound ML coverage of PbTe of the 5th period of the superlattice. The first cycle of PbTe at the interface with PbSe seemed to result in coverage of more than a monolayer compared to the last three cycles of the period, whereas the remaining cycles are nearly a ML. Similar trends were observed by Zhu W. et al. [40] when they grew Bi_2Te_3/Sb_2Te_3 superlattice. They had noticed that at the interface of the unit cells of Bi_2Te_3 and Sb_2Te_3, the current time traces of the first 2-3 cycles looked different from the remaining cycles of the period; the cause of which they attributed to the lattice mismatch between the two compounds. This could explain why the first PbTe cycle in the 5th period resulted in coverage of more than a ML, as PbSe and PbTe have lattice constants of 6.460Ǻ and 6.124Ǻ respectively, and thus a significant mismatch of 6%. However, the average coverage of the PbTe cycles for all the periods of the deposit were found to also be near one compound ML/period as observed in Figure 8.

When observed under the optical microscope, the resulting superlattice deposit appeared homogeneously well distributed, as confirmed by the EPMA data shown in Table 3, where nearly stoichiometric deposit was obtained, although slightly rich in chalcogenides. Film composition of **$Pb_{49}Se_{31}Te_{20}$** and the ratio of the sum of Se and Te to Pb of around **1.06** were obtained. As expected, the higher amounts of Pb and Se are due to the 20 cycle-prelayer of PbSe that was grown prior to growing the superlattice.

Figure 10 displays the as-deposited glancing angle (1^o from the sample plane) X-ray diffraction (XRD) patterns of the 15 period 4PbSe/4PbTe superlattice. The best evidence for a superlattice is the presence of symmetric satellites around the Bragg reflection in X-ray diffraction due to the artificially imposed periodicity in superlattices [2]. The satellite peaks show the crystallographic coherence of the deposited multilayers and confirm the superlattice structure of the electrodeposited film [41-43]. In Figure 10, symmetric shoulders corresponding to satellite peaks are readily seen around the (111) Bragg diffraction peak at 24.3^o and around the (220) Bragg diffraction peak at 40.8^o. The modulation wavelength of the superlattice based on the XRD was found to be around 4.5 nm, whereas the charge based period thickness was estimated to be around 4.0 nm.

3:15 Superlattice. Another superlattice consisting of unequal number of cycles of PbSe and PbTe was then grown using the same deposition potential ranges in Figures 4 and 5. In this case, a deposit of 15 periods of 3 PbSe and 15 PbTe cycles was grown using electrochemical ALD on 20 cycles PbTe prelayer on Au substrate. Figures 11 and 12 depict the average compound ML coverage of the PbSe and PbTe respectively, which resulted once again to coverage of near one compound ML/period similar to the coverage obtained in the previous case of 15P/4PbSe/4PbTe, further confirming the successful ALD potential ranges in Figures 4 and 5.

Upon inspection under the optical microscope, the resulting superlattice deposit appeared homogeneous all throughout the deposit. Table 3 displays the EPMA data of the deposit made of 15 periods of 3 cycles of PbSe and 15 cycles of PbTe, where once again nearly stoichiometric deposit was obtained. Film composition of $\mathbf{Pb_{49}Se_{10}Te_{41}}$ and the ratio of the sum of Se and Te to Pb of around **1.04** were obtained. The higher amounts of Pb and Te are due to the 20 cycle-prelayer of PbTe that was grown on the Au electrode prior to growing the superlattice and the higher number of PbTe cycles in the superlattice.

The XRD pattern of the 3PbSe/15PbTe superlattice was taken as shown by Figures 13 (a) and (b). Once again, the presence of satellite peaks around the (111) Bragg diffraction peak is visible in Figure 13, thus attesting to the well resolved interfaces between PbSe and PbTe of the superlattice. Adjustment of the number of PbSe and PbTe cycles within the period resulted in the expected changes in the position of the satellite peaks in the XRD pattern, when Figure 10 consisting of the superlattice with the shorter modulation wavelength is compared to Figure 13 of the superlattice with longer period thickness. In Figure 13, the distance between the satellites and the (111) Bragg reflection is shorter than the distance in Figure 10. The modulation wavelength of the 3PbSe/15PbTe superlattice based on the XRD was found to be around 8.5 nm, whereas the charge based period thickness was estimated to be around 8.6 nm.

Additional morphological studies of the 3PbSe/15PbTe superlattice were then carried out by Scanning Tunneling Microscopy (STM) as depicted in Figures 15 and 16 which show STM images of Au on glass substrate and 3PbSe/15PbTe superlattice respectively. Grain size of around 200 nm was observed in the image of Au on glass as depicted in Figure 15, whereas much more hexagonal and flatter grain size of around 240 nm is seen in the image of the superlattice in Figure 16, indicating improved crystallinity relative to Au substrate. Steps indicative of the epitaxial nature or layer-by-layer growth nature of the electrochemical ALD process used to form the superlattice are also visible in Figure 16. Roughness (RMS) value of around 4 nm was obtained for both images of Au on glass substrate and the superlattice further indicating that growing the superlattice using the electrochemical ALD did not result in a rougher deposit.

Conclusion

Two different types of PbSe/PbTe superlattices consisting of equal and unequal numbers of cycles were presented in this paper. The coverage of based on the coulometry was found to average one monolayer in both cases due to the optimization of the potential range chosen for the electrochemical ALD program. Electron probe microanalysis characterization determined both deposits to be stoichiometric and the ratio of PbSe and PbTe in the superlattices followed the relative numbers of the cycles. The presence of the satellite peaks was visible in the XRD patterns of both superlattices. In addition, adjusting the number of cycles within a period resulted in changes in the position of the satellite peaks around the (111) peak. Scanning tunneling microscopy indicated that the as-deposited superlattice was essentially conformal with Au on glass substrate and evidence of epitaxial growth was observed in the image of the superlattice deposit as attested by the presence of steps.

Acknowledgements

Support from the National Science Foundation is gratefully acknowledged.

References

1. Vaidyanathan, R., et al., *Preliminary studies in the electrodeposition of PbSe/PbTe superlattice thin films via electrochemical atomic layer deposition (ALD).* Langmuir, 2006. **22**(25): p. 10590-10595.
2. Switzer, J.A., *Electrodeposition of superlattices and multilayers*, in *Electrochemistry of Nanomaterials*, G. Hodes, Editor. 2001, Wiley-VCH: Weinheim. p. 67.
3. Kothari, H.M., et al., *Epitaxial electrodeposition of Pb-Tl-O superlattices on single-crystal Au(100).* Chemistry of Materials, 2002. **14**(6): p. 2750-2756.
4. Esaki, L. and R. Tsu, *Superlattice and negative differential conductivity in semiconductors.* Ibm Journal of Research and Development, 1970. **14**(1): p. 61-&.
5. Abramof, E., et al., *Electrical properties of Pb1-xSnxTe layers with 0<=x<=1 grown by molecular beam epitaxy.* 1997. **82**(5): p. 2405-2410.
6. Caylor, J.C., et al., *Enhanced thermoelectric performance in PbTe-based superlattice structures from reduction of lattice thermal conductivity.* Applied Physics Letters, 2005. **87**(2).
7. Qingbo, Z., et al., *Synthesis of Monodisperse Ag&bond;Au Alloy Nanoparticles with Independently Tunable Morphology, Composition, Size, and Surface Chemistry and Their 3-D Superlattices.* Advanced Functional Materials, 2009. **19**(9): p. 1387-1398.
8. Zhu, W., et al., *Electrochemical atom-by-atom growth of highly uniform thin sheets of thermoelectric bismuth telluride via the route of ECALE.* Journal of Electroanalytical Chemistry, 2008. **614**(1-2): p. 41-48.

9. Oznuluer, T. and U. Demir, *Formation of Bi2S3 thin films on Au(111) by electrochemical atomic layer epitaxy: kinetics of structural changes in the initial monolayers.* Journal of Electroanalytical Chemistry, 2002. **529**(1): p. 34-42.

10. Foresti, M.L., et al., *Ternary CdSxSe1-x deposited on Ag(111) by ECALE. Synthesis and characterization.* Langmuir, 2005. **21**(15): p. 6900-6907.

11. Villegas, I. and P. Napolitano, *Development of a continuous-flow system for the growth of compound semiconductor thin films via electrochemical atomic layer epitaxy.* Journal of the Electrochemical Society, 1999. **146**(1): p. 117.

12. Kolb, D.M., Przasnys.M, and Gerische.H, *Underpotential Deposition of Metals and Work Function Differences.* Journal of Electroanalytical Chemistry, 1974. **54**(1): p. 25-38.

13. Kolb, D.M. and H. Gerisher, *Further aspects concerning the correlation between underpotential depsoition and work function defferences.* SS, 1975. **51**: p. 323.

14. Kolb, D.M., *Physical and Electrochemical Properties of Metal Monolayers on Metallic Substrates*, in *Advances in Electrochemistry and Electrochemical Engineering*, H. Gerischer and C.W. Tobias, Editors. 1978, John Wiley: New York. p. 125.

15. Adzic, R.R., et al., *Electrocatalysis by foreign metal monolayers: oxidation of formic acid on platinum.* JEC, 1975. **65**: p. 587-601.

16. Adzic, R.R., *Electrocatalytic Properties of the Surfaces Modified by Foreign Metal Ad Atoms*, in *Advances in Electrochemistry and Electrochemical Engineering*, H. Gerishcher and C.W. Tobias, Editors. 1984, Wiley-Interscience: New York. p. 159.

17. Harman, T.C., et al., *Quantum dot superlattice thermoelectric materials and devices.* Science, 2002. **297**(5590): p. 2229-2232.

18. Harman, T.C., et al., *Thermoelectric quantum-dot superlattices with high ZT.* 2000. **29**(1): p. L1-L4.

19. Beyer, H., et al., *High thermoelectric figure of merit ZT in PbTe and Bi2Te3-based superlattices by a reduction of the thermal conductivity.* Physica E: Low-dimensional Systems and Nanostructures, 2002. **13**(2-4): p. 965-968.

20. Ueta, A.Y., et al. *IV-VI Compound heterostructures grown by molecular beam epitaxy*. 2002.

21. Nair, P.K. and M.T.S. Nair, *PbS solar control coatings - safety, cost and optimization.* Journal of Physics D-Applied Physics, 1990. **23**(2): p. 150-155.

22. Banga, D., et al., *Optimization of PbSe Nanofilms formation by Electrochemical Atomic Layer Deposition (ALD).* ECS Transactions, 2009. **19**(3): p. 245-272.

23. Banga, D.O., et al., *Formation of PbTe nanofilms by electrochemical atomic layer deposition (ALD).* Electrochimica Acta, 2008. **53**(23): p. 6988-6994.

24. Huang, B.M., T.E. Lister, and J.L. Stickney, *Se adlattices formed on Au (100), studies by LEED, AES, STM and electrochemistry.* Surface Science, 1997. **392**(1-3): p. 27.

25. Lister, T.E., et al., *Electrochemical formation of Se atomic layers on Au(100).* J. Vac. Sci. Technol. B, 1995. **13**: p. 1268.

26. Lister, T.E. and J.L. Stickney, *Atomic level studies of selenium electrodeposition on gold (111) and gold (110).* Journal of Physical Chemistry, 1996. **100**(50): p. 19568-19576.

27. Lister, T.E., et al., *Electrochemical Formation of Se Atomic Layers On Au(100).* Journal of Vacuum Science & Technology B, 1995. **13**(3): p. 1268.

28. Lay, M.D. and J.L. Stickney, *EC-STM Studies of Te and CdTe Atomic Layer Formation from a Basic Te Solution.* Journal of the Electrochemical Society, 2004. **151**(6): p. C431-C435.

29. Flowers, B.H., et al., *Atomic layer epitaxy of CdTe using an automated electrochemical thin-layer flow deposition reactor.* Journal of Electroanalytical Chemistry, 2002. **524-525**: p. 273-285.

30. Kim, Y.-G., et al., *Pb Deposition on I-Coated Au(111). UHV-EC and EC-STM Studies.* Langmuir 2007. **23**(5): p. 2539-45.

31. Bondarenko, A.S., et al., *Potentiodynamic electrochemical impedance spectroscopy of lead upd on polycrystalline gold and on selenium atomic underlayer.* Electrochemistry Communications, 2005. **7**(6): p. 631-636.

32. Conway, B.E. and J.C. Chacha, *Effects of temperature on the states of Pb adatoms underpotentially deposited from various solvents on Au : entropies of adatom states.* Journal of New Materials for Electrochemical Systems, 2004. **7**(3): p. 231-240.

33. Dimitrov, N., R. Vasilic, and N. Vasiljevic, *A Kinetic Model for Redox Replacement of UPD Layers.* Electrochemical and Solid-State Letters, 2007. **10**(7): p. D79-D83.

34. Seo, M. and M. Yamazaki, *Changes in Surface Stress of Gold Electrode during Underpotential Deposition of Pb.* Journal of the Electrochemical Society, 2004. **151**(8): p. E276-E281.

35. Green, M.P. and K.J. Hanson, *Alloy formation in an electrodeposited monolayer.* Surface Science, 1991. **259**(3): p. L743-L749.

36. Vaidyanathan, R., J.L. Stickney, and U. Happek, *Quantum confinement in PbSe thin films electrodeposited by electrochemical atomic layer epitaxy (EC-ALE).* Electrochimica Acta, 2004. **49**(8): p. 1321-1326.

37. Zhu, W., et al., *Optimization of the formation of bismuth telluride thin film by using ECALE.* Journal of Electroanalytical Chemistry, 2005. **585**(1): p. 83-88.

38. Elam, J.W., et al., *Atomic layer deposition of palladium films on Al2O3 surfaces.* Thin Solid Films, 2006. **515**(4): p. 1664-1673.

39. Fabreguette, F.H., et al., *Quartz crystal microbalance study of tungsten atomic layer deposition using WF6 and Si2H6.* Thin Solid Films, 2005. **488**(1-2): p. 103-110.

40. Zhu, W., et al., *Electrochemical aspects and structure characterization of VA-VIA compound semiconductor Bi2Te3/Sb2Te3 superlattice thin films via electrochemical atomic layer epitaxy.* Langmuir, 2008. **24**(11): p. 5919-5924.

41. Switzer, J.A., H.M. Kothari, and E.W. Bohannan, *Thermodynamic to kinetic transition in epitaxial electrodeposition.* Journal of Physical Chemistry B, 2002. **106**(16): p. 4027-4031.

42. Lashmore, D.S. and M.P. Dariel, *Electrodeposited Cu-Ni Textured Superlattices.* JECS, 1988. **135**: p. 1219.

43. Schuller, I.K. and C.M. Falco, *Superconductivity and magnetism in metallic superlattices.* Thin Solid Films, 1982. **90**(2): p. 221-227.

Table 3: Electron Probe Microanalysis (EPMA) Data of 15P:4PbSe:4PbTe and 15P:3PbSe:15PbTe superlattices formed when Se, Te and Pb potentials were ramped. Electrode area: 4 cm^2.

Sample	**15P:4PbTe:4PbSe**	**15P:3PbSe:15PbTe**
Te Atomic %	13.46	33.93
Se Atomic %	20.78	8.67
Pb Atomic %	32.28	40.88
Au Atomic %	33.48	16.52
Film Composition	$Pb_{49}Se_{31}Te_{20}$	$Pb_{49}Se_{10}Te_{41}$
(Te + Se) / Pb	**1.06**	**1.04**

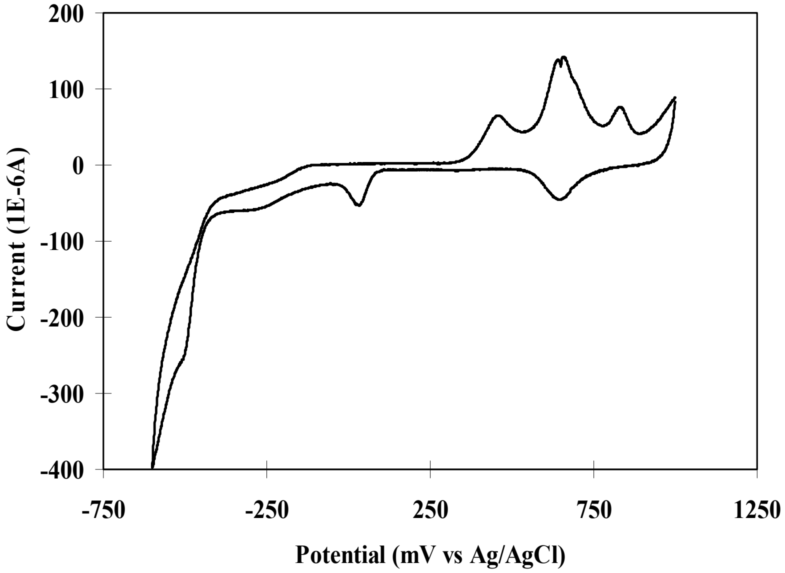

Figure 4.1: Cyclic voltammogram of Au electrode in 0.5 mM $HSeO_3^+$, pH 5, (electrode area: 4 cm^2, scan rate: 10 mV s^{-1}).

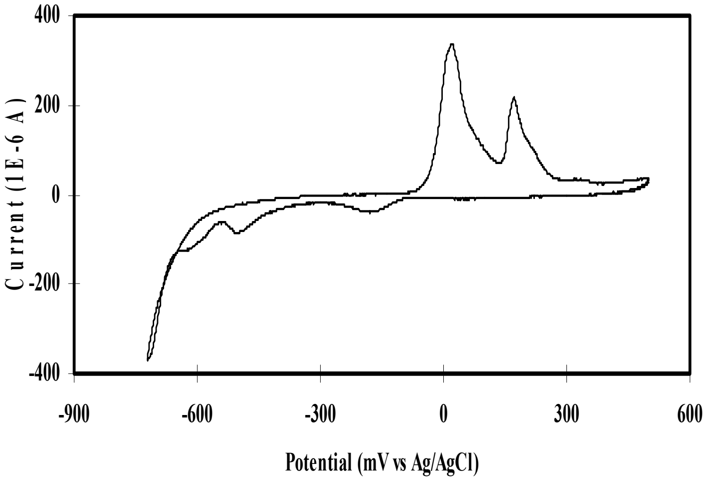

Figure 4.2: Cyclic voltammogram of Au electrode in 0.5 mM $HTeO_2^+$, pH 5, (electrode area: 4 cm^2, scan rate: 10 mV s^{-1}).

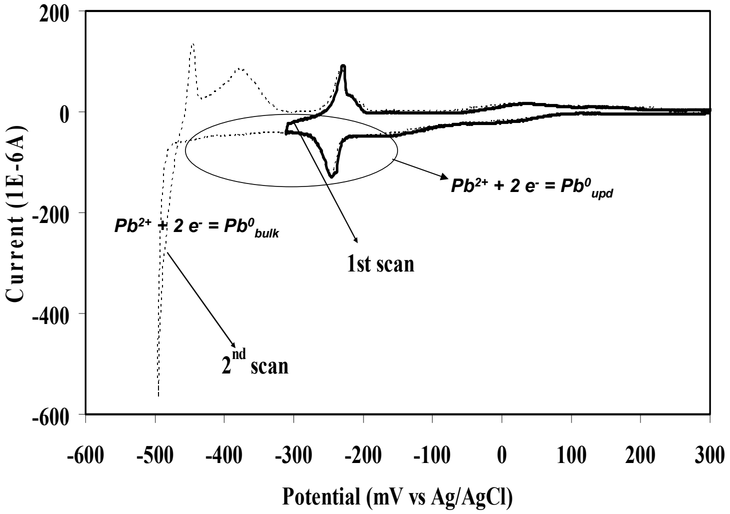

Figure 4.3: Cyclic voltammogram of Au electrode in 0.5 mM Pb^{2+}, pH 3, (electrode area: 4 cm^2, scan rate: 10 mV s^{-1}).

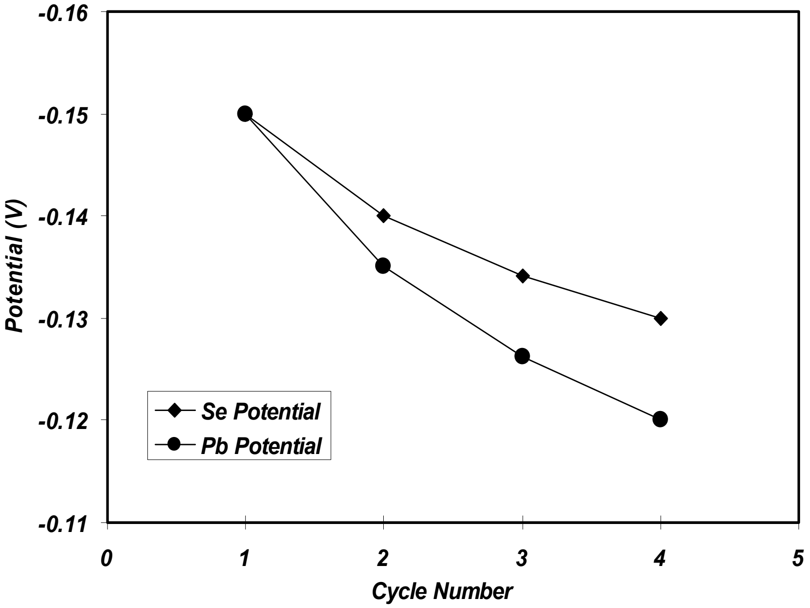

Figure 4.4: PbSe ALD cycle showing Se and Pb deposition potentials of 15P:4PbSe:4PbTe superlattice being shifted positive from -0.15 V to -0.13 V and -0.12 V respectively. Electrode area: 4 cm^2.

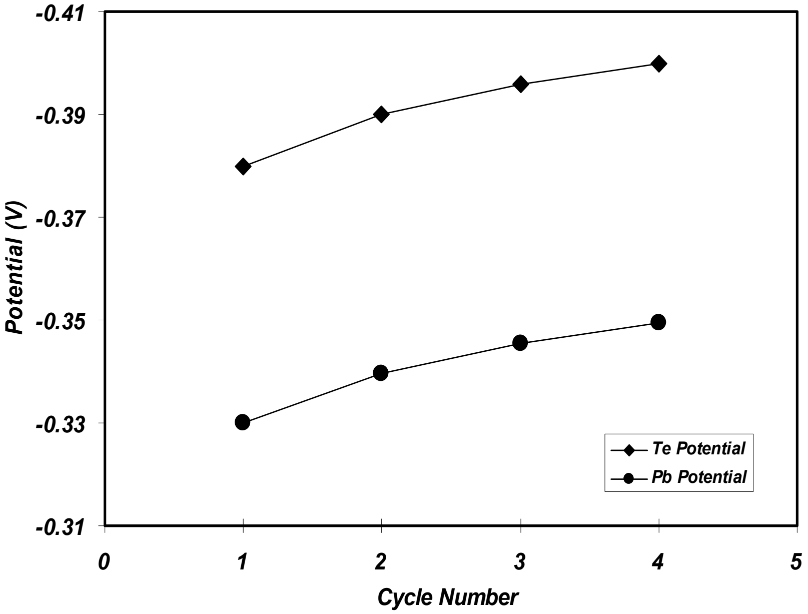

Figure 4.5: PbTe ALD cycle showing Te and Pb deposition potentials of 15P:4PbSe:4PbTe superlattice being shifted negative from -0.38 V to -0.4 V for Te and from -0.33 V to -0.35 V for Pb. Electrode area: 4 cm^2.

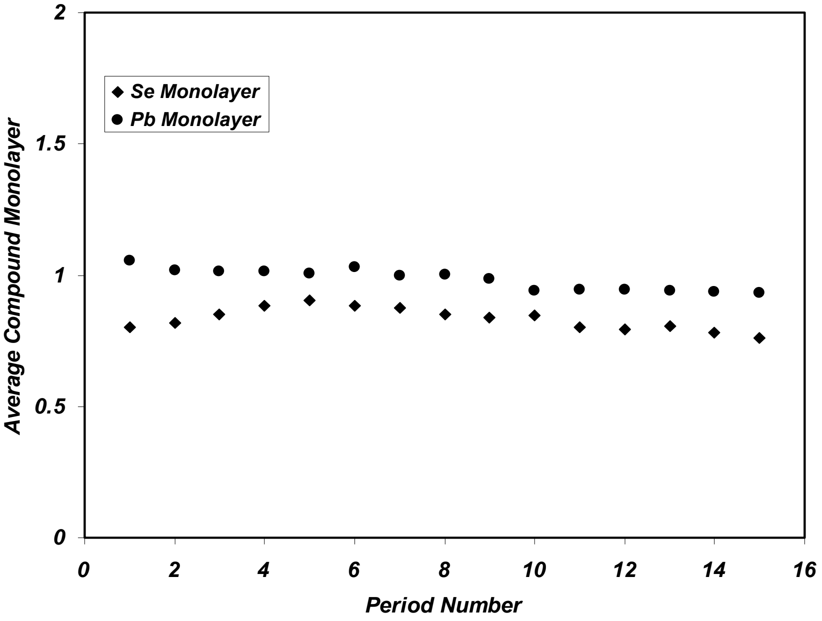

Figure 4.6: Average deposition currents (coverage) of the 15 PbSe ALD periods of 4PbSe:4PbTe superlattice formed when Se, Te and Pb potentials were ramped. Electrode area: 4 cm^2.

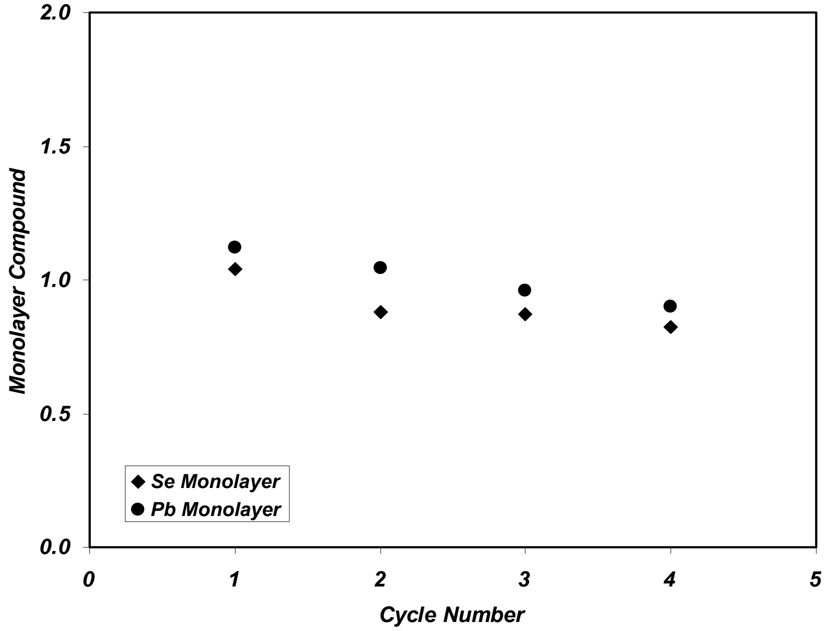

Figure 4.7: Deposition currents (coverage) of PbSe ALD cycles of the 5th period of the 15P:4PbSe:4PbTe superlattice formed when both Se and Pb potentials were ramped. Electrode area: 4 cm^2.

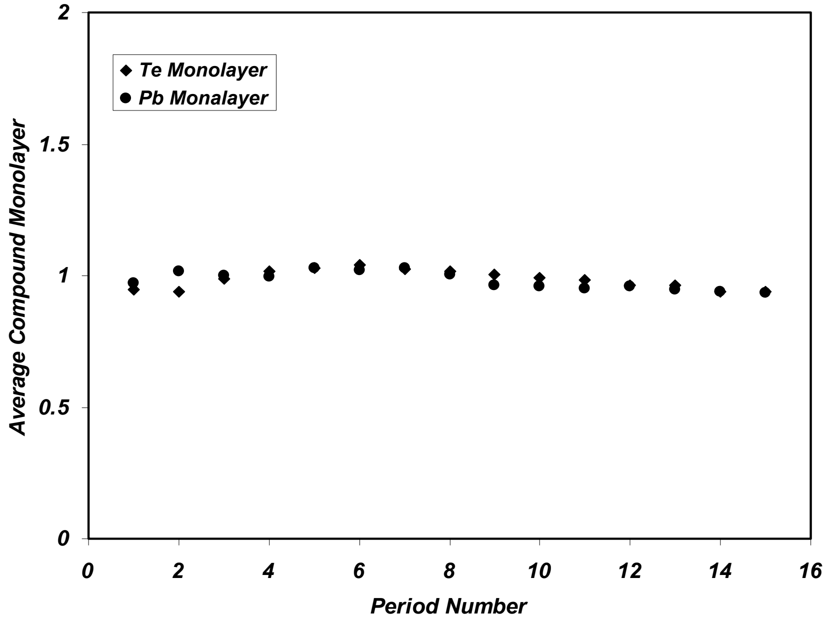

Figure 4.8: Average deposition currents (coverage) of the 15 PbTe ALD periods of 4PbSe:4PbTe superlattice formed when Se, Te and Pb potentials were ramped. Electrode area: 4 cm^2.

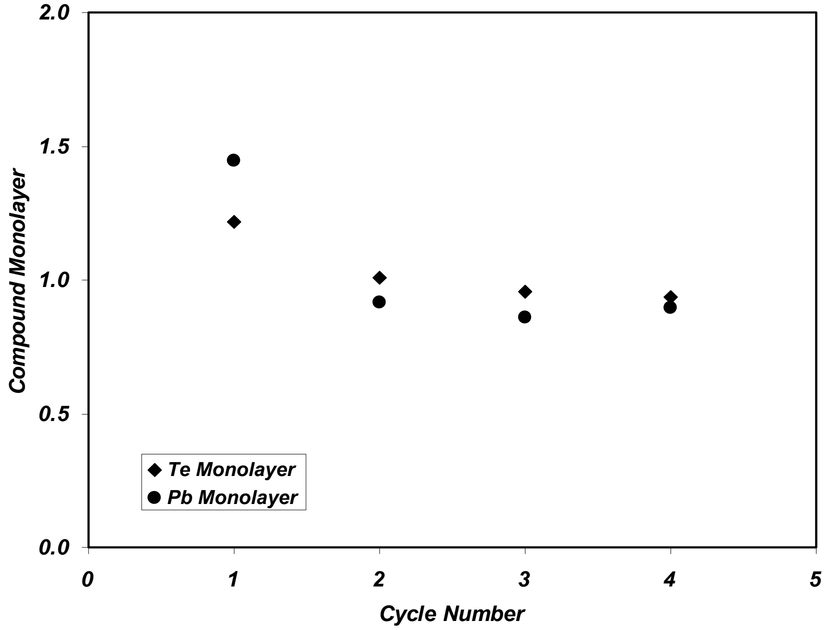

Figure 4.9: Deposition currents (coverage) of PbTe ALD cycles of the 5th period of the 15P:4PbSe:4PbTe superlattice formed when both Te and Pb potentials were ramped. Electrode area: 4 cm^2.

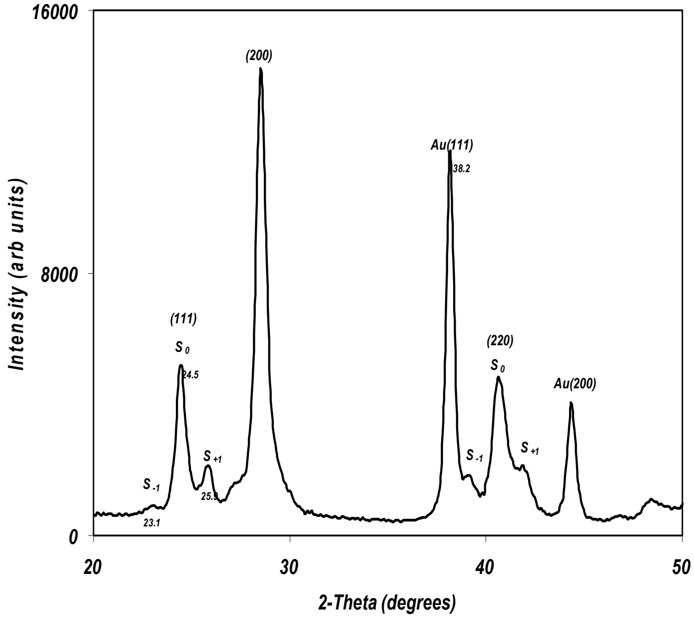

Figure 4.10: X-ray diffraction of 15 ALD periods of 4PbSe:4PbTe superlattice formed when Se, Te and Pb potentials were ramped. Angle of incidence is 1°, Cu Kα source. Electrode area: 4 cm^2.

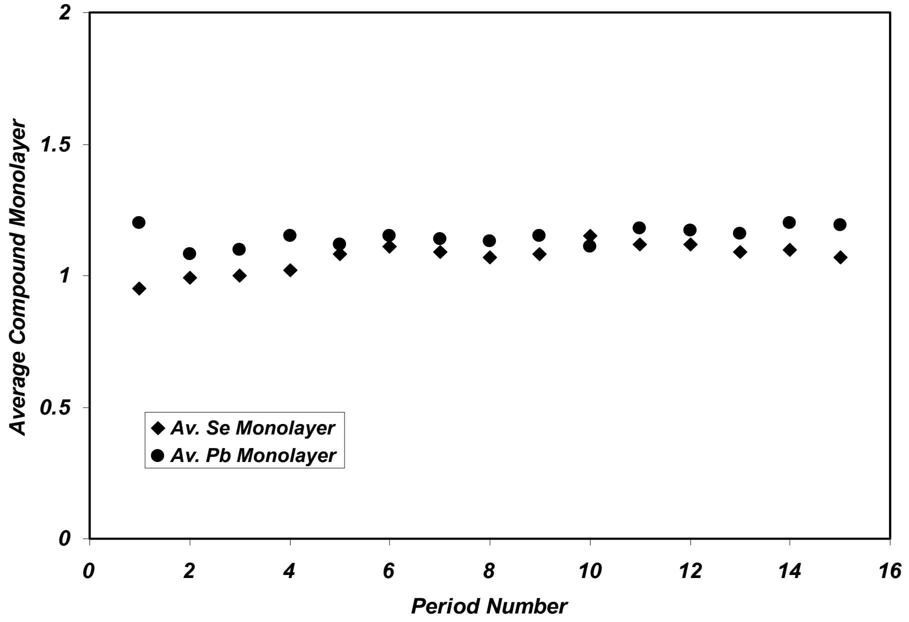

Figure 4.11: Average deposition currents (coverage) of the 15 PbSe ALD periods of 3PbSe:15PbTe superlattice formed when Se, Te and Pb potentials were ramped. Electrode area: 4 cm^2.

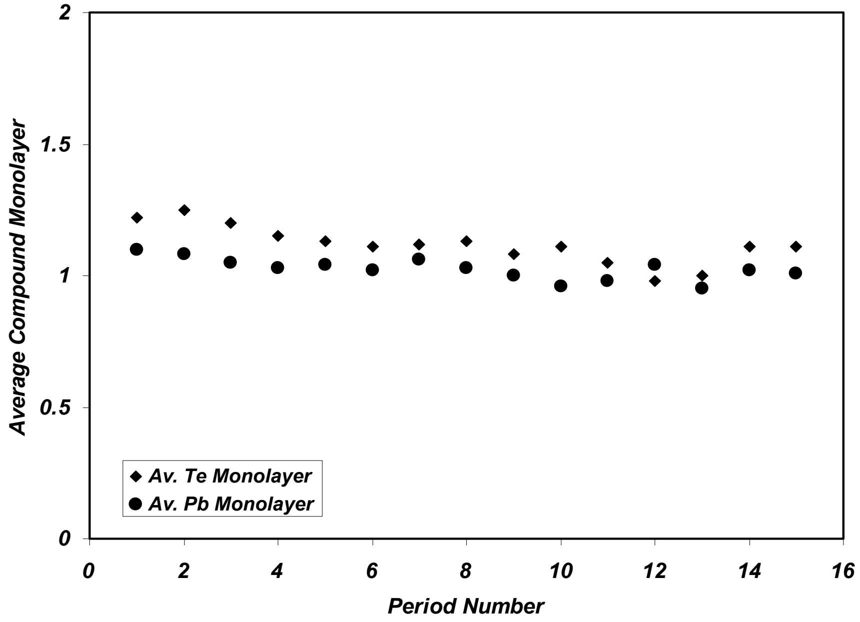

Figure 4.12: Average deposition currents (coverage) of the 15 PbTe ALD periods of 3PbSe:15PbTe superlattice formed when Se, Te and Pb potentials were ramped. Electrode area: 4 cm^2.

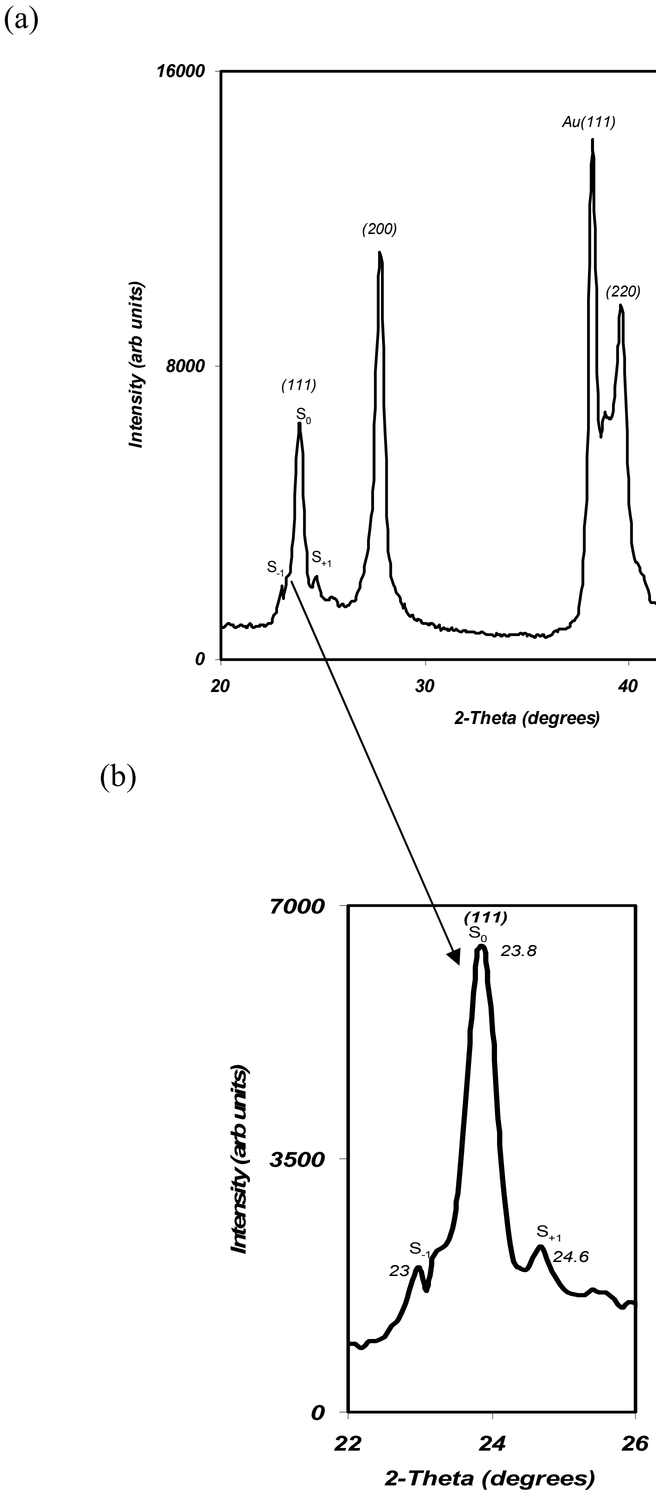

Figure 4.13: X-ray diffraction of 15 ALD periods of 3PbSe:15PbTe superlattice formed when Se, Te and Pb potentials were ramped. Angle of incidence is 1°, Cu Kα source. Electrode area: 4 cm^2.

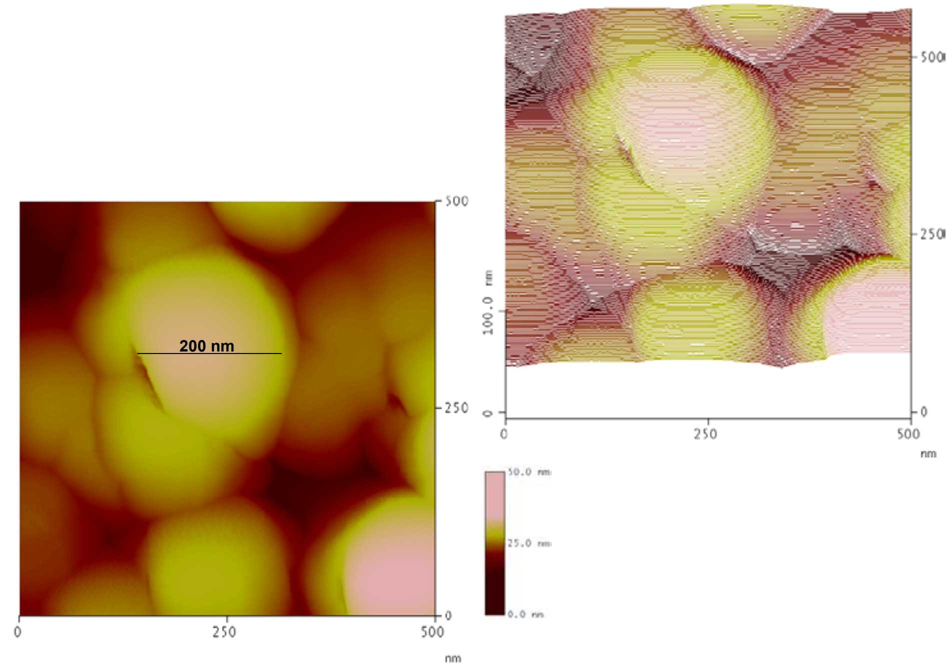

Figure 4.14: STM image of Au on glass substrate (500 nm^2 image). Electrode area: 4 cm^2.

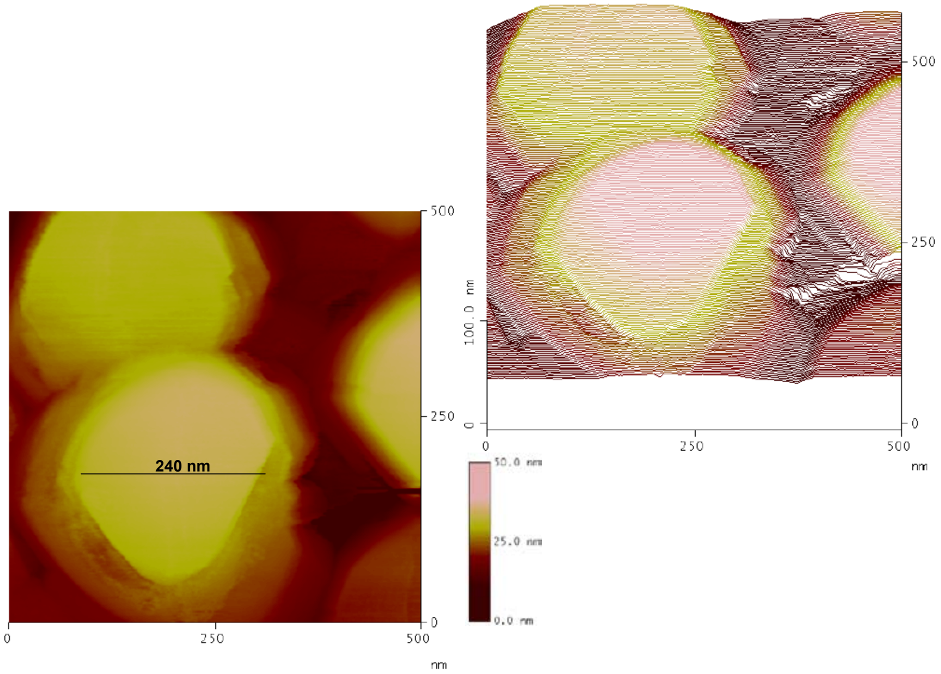

Figure 4.15: STM image of 15P:3PbSe:15PbTe superlattice on Au on glass substrate (500 nm^2 image). Electrode area: 4 cm^2.

CHAPTER 5

ELECTRODEPOSITION OF CdTe AND PbTe/CdTe SUPERLATTICES BY ELECTROCHEMICAL ATOMIC LAYER DEPOSITION (EC-ALD)[4]

---

[4] Banga, D., et al. To be submitted to Langmuir.

Abstract

This article concerns the deposition of a CdTe thin film and a PbTe/CdTe superlattice consisting of 15 periods of 5 cycles of CdTe and 15 cycles of PbTe grown on 15 cycles of PbTe prelayer on Au on glass using electrochemical atomic layer deposition (ALD). In the case of the CdTe thin film, deposition potentials of both Cd and Te are shifted negatively for the first 20 cycles and held constant for the remaining cycles of the deposition process. A stoichiometric and homogeneous CdTe deposit is obtained as the electron probe micro analysis result will show. Peaks corresponding to the cubic phase of CdTe are observed in the XRD pattern of the as-deposited CdTe, with (111) plane being the most predominant one. Optical studies of CdTe reveal a band gap of around 1.45 eV. In the case of PbTe/CdTe superlattice, the period made of the compound monolayers of PbTe and CdTe are repeated 15 times to form the superlattice deposit reported in this paper. Deposition potentials, current time traces and coverages for the deposition cycles of PbTe and CdTe monolayers of the superlattice will be presented. The superlattice is found to be stoichiometric, as determined by the electron probe micro analysis. The X-ray diffraction pattern of the superlattice shows the presence of symmetric shoulders adjacent to (111) peak corresponding to satellite peaks of the (111) Bragg's peak.

Introduction

CdTe, a II-VI compound semiconductor, and PbTe, a IV-VI compound semiconductor, have been extensively studied and grown by various techniques such close sublimation [1], co-evaporation [2], chemical synthesis [3], *rf* sputtering [4], molecular beam epitaxy [5-6], organometallic vapor epitaxy [7], pulse laser deposition [8-10], co-deposition [11-21] and electrochemical atomic layer deposition [22-26], because of their importance in photovoltaic devices, optoelectronic devices, radiation detectors, laser materials, thermoelectric materials, sensors and various other electronic devices [3, 6, 11, 27-28]. CdTe appears to be the semiconductor of choice in photovoltaic and optoelectronic devices because of its high absorption coefficient (> 10^4 cm^{-1}) and an optimum direct band gap (1.5 eV) for the efficient absorption of solar radiation. PbTe, an important thermoelectric material [29] with a rock salt structure, has a narrow band gap (E_g = 0.29 eV) and also a high absorption coefficient (~ 10^{-4} cm^{-1}). The lattice constants of CdTe and PbTe, which are almost identical with a value of 0.648 Ǻ and 0.646 Ǻ for CdTe and PbTe respectively, could favor the growth of a superlattice of the two compound semiconductors as a one of the major requirements in growing superlattices consists in choosing semiconductors with a large difference in band gap between the layers, but a small difference in lattice parameters [30]. The lattice mismatch between the alternating layers is usually chosen to be less than 1% for semiconductor superlattices, although superlattices in systems with larger lattice mismatch could be [30]and have grown [31-32] when the thickness of the alternating layers is kept below a critical thickness. Therefore, the superlattice of CdTe and PbTe could be epitaxially grown because of the low lattice mismatch (~ 0.3 %) between the two compound semiconductors. The formation of PbTe/CdTe have been reported in the literature

[33-43] for probable use a heterosystem for optoelectronic devices [41]. The reported PbTe/CdTe heterosystems were mainly grown by molecular beam epitaxy.

This paper will present the electrodeposition of CdTe thin film and PbTe/CdTe superlattice using electrochemical atomic layer deposition (EC-ALD), which is an electrodeposition technique based on the use of surface limited reactions known as under potential deposition (UPD), a phenomenon where an atomic layer is deposited on the second at a potential prior to that needed to form bulk deposits [44-48] to form deposits with atomic level control. EC-ALD is performed at room temperature thus limiting the interdiffusion in layers of the superlattice and breaks the deposition process into a sequence of individually controllable steps thus allowing the ability to optimize the process. In addition, no annealing has so far been required for the crystal structure of the electrochemical ALD grown thin films [26, 32, 49-51] and superlattices [52] to become visible in their respective X-ray diffraction patterns. In the formation of both CdTe thin film and PbTe/CdTe superlattice, ALD cycles where ramping of the deposition potentials of the first few cycles of Pb, Te and Cd are used will be presented. The probable reason for ramping of the deposition potential of the first few cycles has been extensively discussed previously [26, 49, 53-54].

Experimental

An automated thin layer flow electrodeposition system consisting of a series of solution reservoirs, computer controlled pumps, valves, a thin layer electrochemical flow cell and a potentiostat was used in this study to grow CdTe thin film and PbTe/CdTe superlattice. The reference electrode, Ag/AgCl (3M NaCl) (Bioanalytical systems, Inc., West Lafayette, IN), was held by a simple O-ring and the auxiliary electrode was a Au wire embedded into the Plexiglas flow cell. The electrochemical flow cell was designed to promote laminar flow. The cell volume was about 0.3 mL and solutions were pumped at 50 mL min^{-1}. The system was contained within a nitrogen purged Plexiglas box to reduce the influence of oxygen during electrodeposition.

Substrates used in the study consisted of 300 nm thick vapor deposited gold on glass microscope slides. Prior to insertion into the vapor deposition chamber, the glass slides were cleaned in HF (50% by volume), and rinsed with copious amounts of deionized water from a Nanopure water filtration system (Barnstead, Dubuque, IA), fed from the house distilled water system. Deposition began with 3 nm of Ti, as an adhesion layer, followed by 300 nm of Au deposition at around 250 ^{o}C. The glass slides were then annealed in the deposition chamber at 400 ^{o}C for 12 hours, while the pressure was maintained at 10^{-6} Torr.

Reagent grade or better chemicals and deionized water were used to prepare the three different solutions used in this study. The lead solution consisted of 0.5 mM $Pb(ClO_4)_2$ (Alfa Aesar, Ward Hill, MA), pH 3, with 0.1 M $NaClO_4$ (Fischer Scientific, Pittsburgh, PA) as the supporting electrolyte. The cadmium solution was made of 0.5 mM SeO_2 (Alfa Aesar, Ward Hill, MA), pH 3, with 0.1 M $NaClO_4$ (Fischer Scientific, Pittsburgh, PA) as the supporting electrolyte. The tellurium solution was made of 0.5 mM TeO_2 (Alfa Aesar, Ward Hill, MA), pH 9.2, buffered with 50.0 mM sodium borate and 0.1 M $NaClO_4$ (Fischer Scientific, Pittsburgh, PA) as the supporting electrolyte. A pH 3 blank solution of 0.1 M $NaClO_4$ (Fischer Scientific, Pittsburgh, PA) was used as well. NaOH and $HClO_4$ (Fischer Scientific, Pittsburgh, PA) were used to adjust the pH values of all the solutions in this study.

The electrochemical ALD cycle program used to grow CdTe consisted of the following: the Te solution was flushed in to the cell for 2 s at the chosen potential, and then held quiescent for 15 s for deposition. The blank solution was then flushed through the cell at the same potential for 3 s, to rinse out excess $HTeO_2^+$ ions. The Cd solution was then flushed through the cell for 2 s at the Cd deposition potential, and held quiescent for 15 s for deposition. Blank solution was again flushed through the cell for 3 s to rinse out excess Cd^{2+} ions from the cell. This process was referred to as one cycle, and was repeated as many times as needed to form CdTe cycles of the thin film and the superlattice described in this paper. Whereas the electrochemical ALD cycle program used to form PbTe consisted of the following: the Te solution was flushed in to the cell for 2 s at the chosen potential, and then held quiescent for 15 s for deposition. The blank solution was then flushed through the cell at the same potential for 3 s, to rinse out excess $HTeO_2^+$ ions. The Pb solution was then flushed through the cell for 2 s at the Pb potential, and held quiescent for 15 s for deposition. Blank solution was again flushed through the cell for 3 s to rinse out excess Pb^{2+} ions from the cell. This process was referred to as one cycle, and was repeated as many times as needed to form PbTe cycles of the superlattices described in this report. The deposition area of Au electrode used in experiments described in this paper was 4 cm^2.

Microanalyses (EPMA) of the samples were performed with a Joel JXA-8600 electron probe. Glancing angle X-ray diffraction patterns were obtained on a Scintag PAD V diffractometer, equipped with a 6” long set of Soller slits on the detector to improve resolution in the asymmetric diffraction configuration. The absorption measurement was taken at a normal incidence in the wavelength range of 1100 nm to 500 nm at -1 nm decrement for a total of 1200 s using an Oriel Cornerstone 260 1/4 m monochromator spectrometer.

Results and Discussions

Prior to devising CdTe and PbTe/CdTe programs, the electrochemical behavior of Au on glass electrodes used to grow the deposits needed to be studied in the solutions of Te, Cd and Pb by running cyclic voltammetries of the electrodes. Figure 1(a) and 1(b) show the cyclic voltammetries of Au on glass electrode in 0.5 M $HTeO_2^+$ solution which were discussed in our previous work [26]. The reductive peaks in the negative going scans and their corresponding oxidative features depicted in the first and second scans shown in Figure 1(a) were attributed to Te UPD despite appearing at overpotentials, negative of the formal potential of around -0.05 V. When the negative going scan in Figure 1(a) was held for two minutes at -0.55 V, its corresponding oxidative stripping peak positive of 0.10 V did not increase in size, confirming the characteristics of surface limited deposition. The reason for Te UPD reductive peaks appearing at overpotential has been attributed to the slow kinetics of $HTeO_2^+$ reduction to Te, a known behavior in chalcogenides [22-23, 55-56]. Figure 1(b) shows the case where the scan was reversed at potentials negative of -0.55 V, where it is evident that a new feature equivalent to bulk oxidation of Te is evident around -0.05 V with a peak near 0.05 V, thus clearly differentiating it from the stripping of the surface limited Te seen positive of 0.10 V. The sharp increase observed around -0.70 V has been attributed to hydrogen evolution, more bulk Te deposition and reduction of Te to Te^{2-}, a soluble species, as the bulk Te oxidative peak became larger when scan was reversed from -0.72 V, whereas the surface limited Te oxidative peak positive of 0.10 V stayed the same. Au cyclic voltammogram in Cd^{2+} solution has been previously reported by this group [50, 57], where it was found that bulk Cd deposition did not occur until negative of -0.8 V, while its stripping peak could be observed in its subsequent oxidative scan in a peak at -0.55 V. The extra current that was observed in both reductive and oxidative scans was then attributed to the alloy formation of Au with Cd and its subsequent stripping. Figure 2 represents the cyclic voltammogram of Au on glass electrode in Pb^{2+} solution which was also reported by this group in our previous work [26]. The window shown by the circle in the CV depicts the Pb UPD deposition region with a peak at -0.25 V, characteristic of the reversible Pb^{2+} UPD on Au electrode as reported elsewhere [58-62]. The reduction peak at -

0.47 V is attributed to bulk Pb deposition as its corresponding oxidative peak at -0.45 V and the presence of a hysteresis suggesting nucleation and growth are visible in Figure 2. The broad oxidative peak observed in the positive going scan at -0.38 V is due to Pb oxidation from Pb/Au alloy [63].

CdTe Deposition

We had previously reported a CdTe ALD cycle where Cd was deposited reductively at its UPD potential whereas Te was deposited from an acidic solution (pH 2) at a bulk potential and its excess was reductively stripped at a much more negative potential [25]. This program resulted in a stoichiometric deposit. However in this article, the pH of $HTeO_2^+$ solution was changed to a more basic value (pH 9.2), similar to the tellurium solution that was used in the growth of PbTe thin films [26] with potential ramping of the first few cycles of the deposition process. In this instance, when an ALD cycle deposition program of CdTe using constant potentials of -0.6 V and -0.55 V for Te and Cd respectively was attempted, the deposition currents started at around a monolayer (ML) and gradually decreased to less than a ML as the number of cycles increased. This trend has been observed in the past with most of the compounds grown using EC-ALD by this group [32, 64]. To remedy the loss in currents, the shifting of the deposition potentials to more negative values over the first 10-30 cycles have been used in order to maintain ML/cycle. The successful ALD cycle program used to grow the CdTe deposit presented in this paper was obtained when Te and Cd potentials were ramped down from -0.6 V and -0.55 V to -0.70 V and -0.65 V respectively over 20 cycles. A section of the current time traces of the successful ALD cycle program of CdTe can be seen in Figure 3, where Te and Cd deposition charges are evident.

The resulting CdTe deposit appeared homogeneous when observed under the optical microscope. Table 4 displays the EPMA data which confirms the obtained deposit to be nearly stoichiometric (**$Cd_{49.6}Te_{50.4}$**). Figure 4 is the glancing angle XRD pattern of the as deposited 100 ALD cycle-CdTe thin film that was taken at a 1^{o} incident angle, where peaks consistent with zinc blende structure of CdTe are present. Bragg diffraction peak (111) is the most predominant one in the XRD pattern of the deposit. Absorption measurement, taken on CdTe sample after it had been annealed in an oven under nitrogen environment at 150 ^{o}C for 20 minutes, indicated a direct band gap value of around 1.45 eV similar to values reported in the literature as shown by Figure 5.

PbTe/CdTe Superlattice

We had reported in the previous chapter on the formation of the superlattice of PbSe/PbTe. Despite the high lattice mismatch (~ 5 %) between PbSe and PbTe, we were successful in our attempt to grow PbSe/PbTe superlattice using electrochemical atomic layer deposition, since individual cycles of both compounds had been previously optimized [26, 49]. As stated earlier, in order to successfully form a superlattice, one needs to choose compound semiconductors with a small difference in lattice constants, but a large difference in band gap in layers [30]. Since CdTe and PbTe fit these criteria, an ALD cycle program for the deposition of the superlattice consisting of 15 periods of 5 cycles of CdTe and 15 cycles of PbTe was then devised and attempted on a 15 cycle-PbTe prelayer on Au on glass using CdTe deposition potentials described earlier and the successful PbTe deposition conditions reported in our previous work [26] and shown in Figure 6. In the case of CdTe cycles of the superlattice, Te and Cd potentials were ramped down from -0.6 V and -0.55 V to -0.70 V and -0.65 V respectively over 5 cycles whereas for PbTe cycles of the superlattice, Te deposition potentials were ramped over 15 cycles while Pb potential was held constant throughout the deposition run as shown in Figure 6. To minimize the stress between the superlattice and the polycrystalline Au electrode due to the lattice mismatch, a prelayer consisting of 15 cycles of PbTe was grown on Au on glass electrode based on the optimized ALD program of PbTe [26] prior to the superlattice growth. Figures 7 and 8 depict the average deposition currents (coverage) of CdTe and PbTe cycles respectively in each period of PbTe/CdTe superlattice obtained from the integration of the current time traces of the ALD deposition process. The average PbTe cycles of the superlattice resulted in the desired coverage of near one monolayer (ML) / period as depicted in Figure 8, whereas the average CdTe cycles of the superlattice resulted in a coverage more than the desired one ML / period as shown in Figure 7. The excess amount of CdTe in the superlattice could be due to the difference in the number of cycles over which the potentials for both Te and Cd were negatively shifted prior to reaching the steady state potential values. In the case of CdTe thin film, the potential program was shifted over 20 cycles, whereas in the superlattice program, potentials were only ramped down over 5 cycles. In the case of 4PbSe/4PbTe superlattice, the ALD deposition potentials of both PbTe and PbSe cycles were slightly changed from the programs used for either PbTe or PbSe thin film deposition as the number of cycles of the constituent compounds of the superlattice within each period was only 4 cycles.

The resulting PbTe/CdTe superlattice however appeared homogeneous when observed visually as shown in Figure 9 or under the optical microscope. The EPMA data shown in Table 5 confirmed the superlattice to be stoichiometric as the ratio of the sum of Cd and Pb to Te of around **1.02** was obtained. The glancing angle (1^{o} from the sample plane) X-ray diffraction (XRD) pattern of the as-deposited PbTe/CdTe superlattice is shown in Figure 10. Symmetric small shoulders around the (111) Bragg diffraction peak at 23.7^{o} corresponding to satellites indicative of the crystallographic coherence of the deposited multilayers and the superlattice structure of the electrodeposited film [65-67] could be seen in the XRD pattern of the superlattice. The modulation wavelength of the PbTe/CdTe superlattice based on the XRD was found to be around 11 nm, almost twice the expected amount of around 6.0 nm. The higher thickness value obtained from the XRD could be attributed to the less than optimum condition of CdTe deposition process in the superlattice program, as Figure 7 showed in average that more than a ML was being deposited in each CdTe period. Additional studies of CdTe cycle deposition program of PbTe/CdTe superlattice are still needed in order to optimize CdTe deposition process of the superlattice.

Conclusion

This paper discussed the electrodeposition of CdTe thin film and PbTe/CdTe superlattice in which the deposition potentials of the constituent elements were negatively ramped. The EC-ALD grown CdTe deposit was stoichiometric and homogeneously distributed as confirmed by EPMA. The deposit exhibited a predominantly (111) orientation in XRD and a bandgap of around 1.45 eV. In PbTe/CdTe superlattice, the coverage based on the coulometry was found to average one monolayer per period for PbTe cycles and more than a ML / period for CdTe cycles. The presence of the satellite peaks was visible in the XRD pattern of the superlattice and electron probe microanalysis characterization determined the superlattice to be stoichiometric.

Acknowledgements

Support from the National Science Foundation is gratefully acknowledged.

References

1. Shah, N.A., A. Ali, and A. Maqsood, *Characterization of CdTe thin films fabricated by close spaced sublimation technique and a study of Cu doping by ion exchange process.* Journal of Non-Crystalline Solids, 2009. **355**(28-30): p. 1474-1478.
2. Ribeiro, M.C.R., L.R. Cruz, and R.R. de Avillez, *Thermodynamic evaluation of the CdTe deposition by an elemental co-evaporation method under isothermal transport conditions.* Materials Research Bulletin, 2006. **41**(1): p. 45-53.
3. Sotelo-Lerma, M., R.A. Zingaro, and S.J. Castillo, *Preparation of CdTe coatings using the chemical deposition method.* Journal of Organometallic Chemistry, 2001. **623**(1-2): p. 81-86.
4. Becerril, M., et al., *Crystallization from amorphous structure to hexagonal quantum dots induced by an electron beam on CdTe thin films.* Journal of Crystal Growth, 2009. **311**(5): p. 1245-1249.
5. Matsumura, N., et al., *Preparation of CdTe thin films on Ge substrates by molecular beam epitaxy.* Journal of Crystal Growth. **71**(2): p. 361-370.
6. Beyer, H., et al., *PbTe based superlattice structures with high thermoelectric efficiency.* Appl. Phys. Lett., 2002. **80**(7): p. 1216-1218.
7. Wang, W.S., E. H.E., and B. I.B., *Atomic Layer Epitaxy of CdTe On GaAs, By Organometallic Vapor- Phase Epitaxy.* Journal of Crystal Growth, 1992. **124**(1-4): p. 670.
8. Baleva, M., *Optical properties of laser-deposited PbTe films.* Thin Solid Films, 1986. **139**(2): p. L71-L75.

9. Pandey, S.K., et al., *Growth of cubic and hexagonal CdTe thin films by pulsed laser deposition.* Thin Solid Films, 2005. **473**(1): p. 54-57.

10. Jacquot, A., et al., *Pulsed laser deposition of PbTe films on glass substrates.* Appl. Phys. A-Mater. Sci. Process., 1999. **69**: p. S613-S615.

11. Singh, R.R., D. Painuly, and R.K. Pandey, *Synthesis and characterization of electrochemically deposited nanocrystalline CdTe thin films.* Materials Chemistry and Physics, 2009. **116**(1): p. 261-268.

12. Murali, K.R., P. Thirumoorthy, and V. Sengodan, *Pulse plated cadmium telluride films and their characteristics.* Ionics, 2009. **15**(2): p. 209-213.

13. Murali, K.R., et al., *Characterization of electrodeposited CdTe films.* B. Electrochem., 1989. **5**(12): p. 890-892.

14. Ivanova, Y.A., D.K. Ivanov, and E.A. Strel'tsov. *Electrochemical and photoelectrochemical deposition and oxidation of cadmium atom layers on the surface of n-Si/Te and n-Si/CdTe heterostructures*. 2009.

15. Osipovich, N.P. and S.K. Poznyak, *Underpotential deposition of cadmium adatoms on Te and CdTe.* Electrochimica Acta, 2006. **52**(3): p. 996-1002.

16. Josell, D., et al., *Three Dimensionally Structured CdTe Thin-Film Photovoltaic Devices with Self-Aligned Back-Contacts: Electrodeposition on Interdigitated Electrodes.* Journal of the Electrochemical Society, 2009. **156**(8): p. H654-H660.

17. Murase, K., et al., *Electrodeposition of CdTe films from ammoniacal alkaline aqueous solution at low cathodic overpotentials.* JECS, 1999. **149**(2): p. 531-536.

18. Murase, K., et al., *Electrochemical QCM studies of CdTe formation and dissolution in ammoniacal basic aqueous electrolytes.* Journal of the Electrochemical Society, 2005. **152**(5): p. C304-C309.

19. Arai, K., et al., *Studies of oxidation behaviors of CdTe in ammoniacal basic electrolytes.* Electrochimica Acta, 2006. **51**(23): p. 4987-4993.

20. Beaunier, L., et al., *Epitaxial electrodeposition of lead telluride films on indium phosphide single crystals.* Journal of Electroanalytical Chemistry, 2002. **532**(1-2): p. 215-218.

21. Saloniemi, H., *Electrodeposition of PbS, PbSe and PbTe thin films.* VTT Publications, 2000. **423**: p. 1-137.

22. Flowers, B.H., et al., *Atomic layer epitaxy of CdTe using an automated electrochemical thin-layer flow deposition reactor.* Journal of Electroanalytical Chemistry, 2002. **524-525**: p. 273-285.

23. Lay, M.D. and J.L. Stickney, *EC-STM Studies of Te and CdTe Atomic Layer Formation from a Basic Te Solution.* Journal of the Electrochemical Society, 2004. **151**(6): p. C431-C435.

24. Muthuvel, M., et al., *UHV-EC studies of CdTe electrodeposition on InP(100) using EC-ALE.* ECS Transactions, 2005. **1**(2, SOTAPOCS XLIII and Nitride and Wide Bandgap Semiconductors for Sensors, Photonics, and Electronics VI, 2005): p. 64-74.

25. Venkatasamy, V., et al., *Optimization of CdTe nanofilm formation by electrochemical atomic layer epitaxy (EC-ALE).* Journal of Applied Electrochemistry, 2006. **36**(11): p. 1223-1229.

26. Banga, D.O., et al., *Formation of PbTe nanofilms by electrochemical atomic layer deposition (ALD).* Electrochimica Acta, 2008. **53**(23): p. 6988-6994.

27. Dughaish, Z.H., *Lead telluride as a thermoelectric material for thermoelectric power generation.* 2002. **322**(1-2): p. 205-223.

28. Zimin, D., K. Alchalabi, and H. Zogg, *Heteroepitaxial PbTe-on-Si pn-junction IR-sensors: correlations between material and device properties.* Physica E, 2002. **13**(2-4): p. 1220-1223.

29. Beyer, H., et al., *High thermoelectric figure of merit ZT in PbTe and Bi2Te3-based superlattices by a reduction of the thermal conductivity.* 2002. **13**(2-4): p. 965-968.

30. Switzer, J.A., *Electrodeposition of superlattices and multilayers*, in *Electrochemistry of Nanomaterials*, G. Hodes, Editor. 2001, Wiley-VCH: Weinheim. p. 67.

31. Banga, D. and J.L. Stickney, *PbTe - PbSe superlattice formation by electrochemical atomic layer deposition.* ECS Transactions, 2007. **6**(2, State-of-the-Art Program on Compound Semiconductors 46 (SOTAPOCS 46) and Processes at the Semiconductor/Solution Interface 2): p. 439-449.

32. Vaidyanathan, R., et al., *Preliminary studies in the electrodeposition of PbSe/PbTe superlattice thin films via electrochemical atomic layer deposition (ALD).* Langmuir, 2006. **22**(25): p. 10590-10595.

33. Koike, K., et al., *Photoluminescence characterization of PbTe/CdTe quantum dots grown by lattice-type mismatched epitaxy.* Journal of Crystal Growth, 2007. **301-302**: p. 722-725.

34. Yano, M., I. Makabe, and K. Koike, *Photoluminescence characterized thermal mismatch of PbTe/CdTe single quantum wells grown on GaAs substrates.* Physica E: Low-dimensional Systems and Nanostructures, 2004. **20**(3-4): p. 449-452.

35. Groiss, H., et al. *The coherent {100} and {110} interfaces between rocksalt-PbTe and zincblende-CdTe*. 2007.

36. Groiss, H., et al., *Coherent {001} interfaces between rocksalt and zinc-blende crystal structures.* Physical Review B, 2009. **79**(23).

37. Groiss, H., et al., *Size control and midinfrared emission of epitaxial PbTe/CdTe quantum dot precipitates grown by molecular beam epitaxy.* Applied Physics Letters, 2007. **91**(22).

38. Leitsmann, R., et al. *Structural and electronic properties of PbTe (rocksalt)/CdTe (zinc-blende) interfaces*. 2007.

39. Schwarzl, T., et al., *Temperature-dependent midinfrared photoluminescence of epitaxial PbTe/CdTe quantum dots and calculation of the corresponding transition energy.* Physical Review B, 2008. **78**(16).

40. Heiss, W., et al., *Centrosymmetric PbTe/CdTe quantum dots coherently embedded by epitaxial precipitation.* Applied Physics Letters, 2006. **88**(19).

41. Koike, K., et al., *PbTe/CdTe single quantum wells grown on GaAs (100) substrates by molecular beam epitaxy.* Journal of Crystal Growth, 2003. **257**(1-2): p. 212-217.

42. Leitsmann, R., et al., *Rebonding at coherent interfaces between rocksalt-PbTe/zinc-blende-CdTe.* New Journal of Physics, 2006. **8**.

43. Yano, M., I. Makabe, and K. Koike. *Photoluminescence characterized thermal mismatch of PbTe/CdTe single quantum wells grown on GaAs substrates*. 2004.

44. Adzic, R.R., in *Advances in Electrochemistry and Electrochemical Engineering*, H. Gerishcher and C.W. Tobias, Editors. 1984, Wiley-Interscience: New York. p. 159.

45. Adzic, R.R., et al., *Electrocatalysis by foreign metal monolayers: oxidation of formic acid on platinum.* JEC, 1975. **65**: p. 587-601.

46. Kolb, D.M., *Physical and Electrochemical Properties of Metal Monolayers on Metallic Substrates*, in *Advances in Electrochemistry and Electrochemical Engineering*, H. Gerischer and C.W. Tobias, Editors. 1978, John Wiley: New York. p. 125.

47. Kolb, D.M. and H. Gerisher, *Further aspects concerning the correlation between underpotential depsoition and work function defferences.* SS, 1975. **51**: p. 323.

48. Kolb, D.M., Przasnys.M, and Gerische.H, *Underpotential Deposition of Metals and Work Function Differences.* Journal of Electroanalytical Chemistry, 1974. **54**(1): p. 25-38.

49. Banga, D., et al., *Optimization of PbSe Nanofilms formation by Electrochemical Atomic Layer Deposition (ALD).* ECS Transactions, 2009. **19**(3): p. 245-272.

50. Venkatasamy, V., et al., *Optimization studies of CdTe nanofilm formation by electrochemical atomic layer epitaxy (EC-ALE).* J. Appl. Electrochem., 2006. **36**: p. 1223.

51. Zhu, W., et al., *Electrochemical atom-by-atom growth of highly uniform thin sheets of thermoelectric bismuth telluride via the route of ECALE.* Journal of Electroanalytical Chemistry, 2008. **614**(1-2): p. 41-48.

52. Zhu, W., et al., *Electrochemical aspects and structure characterization of VA-VIA compound semiconductor Bi2Te3/Sb2Te3 superlattice thin films via electrochemical atomic layer epitaxy.* Langmuir, 2008. **24**(11): p. 5919-5924.

53. Vaidyanathan, R., J.L. Stickney, and U. Happek, *Quantum confinement in PbSe thin films electrodeposited by electrochemical atomic layer epitaxy (EC-ALE).* Electrochimica Acta, 2004. **49**(8): p. 1321-1326.

54. Vaidyanathan, R., et al. *Formation of In2Se3 thin films and nanostructures using electrochemical atomic layer epitaxy*. 2003.

55. Lister, T.E., et al., *Electrochemical Formation of Se Atomic Layers On Au(100).* Journal of Vacuum Science & Technology B, 1995. **13**(3): p. 1268.

56. Huang, B.M., T.E. Lister, and J.L. Stickney, *Se adlattices formed on Au (100), studies by LEED, AES, STM and electrochemistry.* Surface Science, 1997. **392**(1-3): p. 27.

57. Mathe, M.K., et al., *Deposition of CdSe by EC-ALE.* Journal of Crystal Growth, 2004. **271**(1-2): p. 55-64.

58. Kim, Y.-G., et al., *Pb Deposition on I-Coated Au(111). UHV-EC and EC-STM Studies.* Langmuir 2007. **23**(5): p. 2539-45.

59. Bondarenko, A.S., et al., *Potentiodynamic electrochemical impedance spectroscopy of lead upd on polycrystalline gold and on selenium atomic underlayer.* Electrochemistry Communications, 2005. **7**(6): p. 631-636.

60. Conway, B.E. and J.C. Chacha, *Effects of temperature on the states of Pb adatoms underpotentially deposited from various solvents on Au : entropies of adatom states.* Journal of New Materials for Electrochemical Systems, 2004. **7**(3): p. 231-240.

61. Dimitrov, N., R. Vasilic, and N. Vasiljevic, *A Kinetic Model for Redox Replacement of UPD Layers.* Electrochemical and Solid-State Letters, 2007. **10**(7): p. D79-D83.

62. Seo, M. and M. Yamazaki, *Changes in Surface Stress of Gold Electrode during Underpotential Deposition of Pb.* Journal of the Electrochemical Society, 2004. **151**(8): p. E276-E281.

63. Green, M.P. and K.J. Hanson, *Alloy formation in an electrodeposited monolayer.* Surface Science, 1991. **259**(3): p. L743-L749.

64. Vaidyanathan, R., et al., *Electrodeposition of Cu2Se thin films by electrochemical atomic layer epitaxy (EC-ALE).* Materials Research Society Symposium Proceedings, 2003. **744**(Progress in Semiconductors II--Electronic and Optoelectronic Applications): p. 289-294.

65. Switzer, J.A., H.M. Kothari, and E.W. Bohannan, *Thermodynamic to kinetic transition in epitaxial electrodeposition.* Journal of Physical Chemistry B, 2002. **106**(16): p. 4027-4031.

66. Lashmore, D.S. and M.P. Dariel, *Electrodeposited Cu-Ni Textured Superlattices.* JECS, 1988. **135**: p. 1219.

67. Schuller, I.K. and C.M. Falco, *Superconductivity and magnetism in metallic superlattices.* Thin Solid Films, 1982. **90**(2): p. 221-227.

Table 4: Electron Probe Microanalysis (EPMA) Data of 100 ALD Cycles of CdTe thin film formed when Te and Cd potentials were ramped. Electrode area: 4 cm^2.

CdTe Sample	**Te at. %**	**Cd at. %**	**Te / Cd**
Inlet	50.5	49.5	**1.02**
Middle	50.4	49.6	**1.02**
Outlet	50.2	49.8	**1.01**

Table 5: Electron Probe Microanalysis (EPMA) Data of 15P/5CdTe/15PbTe superlattice formed on 15 cycle-PbTe prelayer on Au on glass. Electrode area: 4 cm^2.

Sample	**15P:5CdTe:15PbTe**
Te Atomic %	43.7
Cd Atomic %	9.3
Pb Atomic %	32.2
(Pb + Cd) / Te	**1.02**

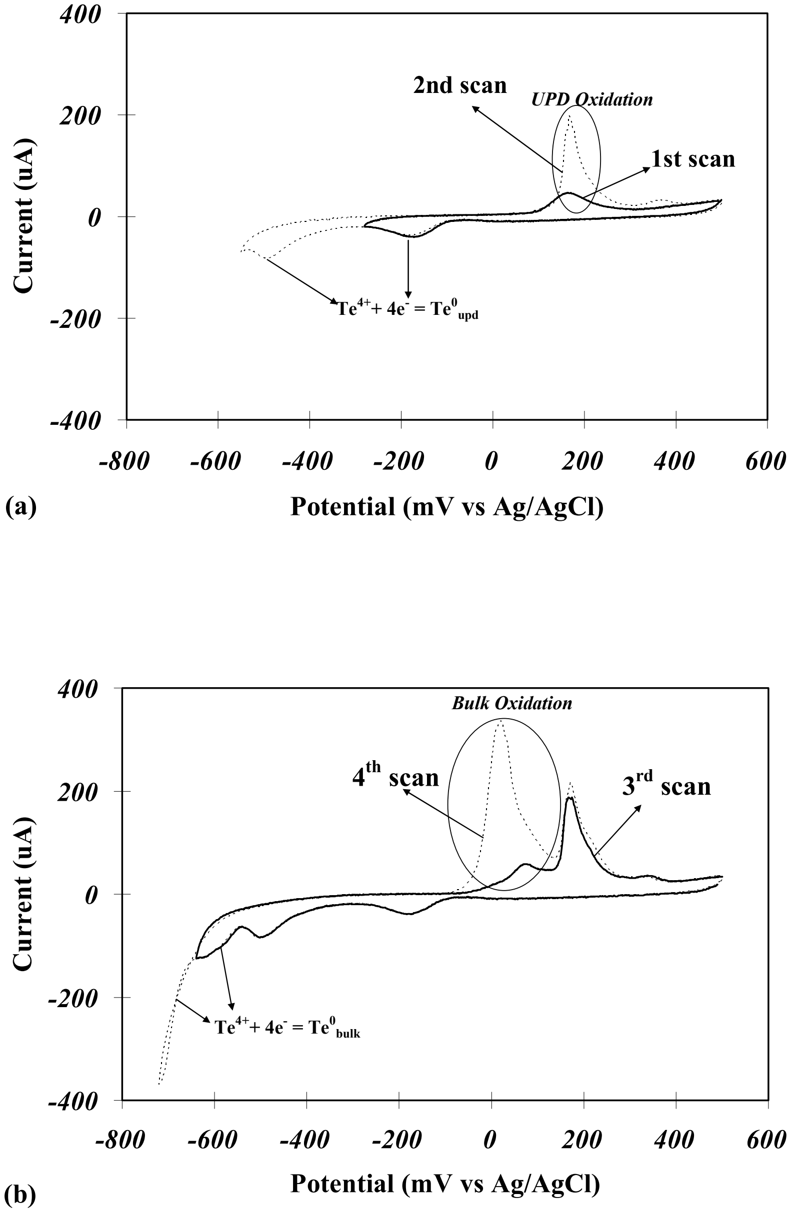

Figure 5.1: Cyclic voltammetry of Au electrode in 0.5 mM $HTeO_2^+$, pH 5, (electrode area: 4 cm^2, scan rate: 10 mV s^{-1}).

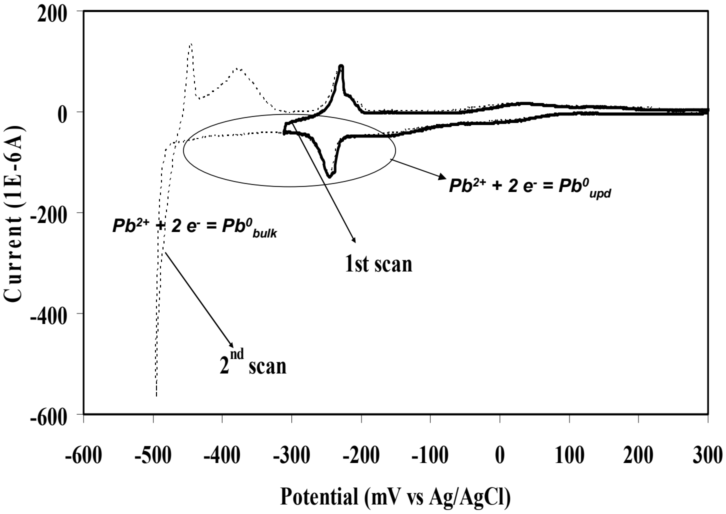

Figure 5.2: Cyclic voltammetry of Au electrode in 0.5 mM Pb^{2+}, pH 3, (electrode area: 4 cm^2, scan rate: 10 mV s^{-1}).

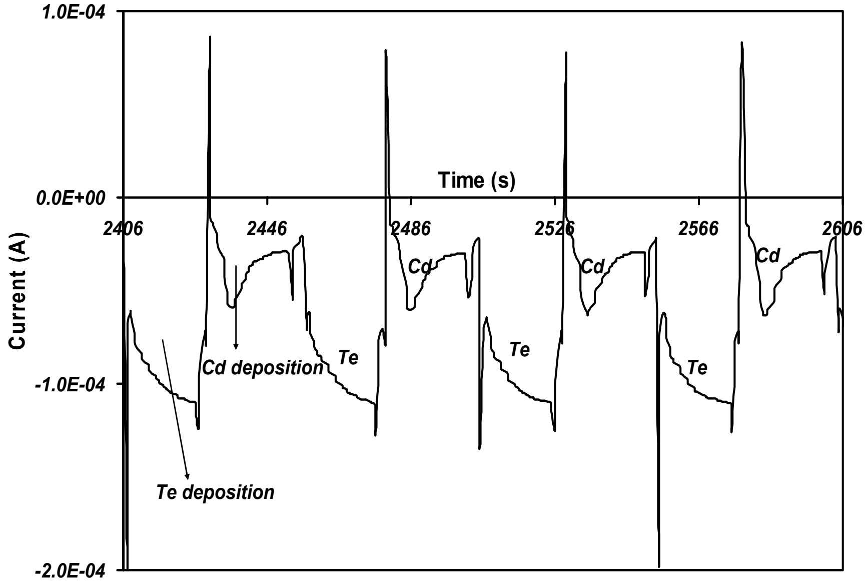

Figure 5.3: A section of current time traces of 100 ALD cycles of CdTe thin film formed when both Te and Cd potentials were ramped over 20 cycles from -0.6 and -0.55 V to steady state -0.7 and -0.65 V respectively. Electrode area: 4 cm^2.

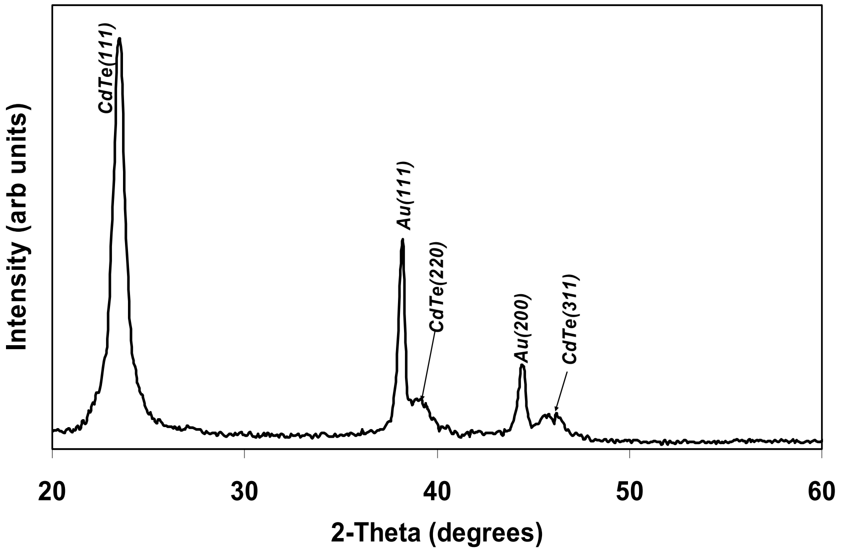

Figure 5.4: X-ray diffraction of 100 ALD cycles of CdTe thin film formed when both Te and Cd potentials were ramped. Angle of incidence is 1°, Cu Kα source. Electrode area: 4 cm^2.

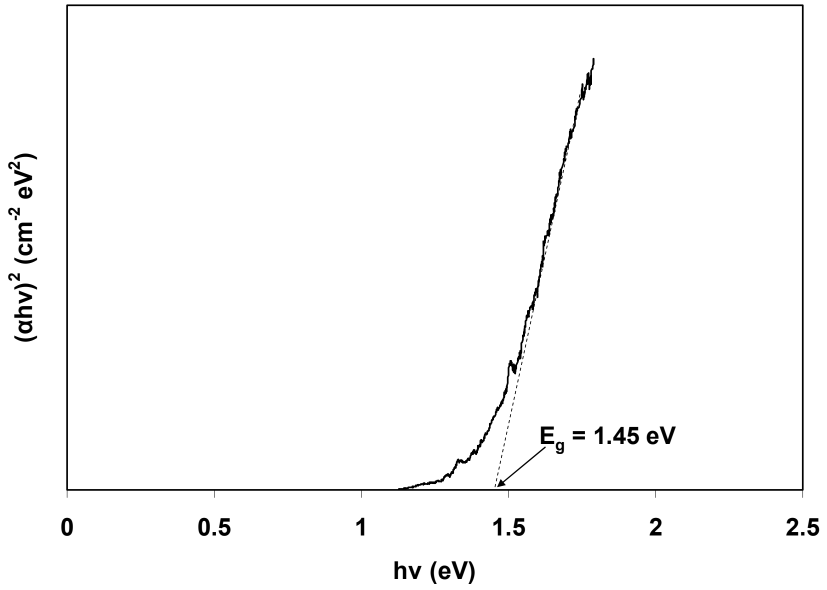

Figure 5.5: Absorption spectrum of 100 cycle CdTe thin film annealed at 150 °C for 20 minutes. Electrode area: 4 cm^2.

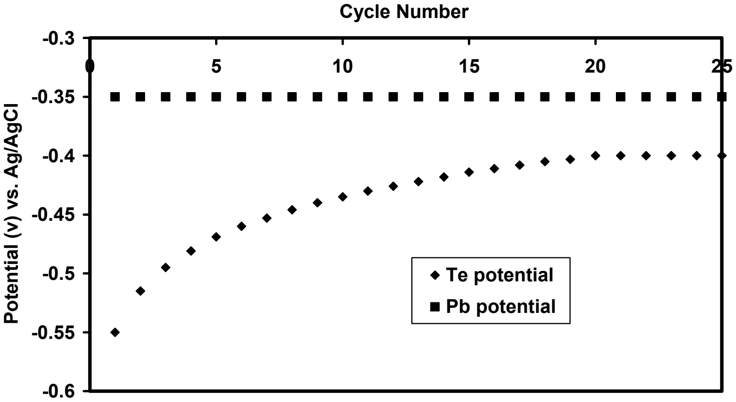

Figure 5.6: PbTe ALD cycle deposition program of a 15P/5CdTe/15PbTe superlattice showing Te deposition potentials of being shifted negative from -0.55 V to -0.4 V and Pb deposition potentials being held constant at -0.35 V. Electrode area: 4 cm^2.

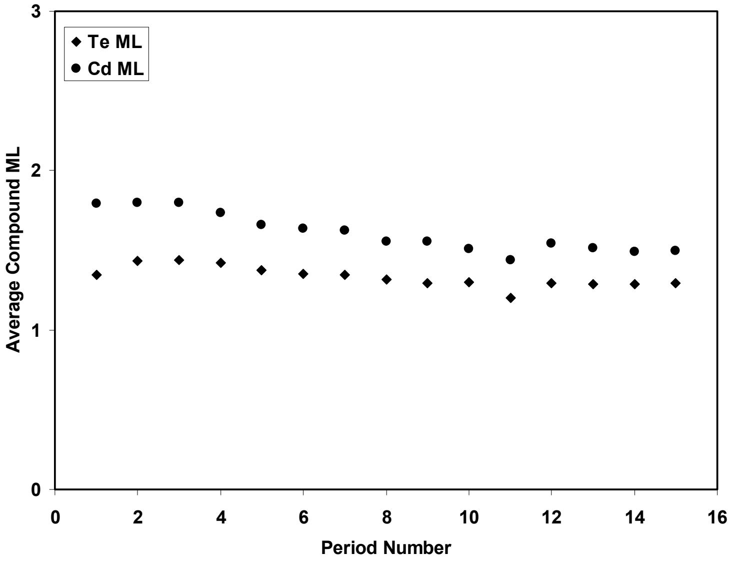

Figure 5.7: Average deposition currents (coverage) of CdTe ALD periods of 5CdTe:15PbTe superlattice with the ramping of potentials. Electrode area: 4 cm^2.

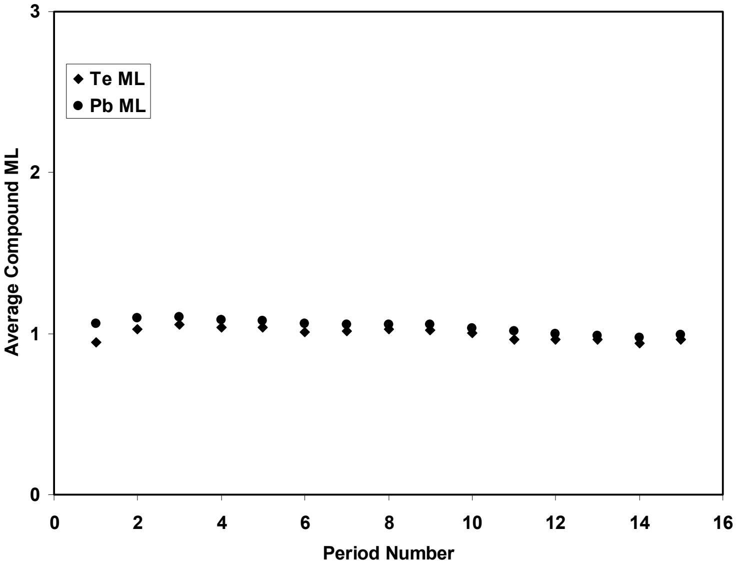

Figure 5.8: Average deposition currents (coverage) of the PbTe ALD periods of 5CdTe:15PbTe superlattice with the ramping of potentials. Electrode area: 4 cm^2.

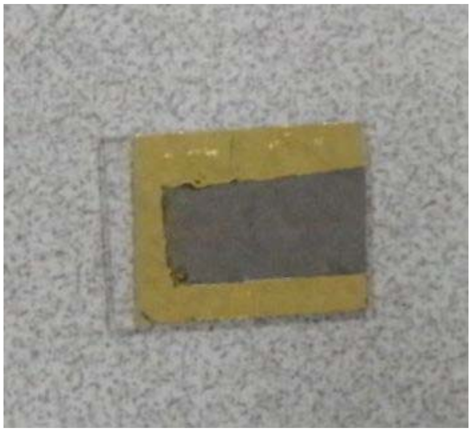

Figure 5.9: Picture of PbTe/CdTe superlattice made of 15 periods of 5 cycles of CdTe and 15 cycles of PbTe on 15 cycle-PbTe prelayer on Au on glass. Electrode area: 4 cm^2.

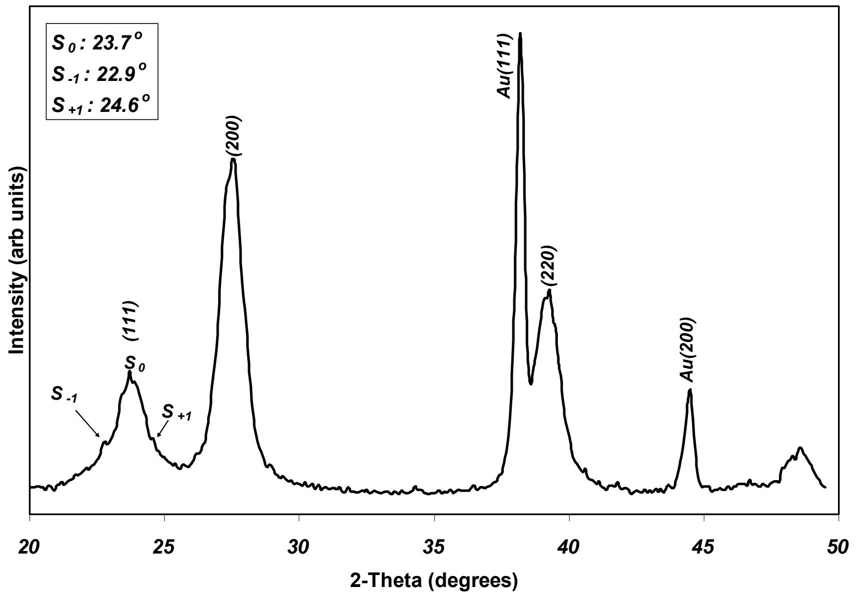

Figure 5.10: X-ray diffraction pattern of 15P/5CdTe/15PbTe superlattice formed on 15 cycle-PbTe prelayer on Au on glass. Angle of incidence is 1°, Cu Kα source. Electrode area: 4 cm^2.

CHAPTER 6

ELECTRODEPOSITION OF $CuInSe_2$ BY ELECTROCHEMICAL ATOMIC LAYER DEPOSITION (ALD)[5]

---

[5] Banga, D., et al. To be submitted to Journal of The Electrochemical Society.

Abstract

This chapter presents the first time electrochemical atomic layer deposition has been successfully used to grow nearly stoichiometric $CuInSe_2$ (CIS). In addition to CIS, studies of the electrodeposition process, composition and crystal structure of the individual binary InSe and Cu_2Se thin films will also be discussed in this report. Potential adjustment of initial few cycles will be used during Cu_2Se formation, in contrast to steady potentials used during InSe deposition process. Different approaches that will be undertaken to grow CIS will include changing various deposition parameters during the ALD cycle program, such as the growth routes of layers of constituent elements (combining the binary compounds of CIS or growing CIS as a superlattice), Se deposition time, Cu deposition time, potential ramping of the elements, maintaining constant deposition potentials for the constituent elements of CIS, etc. The stoichiometric sample was obtained when a superlattice made of 25 periods of 3 cycles of InSe and 1 cycle of CuSe was grown using 3 s as for Cu deposition time and applying constant deposition potentials of 0.14 V, -0.7 V and -0.65 V for Cu, In and Se respectively. Peaks corresponding to the chalcopyrite phase of CIS are observed in the XRD pattern of the as-deposited sample, with (112) plane being the most predominant one. AFM image of the deposit appeared conformal with the image of Au on glass substrate.

Introduction

Photovoltaics, the direct conversion of sunlight into electricity, is one of the most powerful alternatives for future large scale energy production. Of existing photovoltaic materials, $CuInSe_2$, a semiconductor compound belonging to I-III-VI_2 chalcopyrite family, is one of the well known advanced absorber materials for thin film solar cells due to its various properties such as its direct band gap (1.01 eV) [1], high absorption coefficient (10^5 cm^{-1}) [2], extraordinary stability [3] and high conversion efficiency (16 %) [4]. Properties of $CuInSe_2$ have been improved by the replacement of part of indium by gallium or part of selenium by sulfur to form $Cu(In,Ga)(Se,S)_2$ [5] leading to attainment of conversion efficiency of up to 19.9 % [6]. Another attracting advantage of $CuInSe_2$ based materials is that only thin films of CIS (few micrometers) are needed in the solar cells, compared to the thick slices of bulk silicon, thus reducing the consumption of materials during its manufacturing process.

Various techniques used to grow $CuInSe_2$ have included co-evaporation [7-9], flash evaporation[10], fusion [11], chemical vapor deposition [12], sputtering [13], spray pyrolysis [14-15], co-deposition [4, 16-21] and pulse-plated electrodeposition [22]. Selenization of sputtered [13], evaporated [9] or electrodeposited [23] Cu and In stacked layers or alloys have also been carried out.

This chapter will present the electrodeposition of $CuInSe_2$ films where two different deposition routes consisting of growing CIS as a ternary compound and a superlattice using electrochemical atomic layer deposition (EC-ALD), an electrodeposition technique based on the use of surface limited reactions known as under potential deposition (UPD). UPD is a phenomenon where an atomic layer is deposited on the second at a potential prior to its formal potential [24-28] to form deposits with atomic level control. EC-ALD is carried out at room temperature, thus considerably reducing the interdiffusion in layers of the deposits. Furthermore, EC-ALD uses separate solutions of elements of compounds being grown, which provides the ability to break the deposition process into a sequence of individually controllable steps thus allowing the ability to optimize the process. Thus far, no annealing has been required for the crystal structure of the electrochemical ALD grown thin films [29-33] and superlattices [34] to become visible in the X-ray diffraction patterns.

However, prior to forming $CuInSe_2$, results of studies of the formation of individual binary compounds (Cu_2Se and InSe) using electrochemical atomic layer deposition will be reported.

Experimental

In this study, an automated thin layer flow electrodeposition system consisting of a series of solution reservoirs, computer controlled pumps, valves, a thin layer electrochemical flow cell and a potentiostat was used to grow CIS films. The reference electrode, Ag/AgCl (3M NaCl) (Bioanalytical systems, Inc., West Lafayette, IN), was held by a simple O-ring and the auxiliary electrode was a Au wire embedded into the Plexiglas flow cell. The electrochemical flow cell was designed to promote laminar flow. The cell volume was about 0.3 mL and solutions were pumped at 50 mL min^{-1}. A nitrogen purged Plexiglas box was used to contain the system in order to reduce the influence of oxygen during electrodeposition.

Substrates used in the study consisted of 300 nm thick vapor deposited gold on glass microscope slides. Prior to insertion into the vapor deposition chamber, the glass slides were cleaned in HF, and rinsed with copious amounts of deionized water from a Nanopure water filtration system (Barnstead, Dubuque, IA), fed from the house distilled water system. Deposition began with 3 nm of Ti, as an adhesion layer, followed by 300 nm of Au deposition at around 250 °C. The glass slides were then annealed in the deposition chamber at 400 °C for 12 hours, while the pressure was maintained at 10^{-6} Torr.

Reagent grade or better chemicals and deionized water were used to prepare the three different solutions used in this study. The copper solution consisted of 0.5 mM $Cu(SO_4)_2$ (Alfa Aesar, Ward Hill, MA), pH 4.5, with 0.1 M $NaClO_4$ (Fischer Scientific, Pittsburgh, PA) as the supporting electrolyte. The indium solution consisted of 0.5 mM $In_2(SO_4)_3.xH_2O$ (Alfa Aesar, Ward Hill, MA), pH 3, with 0.1 M $NaClO_4$ (Fischer Scientific, Pittsburgh, PA) as the supporting electrolyte. The selenium solution was made of 0.5 mM SeO_2 (Alfa Aesar, Ward Hill, MA), pH 5, buffered with 50.0 mM $CH_3COONa.3H_2O$ and 0.1 M $NaClO_4$ (Fischer Scientific, Pittsburgh, PA) as the supporting electrolyte. A pH 3 blank solution of 0.1 M $NaClO_4$ (Fischer Scientific, Pittsburgh, PA) was used as well. NaOH and $HClO_4$ (Fischer Scientific, Pittsburgh, PA) were used to adjust the pH values of all the solutions in this study.

The electrochemical ALD cycle program used to grow CIS consisted of the following: the Se solution was flushed in to the cell for 5 s at the chosen potential, and then held quiescent for 15 s for deposition. The blank solution was then flushed through the cell at the same potential for 5 s, to rinse out excess $HSeO_3^-$ ions. The In solution was then flushed in to the cell for 5 s at In chosen potential and held quiescent for 15 s for deposition. The blank solution was then flushed through the cell at the same potential to remove excess In^{2+} ions from the cell. The Se solution was again flushed in to the cell for 5 s at the chosen Se potential, and then held quiescent for 15 s for deposition. The blank solution was then flushed through the cell at the same potential for 5 s, to rinse out excess $HSeO_3^-$ ions. Finally, the Cu solution was flushed through the cell for 5 s at the Cu deposition potential, and held quiescent for 15 s for deposition. Blank solution was again flushed through the cell for 5 s to rinse out excess Cu^{2+} ions from the cell. This process was referred to as one ALD cycle, and was repeated as many times as needed to form CIS deposits described in this report. The Cu_2Se deposit that will be reported in this paper was grown using the same ALD process without the InSe steps, whereas the InSe sample was grown similarly without the CuSe steps.

Microanalyses (EPMA) of the samples (Cu_2Se, InSe and CIS) were performed with a Joel JXA-8600 electron probe. Glancing angle X-ray diffraction patterns were obtained on a Scintag PAD V diffractometer, equipped with a 6" long set of Soller slits on the detector to improve resolution in the asymmetric diffraction configuration. The morphology of the deposits was characterized by a Molecular Imaging PicoPlus AFM instrument.

Results and Discussions

Prior to devising an EC-ALD cycle program, voltammetric behavior of Au on glass substrate into the solutions of the constituent elements of CIS compound being grown was assessed in order to determine to determine suitable UPD deposition of each element. Figure 1(a) shows the cyclic voltammetry of Au on glass electrode in 0.5 M $Cu(SO_4)_2$ solution where two distinctive reductive features are visible in the negative going scan at 0.28 V and -0.13 V corresponding to UPD Cu deposition and bulk Cu deposition respectively. In the positive going scan, oxidative peaks seen at 0.05 V and 0.34 V could be attributed to bulk Cu stripping and UPD Cu oxidation respectively. More surface limited Cu deposition could be obtained at potential values prior to -0.06 V which seems to be the formal potential of this system. Similar features had been previously reported by Vasiljevic et al. [35]. When the cyclic voltammetry of Se upd covered Au electrode was run in 0.5 M $Cu(SO_4)_2$ solution buffered with 50.0 mM $CH_3COONa.3H_2O$ as depicted in Figure 1(b), the Cu UPD peak seemed to have shifted to a more negative potential value of around 0.07 V (peak C2) compared to the Cu UPD peak on Au (peak

C1). When peak C1 was integrated, a coverage of around 0.4 monolayer was obtained indicating a surface limited deposition of Cu. Similar trend was observed during the positive going scan, where the oxidative stripping of Cu UPD appeared at 0.18 V (peak A2), a potential lower than the Cu UPD on Au (peak A1). The shift to more negative potential values seen in Figure 1(b) could be attributed to Cu atoms needing more energy or driving force in order to form a compound with Se than simply depositing on bare Au substrate.

Figure 2 shows the cyclic voltammetry of Au on glass electrode in 0.5 M $In_2(SO_4)_3.xH_2O$ solution to successive decreasing potentials. In the negative going scan, two reductive features are evident at around -0.35 V and -0.58 V which could be attributed to In UPD and bulk In deposition respectively. However, when the scan was reversed at -0.58 V, no clear oxidative was seen in the positive going scan. When the scan was reversed at -0.67 V, the only oxidative feature present in the positive going scan was the peak at around -0.28 V, which could be attributed to In UPD stripping. On the other hand, when the negative going scan is reversed at -0.8 V, a new oxidative feature which could be attributed to bulk In stripping appears at around -0.4 V in addition to a shoulder peak at -0.28 V (UPD In stripping).

Au cyclic voltammetry in 0.5 mM SeO_2 depicted in Figure 3 has been reported previously [29], where we had demonstrated that when the scan was reversed at potential range between -0.025 V and -0.3 V, the only oxidative feature present was the one at 0.6 V, positive of the formal potential. When the scan was reversed at potentials more negative than -0.3 V, the oxidative feature just positive of 0.4 V, attributed to bulk Se stripping, appeared. Selenium deposition is known to be kinetically slow [36-38]. Because of the slow kinetics, the peaks occurring from 0.1 V to -0.3 V in the negative going scan exhibit all the characteristics of surface limited deposition although they appear negative of the formal potential 0.4 V of HSO_3^-/Se.

Based on previous Se studies, the increase in reductive spike around -0.5 V is due to a combination of bulk Se deposition, hydrogen evolution and Se reduction to Se^{-2}, a soluble species [36, 38-39].

After careful studies of the cyclic voltammetries in Figures 1, 2 and 3, EC-ALD cycle programs were devised for the formation of Cu_2Se, InSe and CIS thin films respectively.

Cu_2Se Thin Film Deposition

Based on the cyclic voltammetries of Au on glass electrode in both Cu and Se solutions, potentials of -0.2 V and 0.05 V, which are both well in the surface limited regions in Figures 1 and 3, were chosen as possible starting points for Se and Cu respectively. Thus the initial Cu_2Se cycle consisted of filling the $HSeO_3^-$ solution into the cell for 5s at -0.2 V and holding quiescent for 15 s for deposition. The blank solution was then flushed through the cell at the same potential for 5 s, to rinse out excess $HSeO_3^-$ ions. The Cu^{2+} solution was then flushed in to the cell for 5 s at 0.05 V and held quiescent for 15 s for deposition. The blank solution was then flushed through the cell at the same potential to remove excess Cu^{2+} ions from the cell. This cycle was intended to form one monolayer of Cu_2Se, and was repeated as many times as needed to form compound films. However, when this program was attempted, Se deposition charges decreased over the first few cycles and no film growth was observed past the fifth cycle. This behavior which had been previously observed by this group and others [40-44] could be due to the fact that potentials were chosen based on the deposition on a Au surface and not on the growing compound. As the semiconductor film grows, especially over the first few cycles, the nature of the substrate greatly varies from the initial Au surface to the compound covered Au surface. The initial wider lattice mismatch between Au electrode and the growing compound evolves to epitaxial Cu_2Se layers being grown on Cu_2Se covered Au substrate.

Various EC-ALD programs were attempted, where only the deposition potential of one of the constituent element (either Cu or Se) was shifted. They all resulted in Cu to Se ratio values other than the expected 2. The successful EC-ALD cycle program for the growth of Cu_2Se was obtained when deposition potentials of Se and Cu were adjusted in different directions over 20 cycles and then held constant at final potential values for the remaining cycles of the EC-ALD deposition run. Se deposition potential was negatively shifted negatively over 20 cycles from -0.2 V to -0.35 V, while Cu deposition potential was positively ramped from 0.05 V to 0.1 V over the first 20 cycles. This particular sample was a 200 EC-ALD cycle deposit.

This sample resulted in a homogeneous deposit when observed under the optical microscope. Electron probe microanalysis (EPMA) results shown in Table 6 indicate a nearly stoichiometric (**$Cu_{2.1}Se$**) deposit. Similarly, a section of the current time traces recorded during the EC-ALD program of this sample shown in Figure 4 indicates that after the initial adjustment of deposition potentials of the first few cycles, the currents proceeded steadily throughout the remaining cycles of the deposition process.

Peaks (111), (220) and (311) corresponding to cubic Cu_2Se phase of face-centered lattice structure along with Au substrate peaks are evident in the x-ray diffraction pattern of the as deposited sample as shown in Figure 5. A well resolved strong (111) peak is the most predominant one. The intensity of Cu_2Se(220) peak remained unknown as it overlapped with Au(200) peak. However, no elemental peak due to either Se or Cu was seen in the XRD pattern attesting to the quality of the EC-ALD grown deposit.

InSe Thin Film Deposition

After successfully growing Cu_2Se, attempts were then made to form InSe thin films. The successful EC-ALD cycle program was obtained when constant deposition potentials for both In and Se were applied during the deposition process. The InSe cycle consisted of filling the $HSeO_3^-$ solution into the cell for 5s at -0.6 V and holding quiescent for 15 s for deposition. The blank solution was then flushed through the cell at the same potential for 5 s, to rinse out excess $HSeO_3^-$ ions. The In^{2+} solution was then flushed through the cell for 5 s at -0.75 V and held quiescent for 15 s for deposition. The blank solution was then flushed through the cell at the same potential to remove excess In^{2+} ions from the cell. This cycle was intended to form one monolayer of InSe, and was repeated as many times as needed to form compound films. In this case, the deposit consisted of 100 EC-ALD cycles.

Figure 6 shows a section of the current and potential time traces of successfully grown InSe deposit which appeared homogeneous when observed under the optical microscope. In contrast to Cu_2Se EC-ALD program, when constant potentials were applied for InSe EC-ALD program, the deposition currents remained steady throughout the deposition process. Electron probe microanalysis results of this sample resulted in nearly stoichiometric (**$InSe_{1.1}$**) deposit as shown by data in Table 7. Two peaks (101) and (004) corresponding to InSe were clearly evident in the XRD pattern of the as grown deposit shown in Figure 7. Once again no elemental peaks corresponding to either In or Se were seen in the XRD pattern of this sample.

$CuInSe_2$ Thin Films Deposition

As stated earlier, two major growth routes were attempted to grow CIS. In the first case, a ternary EC-ALD cycle program of CIS was attempted where a period consisting of one cycle of the binary compounds InSe and Cu_2Se was alternately deposited and repeated as many times as needed to form the desired CIS sample. In the second case, CIS was grown as a superlattice where more than one cycle of InSe was deposited within a period while the number of Cu_2Se

cycle was maintained at one. In addition to growing CIS as a superlattice, various other deposition parameters were varied in order to obtain the desired stoichiometric deposit.

Figure 8 shows a cartoon representation of the sequence in which the EC-ALD cycle program of the ternary CIS was grown. This period was repeated 50 times to grow the ternary CIS sample. Based on the cyclic voltammetries of Au on glass in the solutions of CIS constituent elements, potentials of 0.14 V, -0.7 V and -0.22 V were for the deposition of Cu, In and Se respectively. No 3-D growth was expected during this deposition program as all the chosen potential values are in the surface limited regions of the cyclic voltammetries of Au in the aforementioned solutions. Figure 9 shows a section of the current and potential time traces of the ternary CIS sample where the deposition potentials and the resulting currents of each constituent element of CIS are evident. However, oxidative currents are also observed every time the deposition potential is switched from In to Se steps, most likely due to In stripping since the chosen potential of -0.22 V for Se deposition is positive of In stripping potential of around -0.5 V. A similar behavior is observed when Se deposition potential of -0.22 V is switched to Cu deposition potential of 0.14 V, once again due to more In stripping as Se does not oxidatively strip until around 0.4 V. This sample appeared homogeneously grown when observed under the optical microscope. However when its composition measurements were taken by EPMA, this program resulted in a nonstoichiometric (**$Cu_{2.4}InSe_{2.4}$**) deposit as depicted by the data at the bottom left corner of Figure 9. More than needed Cu amount and a little excess of Se were present in the sample. The loss of In, suspected earlier during both Cu and Se deposition time, was confirmed by the EPMA results. The question was then how do we keep enough In amount in the deposit and still have enough amounts Cu and Se to attain the ideal CIS stoichiometry? One possible way of solving this problem would be to reduce Cu deposition time in the ternary

EC-ALD program to reduce the amount of In that could be stripped. Reducing Cu deposition time is not expected to affect the amount of Cu in the deposit by much as Cu UPD deposition is a reversible and kinetically fast process [45-46]. Another possibility would be to grow CIS as a superlattice by increasing the number of InSe cycles within the CIS period while the number of Cu_2Se cycle is maintained at one. As In would be bound to Se and some of its layers would be buried by the InSe layer closest to Cu_2Se layer, growing CIS as superlattice could result in fewer In being lost during Cu deposition time.

An attempt to grow CIS as a superlattice was then undertaken, where constant potentials of 0.14 V, -0.7 V and -0.65 V were applied for Cu, In and Se respectively. Knowing that Se deposition process is a slow process [36-38] as its irreversibility is clearly evident in the cyclic voltammetry in Figure 3, its deposition time was doubled from 15 s to 30 s, in order to allow its reactions to reach completion. Three experiments were carried out where the samples shown in Table 8 were grown with varying number of InSe cycles. The three films looked more or less homogeneous when inspected by the optical microscope. However, varying InSe cycles from 2, 3 to 4 did not result in the expected increase of In amount in the CIS stoichiometry as the EPMA data showed in Table 8, where it is evident that all the three samples appeared to have similar In amount and CIS stoichiometry. However there was a slight increase in In amount and better CIS stoichiometry in superlattice CIS deposits compared to ternary CIS deposit.

Having attained an average CIS stoichiometry of $\mathbf{Cu_{1.5}InSe_2}$ in the superlattice CIS deposit, studies of the effects of Cu deposition time on CIS stoichiometry were then carried out, since less In would be expected to strip, the less Cu deposition time became. Four superlattice experiments during which four samples consisting of 25 periods of 3 InSe cycles and 1 CuSe cycle were grown with Cu deposition time held for 15, 10, 5 and 3 s, were carried out. To grow these samples, constant deposition potentials of 0.14 V, -0.7 V and -0.65 V were used for Cu, In and Se respectively. Figure 10 shows the effects of varying Cu deposition time on the atomic percentage values of constituent elements of CIS samples. As expected, In amount in the CIS stoichiometry increased, while Cu went down as Cu deposition time was decreased from 15 to 3 s. Se amount in the CIS stoichiometry remained steady when comparing sample IV grown with 15 s Cu deposition time to sample I grown with 3 s deposition time. The CIS sample with the best stoichiometry (**$Cu_{1.1}InSe_{1.9}$**) was sample I, grown with 3 s Cu deposition time. A section of its current and potential time traces and EPMA data are shown in Figure 11, where the deposition currents of the cycles of constituent elements of CIS are evident. Cu deposition time of 3 s appears to be enough for the reductive currents of Cu deposition to be evident in Figure 11. The X-ray diffraction pattern of the as grown deposit of this superlattice CIS sample is shown in Figure 12, where (111), (116/246) and (204/220) peaks corresponding to the chalcopyrite structure are present. Morphological studies of this sample was carried out by intermittent contact mode atomic force microscopy as shown by the images in Figure 13 that depicts an image of Au on glass electrode and an image of (**$Cu_{1.1}InSe_{1.9}$**) CIS sample. The image resolution was 512/512 and all the images were processed and analyzed using WSXM software. The image of the deposit seems more or less conformal to the image of the substrate. Further morphological studies using scanning tunneling microscope are currently being carried out and pending.

Conclusion

This report presented the electrodeposition of Cu_2Se, InSe and $CuInSe_2$ thin films using electrochemical atomic layer deposition. Nearly stoichiometric $Cu_{2.1}Se$ and $InSe_{1.1}$ were obtained as confirmed by EPMA data of their deposits. Expected peaks were obtained in their X-ray diffraction patterns. CIS samples grown using the ternary and superlattice EC-ALD cycle programs were presented. The nearly stoichiometric (**$Cu_{1.1}InSe_{1.9}$**) CIS sample, as confirmed by EPMA results, was obtained from the 25P/3InSe/1CuSe superlattice program where Cu deposition time was reduced to 3 s, while steady potentials were applied for the constituent elements of CIS. The film appeared homogeneously distributed when observed under the optical microscope as it was confirmed by EPMA results. The crystal structure studies revealed that the stoichiometric CIS sample was chalcopyrite in nature. AFM indicated the images of the Au substrate and the CIS sample to be conformal. Additional studies are being carried out for the determination of the optical and electronic properties of the EC-ALD grown CIS samples, while further morphological studies by scanning tunneling microscope are also pending.

Acknowledgements

Support from the National Science Foundation is gratefully acknowledged.

References

1. Pathan, H.M. and C.D. Lokhande, *Chemical deposition and characterization of copper indium diselenide (CISe) thin films.* Applied Surface Science, 2005. **245**(1-4): p. 328-334.
2. Yoon, S., et al. *Nanoparticle-based approach for the formation of CIS solar cells*. 2009.
3. Postnikov, A.V. and M.V. Yakushev. *Lattice dynamics and stability of CuInSe2*. 2004.
4. Al-Bassam, A.A.I., *Electrodeposition of CuInSe2 thin films and their characteristics.* Physica B: Condensed Matter, 1999. **266**(3): p. 192-197.
5. Kemell, M., M. Ritala, and M. Leskela, *Thin film deposition methods for CulnSe(2) solar cells.* Critical Reviews in Solid State and Materials Sciences, 2005. **30**(1): p. 1-31.
6. Ingrid, R., et al., *Short Communication: Accelerated Publication 19·9%-efficient ZnO/CdS/CuInGaSe2 solar cell with 81·2% fill factor.* Progress in Photovoltaics: Research and Applications, 2008. **16**(3): p. 235-239.
7. Ashida, A., et al., *CuInSe2 Thin-Film Prepared by Evaporation of Cu2Se and In2Se3.* Japanese Journal of Applied Physics Part 1-Regular Papers Short Notes & Review Papers, 1993. **32**: p. 84-85.
8. Dejene, F.B., *The structural and material properties of CuInSe2 and Cu(In,Ga)Se2 prepared by selenization of stacks of metal and compound precursors by Se vapor for solar cell applications.* Solar Energy Materials and Solar Cells, 2009. **93**(5): p. 577-582.
9. Guillen, C. and J. Herrero, *Structure, morphology and photoelectrochemical activity of CuInSe2 thin films as determined by the characteristics of evaporated metallic precursors.* Solar Energy Materials and Solar Cells, 2002. **73**(2): p. 141-149.
10. Ashida, A., et al., *CuInSe2 Thin-Films Prepared by Quasi-Flash Evaporation of In2Se3 and Cu2Se.* Journal of Materials Science Letters, 1994. **13**(16): p. 1181-1184.

11. Djellal, L., et al., *Bulk p-CuInSe2 photo-electrochemical solar cells.* Solar Energy Materials & Solar Cells, 2008. **92**(5): p. 594-600.

12. Fischer, D., et al., *Structural properties and growth mechanism of CuGaSe2 thin films for solar cells grown by two-source CVD*, in *Polycrystalline Semiconductors Iv Materials, Technologies and Large Area Electronics*. 2001, Trans Tech Publications Ltd: Zurich-Uetikon. p. 275-280.

13. Guillen, C., M.A. Martinez, and J. Herrero, *CuInSe2 thin films obtained by a novel electrodeposition and sputtering combined method.* Vacuum, 2000. **58**(4): p. 594-601.

14. Shirakata, S., et al., *Preparation of CuInSe2 thin-films by chemical spray-pyrolysis.* Japanese Journal Of Applied Physics Part, 1996. **35**: p. 191-199.

15. Terasako, T., S. Shirakata, and S. Isomura, *Photoacoustic spectra of CuInSe2 thin films prepared by chemical spray pyrolysis.* Japanese Journal of Applied Physics Part 1-Regular Papers Short Notes & Review Papers, 1999. **38**(8): p. 4656-4660.

16. Chassaing, E., et al., *New insights in the electrodeposition mechanism of CuInSe2 thin films for solar cell applications.* Physica Status Solidi C: Current Topics in Solid State Physics, 2008. **5**(11): p. 3445-3448.

17. Bhattacharya, R.N., *Solution growth and electrodeposited CuInSe2 thin films.* J. Electrochem. Soc., 1983. **130**: p. 2040.

18. C. Guillen, J.H., *Effects of thermal and chemical treatments on the composition and structure of electrodeposited CuInSe2 thin films.* J. Electrochem. Soc., 1994. **141**: p. 225.

19. Calixto, M.E., et al. *Compositional and optoelectronic properties of CIS and CIGS thin films formed by electrodeposition*. 1999.

20. Dharmadasa, I.M., R.P. Burton, and M. Simmonds, *Electrodeposition of CuInSe2 layers using a two-electrode system for applications in multi-layer graded bandgap solar cells.* Solar Energy Materials & Solar Cells, 2006. **90**(15): p. 2191-2200.

21. Valdes, M., M. Vazquez, and A. Goossens, *Electrodeposition of CuInSe2 and In2Se3 on flat and nanoporous TiO2 substrates.* Electrochimica Acta, 2008. **54**(2): p. 524-529.

22. Endo, S., Y. Nagahori, and S. Nomura, *Preparation of CuInSe2 thin films by the pulse-plated electrodeposition.* JJAP, 1996. **35**: p. L1101.

23. Guillen, C. and J. Herrero, *Improved Selenization procedure to obtain CuInSe2 thin films from sequentially electrodeposited precursors.* JECS, 1996. **143**: p. 493.

24. Adzic, R.R., in *Advances in Electrochemistry and Electrochemical Engineering*, H. Gerishcher and C.W. Tobias, Editors. 1984, Wiley-Interscience: New York. p. 159.

25. Adzic, R.R., et al., *Electrocatalysis by foreign metal monolayers: oxidation of formic acid on platinum.* JEC, 1975. **65**: p. 587-601.

26. Kolb, D.M., *Physical and Electrochemical Properties of Metal Monolayers on Metallic Substrates*, in *Advances in Electrochemistry and Electrochemical Engineering*, H. Gerischer and C.W. Tobias, Editors. 1978, John Wiley: New York. p. 125.

27. Kolb, D.M. and H. Gerisher, *Further aspects concerning the correlation between underpotential depsoition and work function defferences.* SS, 1975. **51**: p. 323.

28. Kolb, D.M., Przasnys.M, and Gerische.H, *Underpotential Deposition of Metals and Work Function Differences.* Journal of Electroanalytical Chemistry, 1974. **54**(1): p. 25-38.

29. Banga, D., et al., *Optimization of PbSe Nanofilms formation by Electrochemical Atomic Layer Deposition (ALD).* ECS Transactions, 2009. **19**(3): p. 245-272.

30. Banga, D.O., et al., *Formation of PbTe nanofilms by electrochemical atomic layer deposition (ALD).* Electrochimica Acta, 2008. **53**(23): p. 6988-6994.

31. Venkatasamy, V., et al., *Optimization studies of CdTe nanofilm formation by electrochemical atomic layer epitaxy (EC-ALE).* J. Appl. Electrochem., 2006. **36**: p. 1223.

32. Zhu, W., et al., *Electrochemical atom-by-atom growth of highly uniform thin sheets of thermoelectric bismuth telluride via the route of ECALE.* Journal of Electroanalytical Chemistry, 2008. **614**(1-2): p. 41-48.

33. Vaidyanathan, R., et al., *Preliminary studies in the electrodeposition of PbSe/PbTe superlattice thin films via electrochemical atomic layer deposition (ALD).* Langmuir, 2006. **22**(25): p. 10590-10595.

34. Zhu, W., et al., *Electrochemical aspects and structure characterization of VA-VIA compound semiconductor Bi2Te3/Sb2Te3 superlattice thin films via electrochemical atomic layer epitaxy.* Langmuir, 2008. **24**(11): p. 5919-5924.

35. Vasiljevic, N., et al., *High resolution electrochemical STM: New structural results for underpotentially deposited Cu on Au(111) in acid sulfate solution.* Journal of Electroanalytical Chemistry, 2008. **613**(2): p. 118-124.

36. Huang, B.M., T.E. Lister, and J.L. Stickney, *Se adlattices formed on Au (100), studies by LEED, AES, STM and electrochemistry.* Surface Science, 1997. **392**(1-3): p. 27.

37. Lister, T.E., et al., *Electrochemical formation of Se atomic layers on Au(100).* J. Vac. Sci. Technol. B, 1995. **13**: p. 1268.

38. Lister, T.E. and J.L. Stickney, *Atomic level studies of selenium electrodeposition on gold (111) and gold (110).* Journal of Physical Chemistry, 1996. **100**(50): p. 19568-19576.

39. Lister, T.E., et al., *Electrochemical Formation of Se Atomic Layers On Au(100).* Journal of Vacuum Science & Technology B, 1995. **13**(3): p. 1268.

40. Vaidyanathan, R., et al., *Electrodeposition of Cu2Se thin films by electrochemical atomic layer epitaxy (EC-ALE).* Materials Research Society Symposium Proceedings, 2003. **744**(Progress in Semiconductors II--Electronic and Optoelectronic Applications): p. 289-294.

41. Vaidyanathan, R., J.L. Stickney, and U. Happek, *Quantum confinement in PbSe thin films electrodeposited by electrochemical atomic layer epitaxy (EC-ALE).* Electrochimica Acta, 2004. **49**(8): p. 1321-1326.

42. Wade, T.L., et al. *Morphology control in the formation of compound semiconductors using electrochemical atomic layer epitaxy (EC-ALE)*. in *Electrochemical Society National Meeting*. 2001. Washington D.C.: Electrochemcial Society.

43. Yang, J.Y., et al., *Formation and characterization of Sb2Te3 nanofilms on Pt by electrochemical atomic layer epitaxy.* Journal of Physical Chemistry B, 2006. **110**(10): p. 4599-4604.

44. Zhu, W., et al., *Effect of potential on bismuth telluride thin film growth by electrochemical atomic layer epitaxy.* Electrochimica Acta, 2005. **50**(20): p. 4041-4047.

45. Herrero, E., L.J. Buller, and H.D. Abruna, *Underpotential Deposition at Single Crystal Electrodes Surfaces of Au, Pt, Ag and other Materials.* Chemical Reviews, 2001. **101**: p. 1897-1930.

46. Kim, J.Y., Y.-G. Kim, and J.L. Stickney, *Cu nanofilm formation by electrochemical atomic layer deposition (ALD) in the presence of chloride ions.* Journal of Electroanalytical Chemistry, 2008. **621**(2): p. 205-213.

Table 6: Electron Probe Microanalysis (EPMA) data of a 200 ALD cycle Cu_2Se sample grown on Au on glass when Se and Cu were ramped from -0.2 V and 0.05 V to -0.35 V and 0.1 V respectively. Electrode area: 4 cm^2.

Sample	Cu_2Se Thin Film
Cu Atomic %	44
Se Atomic %	21
Au Atomic %	35
Cu/Se Ratio	2.1
Stoichiometry	$Cu_{2.1}Se$

Table 7: Electron Probe Microanalysis (EPMA) data of a 100 ALD cycle InSe sample grown on Au on glass when both Se and In were held constant at -0.6 V and -0.75 V respectively. Electrode area: 4 cm^2.

Sample	InSe Thin Film
In Atomic %	14.0
Se Atomic %	15.9
Au Atomic %	70.1
Se/In Ratio	1.1
Stoichiometry	$InSe_{1.1}$

Table 8. Electron Probe Microanalysis (EPMA) data of Superlattice CIS samples grown on Au on glass electrode with Se, In and Cu deposited at -0.65 V, -0.7 V, and 0.14 V respectively. Se deposition time was doubled from 15 s to 30 s. Electrode area: 4 cm^2.

Superlattice CIS Samples	Cu at.%	In at.%	Se at.%	Stoichiometry
34P:2InSe:1CuSe	33	22	44	**$Cu_{1.5}InSe_2$**
25P:3InSe:1CuSe	35	22	43	**$Cu_{1.5}InSe_{1.9}$**
20P:4InSe:1CuSe	35	22	43	**$Cu_{1.6}InSe_2$**

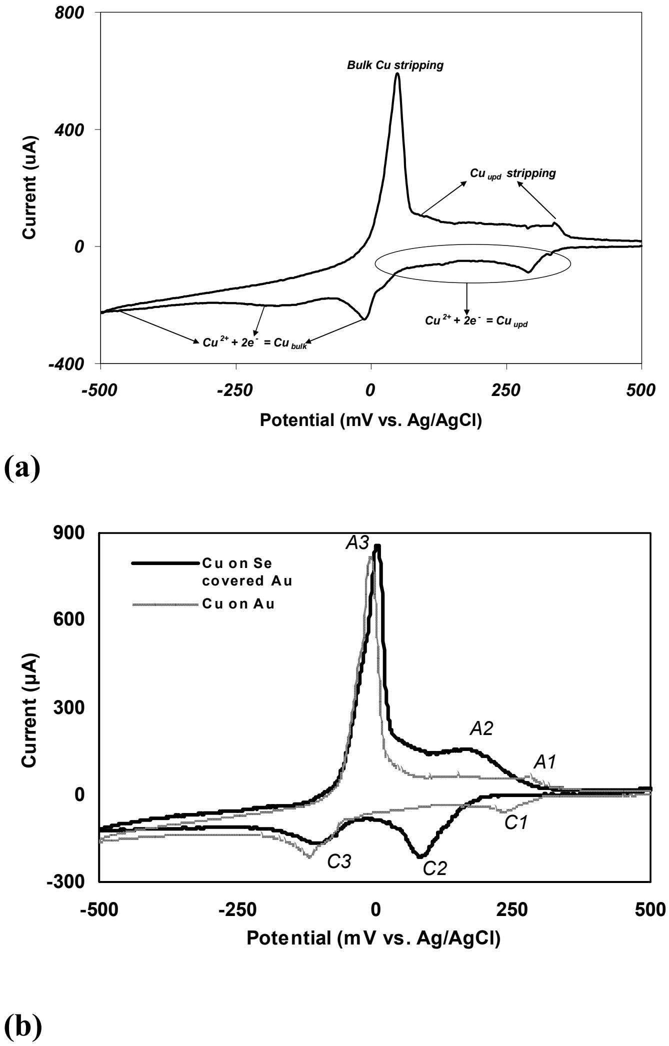

(a)

(b)

Figure 6.1: Cyclic voltammetries of (a) Au electrode in 0.5 mM $Cu(SO_4)_2$ buffered with 50.0 mM $CH_3COONa.3H_2O$, and (b) comparison of Au electrode to Se covered Au electrode in 0.5 mM $Cu(SO_4)_2$, pH 4.5, (electrode area: 4 cm^2, scan rate: 10 mV s^{-1}).

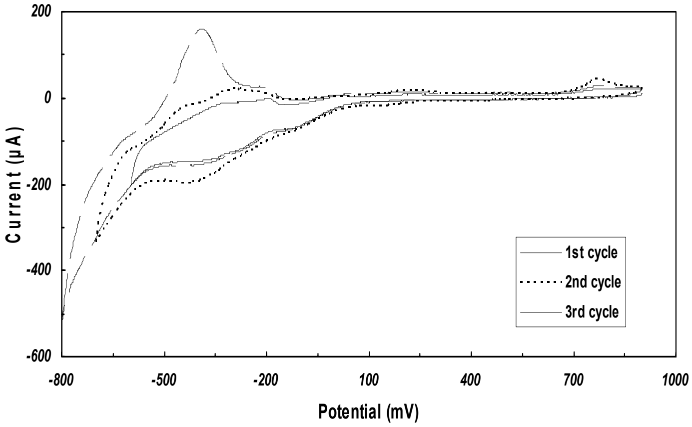

Figure 6.2: Cyclic voltammetry of Au electrode in 0.5 mM $In_2(SO_4)_3.xH_2O$, pH 3, (electrode area: 4 cm^2, scan rate: 10 mV s^{-1}).

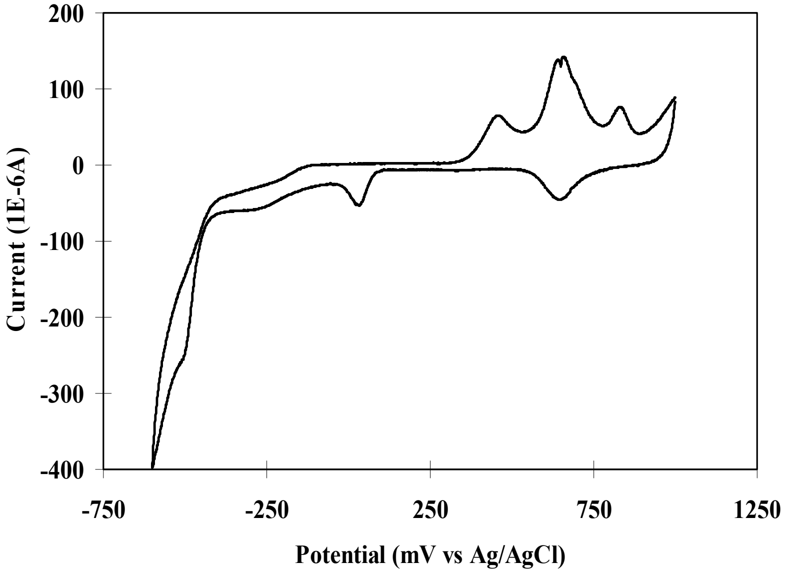

Figure 6.3: Cyclic voltammetry of Au electrode in 0.5 mM $HSeO_3^+$, pH 5, (electrode area: 4 cm^2, scan rate: 10 mV s^{-1}).

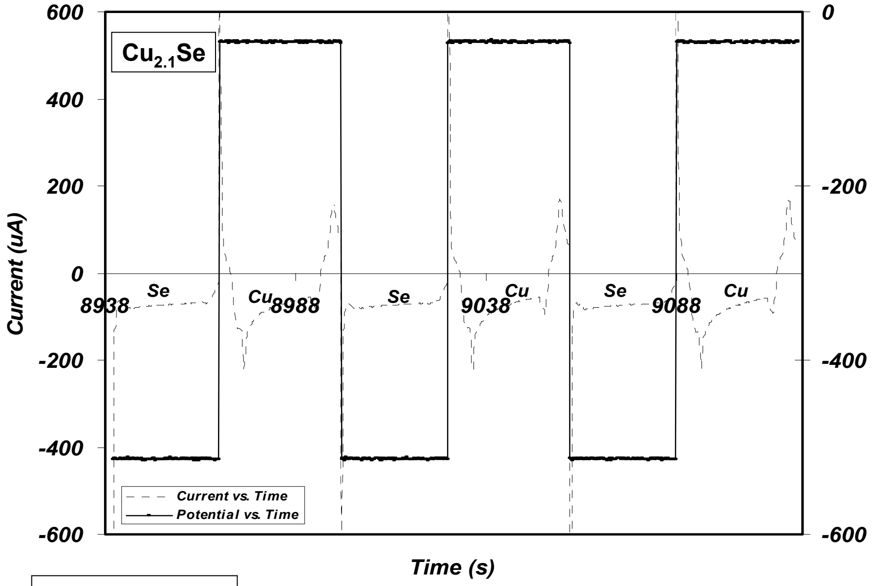

EPMA Atomic %
Se: 32
Cu: 68

Figure 6.4: A section of current time traces the 200 ALD-cycle Cu_2Se sample grown on Au on glass when Se and Cu were ramped from -0.2 V and 0.05 V to -0.35 V and 0.1 V respectively. Electrode area: 4 cm^2.

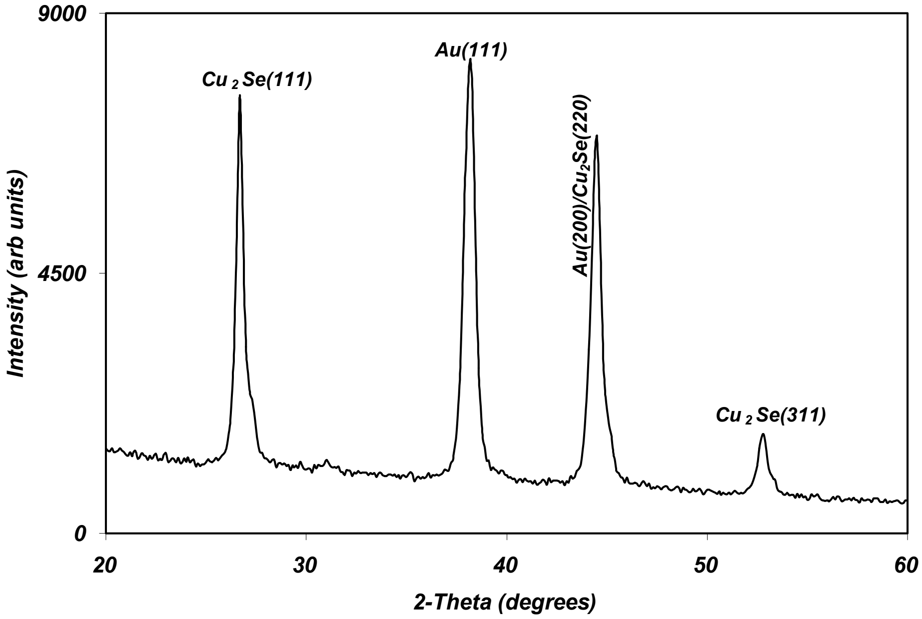

Figure 6.5: X-ray diffraction pattern of the 200 ALD-cycle Cu_2Se sample grown on Au on glass when Se and Cu were ramped from -0.2 V and 0.05 V to -0.35 V and 0.1 V respectively. Angle of incidence is 0.1°, Cu Kα source. Electrode area: 4 cm^2.

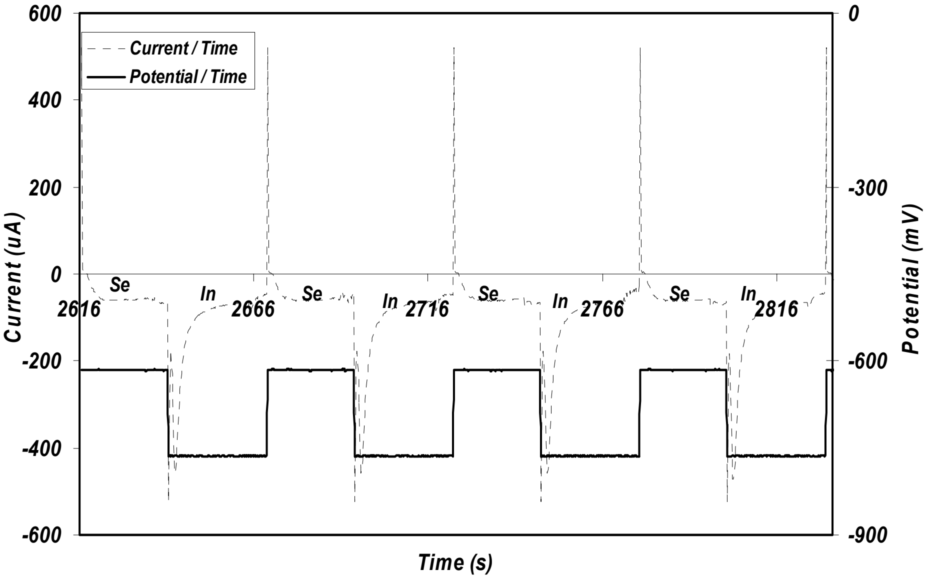

EPMA Atomic %
Se: 53
In: 47

Figure 6.6: A section of current time traces the 100 ALD-cycle InSe sample grown on Au on glass when both Se and In were held steady at -0.6 V and -0.75 V respectively throughout the deposition run. Electrode area: 4 cm^2.

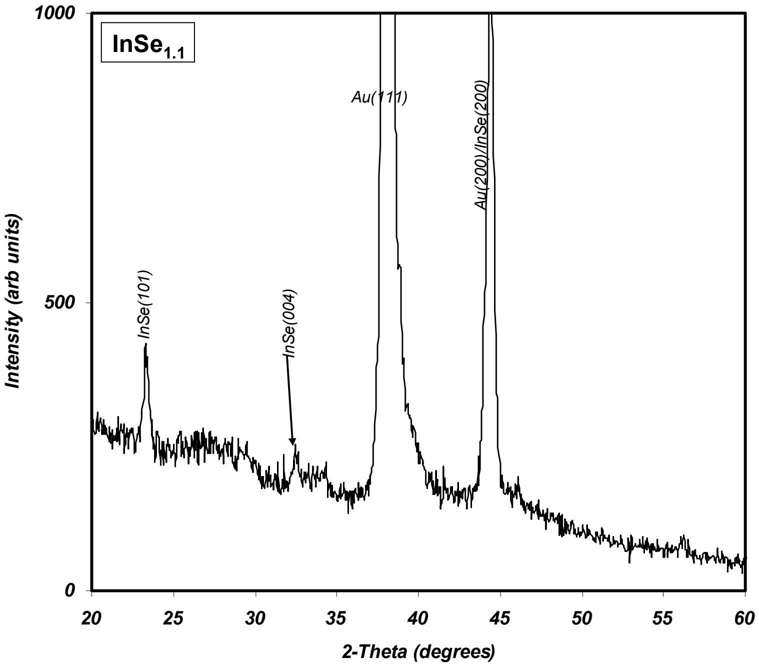

Figure 6.7: X-ray diffraction pattern of the 100 ALD-cycle InSe sample grown on Au on glass when both Se and In were held steady at -0.6 V and -0.75 V respectively throughout the deposition run. Angle of incidence is 0.1°, Cu Kα source. Electrode area: 4 cm^2.

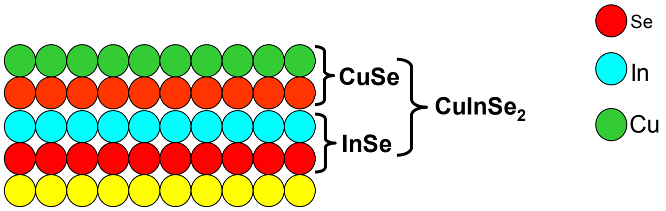

Figure 6.8: A cartoon of CIS sequence grown as a ternary In, Se, and Cu

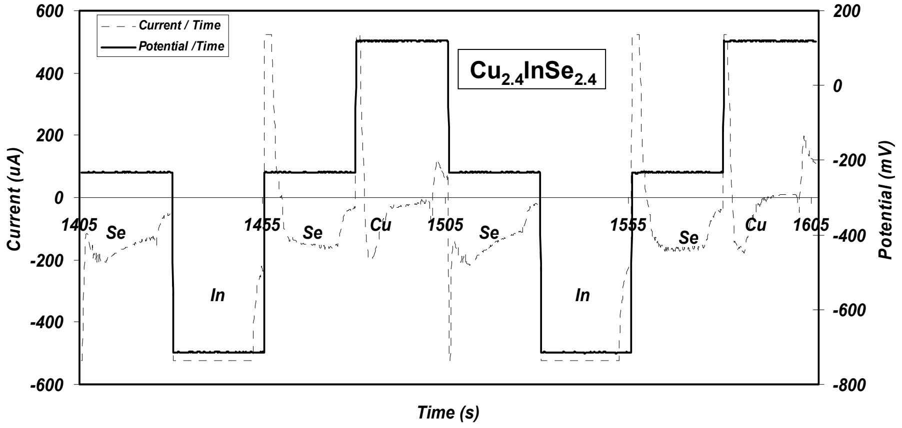

EPMA Atomic %
Cu: 41.5
In: 17
Se: 41.5

Figure 6.9: A section of current and potential time traces of the ternary CIS with Se, In and Cu deposited at -0.22 V, -0.7 V, and 0.14 V and the resulting EPMA data of the deposit. Electrode area: 4 cm^2

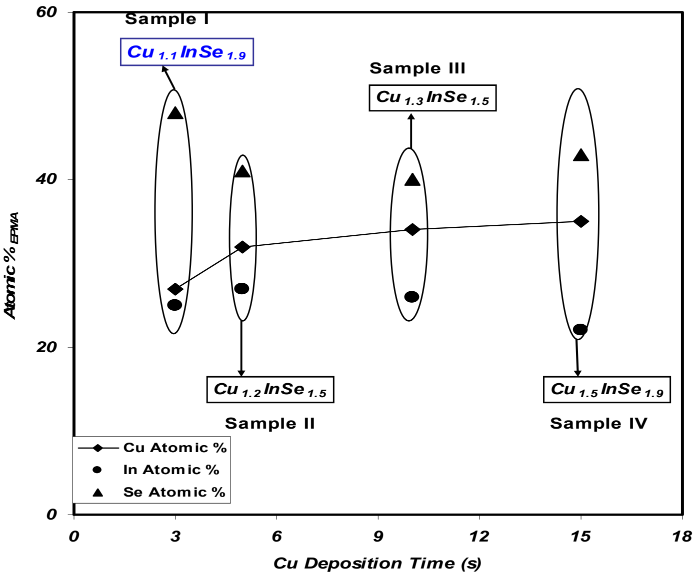

Figure 6.10: The effects of varying Cu deposition time on the atomic percentage values of constituent elements of 25P/3InSe/CuSe CIS samples grown on Au on glass electrode at varying Cu deposition time. Electrode area: 4 cm^2.

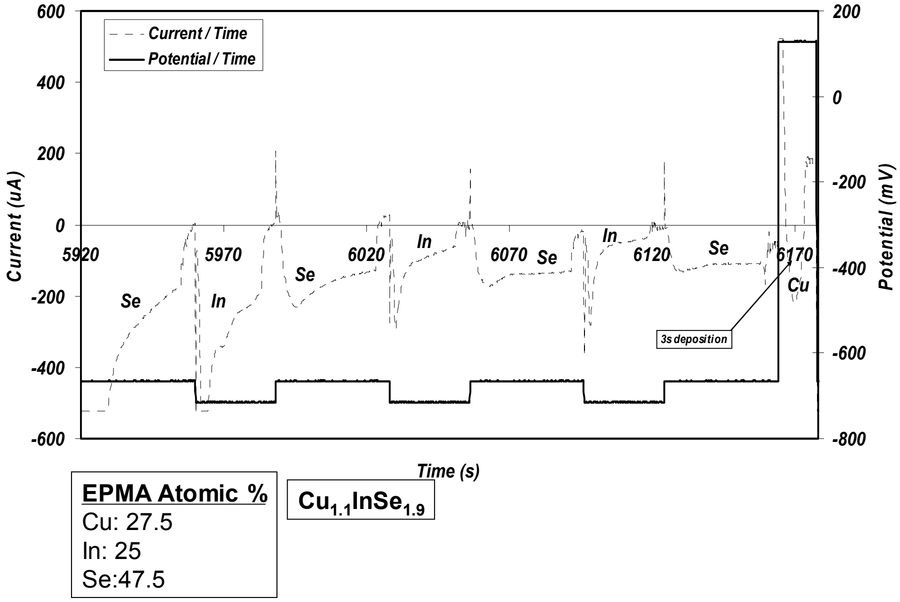

EPMA Atomic %
Cu: 27.5
In: 25
Se:47.5

$Cu_{1.1}InSe_{1.9}$

Figure 6.11: A section of current and potential time traces and the resulting EPMA data of a 25P/3InSe/CuSe CIS sample grown on Au on glass electrode with Cu deposition time of 3 s and constant deposition potentials of -0.65 V, -0.7 V, and 0.14 V for Se, In and Cu respectively. Electrode area: 4 cm^2.

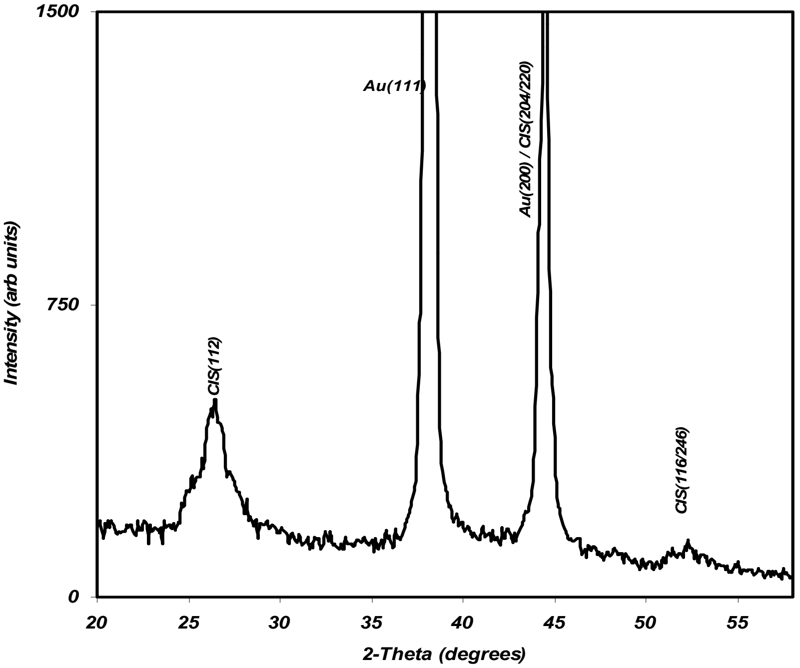

Figure 6.12: XRD pattern of a 25P/3InSe/1CuSe superlattice CIS sample with Cu deposition time of 3 s and constant deposition potentials of -0.65 V, -0.7 V and 0.14 V for Se, In and Cu respectively. Electrode area: 4 cm^2.

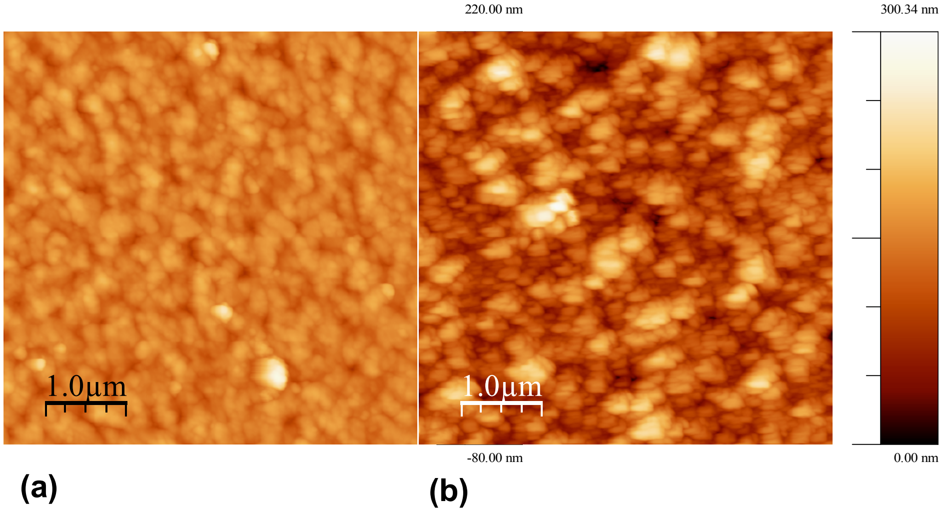

Figure 6.13: AFM images of (a) Au on glass electrode and (b) a 25P/3InSe/1CuSe superlattice CIS sample with Cu deposition time of 3 s and constant deposition potentials of -0.65 V, -0.7 V, and 0.14 V for Se, In and Cu respectively. Electrode area: 4 cm^2.

CHAPTER 7

FORMATION OF $CuIn_{(1-x)}Ga_xSe_2$ BY ELECTROCHEMICAL ATOMIC LAYER DEPOSITION (ALD)[6]

---

[6] Banga, D., et al. To be submitted to Journal of The Electrochemical Society.

Abstract

The formation of $CuIn_{(1-x)}Ga_xSe_2$ will be reported using electrochemical atomic layer deposition in this paper. Two different deposition routes of CIGS consisting of growing a quaternary CIGS by combining individual binary compounds, and growing CIGS as a superlattice by depositing more than an ALD cycle for one of the binary compounds of CIGS in order to obtain the desired stoichiometry will be presented. Electron probe micro analysis will be used for the studies of the composition of the various deposits that will be reported. Discussions on how samples with various CIGS stoichiometry values ($Cu_{2.3}In_{0.6}Ga_{0.4}Se_{2.3}$, $Cu_{1.2}In_{0.9}Ga_{0.1}Se_{1.9}$, $Cu_{1.2}In_{0.8}Ga_{0.2}Se_{2.1}$, and $\mathbf{CuIn_{0.7}Ga_{0.3}Se_2}$) were obtained will be discussed. XRD patterns depicting the chalcopyrite nature of the ALD grown CIGS samples will also be reported.

Introduction

The interest in renewable energy source has pushed intense research in technologies of solar energy conversion as the energy source is readily available and provides such an enormous supply of renewable energy that could solve the whole global energy demand. The reason behind the interest in solar cells is that they are easy to install and use, and they have proven to be very stable under both normal operating conditions as well as under irradiation by X-rays, electrons and protons, and are reliable [1], thus minimizing the need for continuous maintenance. Various solar cells consisting of various materials such as single crystal silicon [2], polycrystalline silicon [3], thin films (amorphous silicon [4], CdTe [5-6], $CuInSe_2$ [7-8], $Cu(InGa)Se_2$ [9-12]) and multi-junction $GaInP_2/GaAs/Ge$ [13] have been studied or manufactured. One of the most studied photovoltaic materials has been $CuIn_{(1-x)}Ga_xSe_2$ (CIGS) absorber, as recent publications have demonstrated laboratory scale solar devices having up to 19.5 % or higher (19.9 %) conversion efficiency and favorable optical properties due to its direct tunable band gap and high absorption coefficient ($\alpha > 10^5$ cm^{-2})[12, 14-17]. Moreover, only thin films of CIGS (few micrometers) are needed in the solar cells, compared to the thick slices of bulk silicon, thus reducing the consumption of materials during its manufacturing process.

Various techniques known to have been used to grow CIGS have included co-evaporation [17], flash evaporation [18], sputtering [19], molecular beam epitaxy [20], spray pyrolysis [21], chemical bath deposition [22] and co-deposition [12, 23-31]. Another very common methods used in the industry have consisted in depositing Cu, In and Ga layers and using the selenization process to incorporate Se [32-33].

This chapter will present the electrodeposition of $CuIn_{(1-x)}Ga_xSe_2$ films using electrochemical atomic layer deposition (EC-ALD). EC-ALD is an electrodeposition technique based on the use of surface limited reactions known as under potential deposition (UPD), a phenomenon where an atomic layer is deposited on the second at a potential prior to its formal potential [34-38] to form deposits with atomic level control. The advantages of EC-ALD include the ability to perform at room temperature, which considerably minimizes the interdiffusion in layers of the deposits and the ability to break the deposition process into a sequence of individually controllable steps thus allowing the ability to optimize the process. In addition, no annealing has so far been required for the crystal structure of the electrochemical ALD grown thin films [39-43] and superlattices [44] to become visible in the X-ray diffraction pattern.

Two major deposition routes will be discussed in this report. The first case will show an unsuccessful attempt to grow CIGS using a quaternary ALD cycle program where single binary compounds of the constituent elements will be combined and repeated in as many cycles as needed. In the second case, CIGS will be grown as superlattice where more than one ALD cycle of one of the binary compounds will be deposited within the period of CIGS. Then the period will be repeated as many times as needed to form the superlattice.

Experimental

An automated thin layer flow electrodeposition system consisting of a series of solution reservoirs, computer controlled pumps, valves, a thin layer electrochemical flow cell and a potentiostat was used in this study to grow CIGS films. The reference electrode, Ag/AgCl (3M NaCl) (Bioanalytical systems, Inc., West Lafayette, IN), was held by a simple O-ring and the auxiliary electrode was a Au wire embedded into the Plexiglas flow cell. The electrochemical flow cell was designed to promote laminar flow. The cell volume was about 0.3 mL and solutions were pumped at 50 mL min^{-1}. The system was contained within a nitrogen purged Plexiglas box to reduce the influence of oxygen during electrodeposition.

Substrates used in the study consisted of 300 nm thick vapor deposited gold on glass microscope slides. Prior to insertion into the vapor deposition chamber, the glass slides were cleaned in HF, and rinsed with copious amounts of deionized water from a Nanopure water filtration system (Barnstead, Dubuque, IA), fed from the house distilled water system. Deposition began with 3 nm of Ti, as an adhesion layer, followed by 300 nm of Au deposition at around 250 ^{o}C. The glass slides were then annealed in the deposition chamber at 400 ^{o}C for 12 hours, while the pressure was maintained at 10^{-6} Torr.

Reagent grade or better chemicals and deionized water were used to prepare the three different solutions used in this study. The copper solution consisted of 0.5 mM $Cu(SO_4)_2$ (Alfa Aesar, Ward Hill, MA), pH 4.5, with 0.1 M $NaClO_4$ (Fischer Scientific, Pittsburgh, PA) as the supporting electrolyte. The indium solution consisted of 0.5 mM $In_2(SO_4)_3.xH_2O$ (Alfa Aesar, Ward Hill, MA), pH 3, with 0.1 M $NaClO_4$ (Fischer Scientific, Pittsburgh, PA) as the supporting electrolyte. The gallium solution was obtained from 1 mM $Ga_2(SO_4)_3$ (Alfa Aesar, Ward Hill, MA), pH 3, with 0.1 M $NaClO_4$ (Fischer Scientific, Pittsburgh, PA) as the supporting electrolyte. The selenium solution was made of 0.5 mM SeO_2 (Alfa Aesar, Ward Hill, MA), pH 5, buffered with 50.0 mM $CH_3COONa.3H_2O$ and 0.1 M $NaClO_4$ (Fischer Scientific, Pittsburgh, PA) as the supporting electrolyte. A pH 3 blank solution of 0.1 M $NaClO_4$ (Fischer Scientific, Pittsburgh, PA) was used as well. NaOH and $HClO_4$ (Fischer Scientific, Pittsburgh, PA) were used to adjust the pH values of all the solutions in this study.

The electrochemical ALD cycle program used to grow CIGS in the first case consisted of the following: the Se solution was flushed in to the cell for 5 s at the chosen potential, and then held quiescent for 15 s for deposition. The blank solution was then flushed through the cell at the same potential for 5 s, to rinse out excess $HSeO_2^-$ ions. The Ga solution was then flushed in to the cell for 5 sec at Ga chosen potential and held quiescent for 15 s for deposition. The blank solution was then flushed through the cell at the same potential to remove excess Ga^{2+} ions from the cell. The Se solution was again flushed in to the cell for 5 s at the chosen Se potential, and then held quiescent for 15 s for deposition. The blank solution was then flushed through the cell at the same potential for 5 s, to rinse out excess $HSeO_3^+$ ions. The In solution was then flushed through the cell for 5 s at the In deposition potential, and held quiescent for 15 s for deposition. Blank solution was again flushed through the cell for 5 s to rinse out excess In^{2+} ions from the cell. The Se solution was repeated again as described earlier using the Se chosen potential. Finally, the Cu solution was flushed through the cell for 5 s at the Cu deposition potential, and held quiescent for 15 s for deposition. Blank solution was again flushed through the cell for 5 s to rinse out excess Cu^{2+} ions from the cell. This process was referred to as one ALD cycle, and was repeated as many times as needed to form CIGS described in the first case reported in this report.

In the second case where CIGS was grown as a superlattice, the ALD cycle deposition program is similar to the one described in the previous paragraph, except the number of cycles for the binary compounds was varied and its effects on the composition of the obtained CIGS samples deposits will be evaluated. Moreover, the effects of changing the sequence of the binary compounds within the period of the superlattice deposit will also be assessed. Three different samples consisting of superlattices of 2InSe/1GaSe/1CuSe, 2InSe/2GaSe/1CuSe and 2GaSe/2InSe/1CuSe binary compound cycles will be grown using the superlattice ALD program and discussed. In all the three CIGS samples obtained as superlattices, Cu deposition time was reduced to 5 s whereas Se deposition time was doubled to 30 s.

Microanalyses (EPMA) of the samples were performed with a Joel JXA-8600 electron probe. Glancing angle X-ray diffraction patterns were obtained on a Scintag PAD V diffractometer, equipped with a 6” long set of Soller slits on the detector to improve resolution in the asymmetric diffraction configuration.

Results and Discussions

Cyclic voltammograms of Au in separate Cu, In, Ga and Se solutions were studied to determine suitable UPD deposition of each element. Figure 1 shows the cyclic voltammogram of Au on glass electrode in 0.5 M $Cu(SO_4)_2$ solution where 3 distinctive reductive features are visible in the negative going scan at 0.25 V, -0.03 V and -0.53 V corresponding to the onset of UPD Cu deposition, the onset of bulk Cu deposition and the onset of hydrogen evolution respectively. In the positive going scan, oxidative peaks seen at 0.03 V and 0.23 V could be attributed to bulk Cu stripping and UPD Cu oxidation respectively. Similar features had been previously reported by Vasiljevic et al. [45]. Figure 2 shows the cyclic voltammograms of Au on glass electrode in 0.5 M $In_2(SO_4)_3.xH_2O$ solution to successive decreasing potentials. In the negative going scan, two reductive features are evident at around -0.35 V and -0.58 V which could be attributed to In UPD and bulk In deposition respectively. However, when the scan was reversed at -0.58 V, no clear oxidative was seen in the positive going scan. When the scan was reversed at -0.67 V, the only oxidative feature present in the positive going scan was the peak at around -0.28 V, which could be attributed to In UPD stripping. On the other hand, when the negative going scan is reversed at -0.8 V, a new oxidative feature which could be attributed to bulk In stripping appears at around -0.4 V in addition to the one at -0.28 V (UPD In stripping). Au cyclic voltammetry in 0.5 mM SeO_2 depicted in Figure 3 has been reported previously [39]. We had previously demonstrated that only the oxidative feature at 0.6 V, positive of the formal potential, was present when the scan was reversed at potential range between -0.025 V and -0.3 V. When the scan was reversed at potentials more negative than -0.3 V, the oxidative feature just positive of 0.4 V, attributed to bulk Se stripping, appeared. Selenium deposition is known to be kinetically slow [46-48]. Because of the slow kinetics, the peaks occurring from 0.1 V to -0.3 V in the negative going scan exhibit all the characteristics of surface limited deposition although they appear negative of the formal potential 0.4 V of HSO_3^-/Se. Based on previous Se studies, the increase in reductive spike around -0.5 V is due to a combination of bulk Se deposition, hydrogen evolution and Se reduction to Se^{-2}, a soluble species [46, 48-49]. Figure 4(a) shows the Au on glass electrode cyclic voltammetry in 1 mM $Ga_2(SO_4)_3$ solution where a shoulder is visible in the negative going scan around -0.55 V with a sharp peak at -0.6 V which could be attributed to Ga UPD deposition and hydrogen evolution reaction respectively. This seems to be similar to the work this group had previously reported where Ga UPD deposition in $NaClO_4$ electrolyte was observed around -0.55 V whereas bulk Ga appeared negative of hydrogen evolution reaction [50]. Figure 4(b) depicts an attempt where Au scan run in 1 mM $Ga_2(SO_4)_3$ was held for 2 minutes at successive decreasing potential values in order to check Ga UPD deposition on Au electrode since there was no definitive reductive feature in the negative going scan in the region prior to the system's formal potential of around -0.5 V in Figure 4(a). As the potential is held for 2 minutes at various decreasing potential values in Figure 4(b), clear oxidative features started appearing in the positive going scans at around -0.45 V attesting to the stripping of Ga from Au electrode. Not much of Ga stripping charge is seen when the potential is held at -0.6 V for 2 minutes in the positive going scan which could lead to conclude that no bulk Ga is deposited at -0.6 V. The oxidative feature in the positive going scan did increase when the potential is held and reversed at -0.7 V and -0.75 V indicating some bulk Ga presence. This further confirms that bulk Ga appeared negative of hydrogen evolution reaction.

Figure 5 shows the cartoon of the sequence in which the ALD cycle program for the quaternary CIGS program was grown in the first case mentioned earlier, which was repeated 34 times to reach around 100 cycles of compound monolayers. Se, Ga, In and Cu were respectively deposited at -0.18 V, -0.8 V, -0.7 V and 0.14 V as depicted by a section of the current and potential time traces shown in Figure 6. Deposition time for all the four elements of CIGS were maintained for 15 s. Deposition currents due to each constituent element of CIGS are clearly evident in Figure 6. What is also obvious in the current and potential traces is the presence of oxidative currents when the deposition potentials are switched from either Ga or In steps to Se step as Se deposition potential of -0.18 V is in the region where both In and Ga oxidize. Additionally some Ga or In are expected to strip during Cu deposition time. The film grown using this program appeared homogeneously well distributed when observed under the optical microscope although its electron probe microanalysis (EPMA) data at the bottom left corner of Figure 6 showed a deposit richer in Cu and slightly higher in Se content corresponding to a stoichiometry of $\mathbf{Cu_{2.3}In_{0.6}Ga_{0.4}Se_{2.3}}$. In and Ga contents of 11 and 7 atomic % appeared to be a reasonable amount for 34 cycles. The reason for choosing Ga and In deposition potentials -0.8 V and -0.7 respectively, values that appear in their bulk regions, was because bulk Ga and bulk In were expected to strip during both Se (at -0.18 V) and Cu (at 0.14 V) deposition since both Se and Cu deposition potentials are well positive of the oxidative features observed in Figures 2 and 4. This was confirmed by the oxidative currents mentioned previously that were present in the current and potential time traces.

In an attempt to reduce Cu amount in the CIGS grown in the previous paragraph, we devised three experiments in which an attempt to grow CIGS as superlattices was undertaken, and the number of cycles of InSe and GaSe was varied, while the number of CuSe cycle was maintained at one. In the case of CIGS grown as superlattices, the studies of the effects of changing the sequence of the binary compounds within the period were also carried out. As stated earlier, Cu deposition time was reduced from 15 s to 5 s whereas Se deposition time was increased from 15 s to 30 s in the three experiments of the superlattice program. The reason for reducing Cu deposition time was to minimize the loss of Ga and In that would occur during Cu deposition as Cu deposition potential of 0.14 V used in these experiments was positive of both Ga and In oxidative peaks observed in their respective cyclic voltammograms in Figures 2 and 4. At the same time, reducing Cu deposition time should not affect Cu amount in the deposits as its UPD deposition is a reversible [51-52] and kinetically fast process. On the other hand, the reason for increasing Se deposition time resides in the slow kinetics of the deposition process of chalcogenides [46-48, 53]. The slow kinetics of Se was clearly visible by the pronounced irreversibility observed in the cyclic voltammogram in Figure 3.

In the first experiment of the superlattice CIGS, a superlattice consisting of 25 periods of **2InSe/1GaSe/1CuSe** cycles was grown with Se, In, Ga and Cu potentials of -0.6 V, -0.7 V, -0.9 V and 0.14 V respectively as shown in Figure 7 representing a section of the current and potential time traces of the ALD period of the superlattice. Se deposition potential was lowered from -0.18 V used in the quaternary CIGS ALD program to -0.6 V in the superlattice CIGS ALD program to prevent Ga and In losses which were evident in the current and potential traces in Figure 6. Changing Se deposition potential to -0.6 V drastically minimized or prevented the oxidative features that were present in Figure 6 after switching from Ga or In deposition to Se deposition. Moreover, the use of Se deposition potential around -0.6 V proved to be successful during the formation of $CuInSe_2$ using the superlattice ALD program. As both In and Ga were deposited at more negative potentials than Se, we expected most if not all of bulk Se to strip during In and Ga deposition since bulk Se is known to reductively strip by Se reduction to Se^{2-}, a soluble species [39]. Once again the sequence and currents for the deposition of each constituent element of CIGS are visible in Figure 7, where it is evident that the oxidative currents that were present in Figure 6 after Ga and In deposition are noticeably missing. The only time any oxidative currents are present in Figure 7 is when Cu deposition potential (0.14V) is applied. As expected the oxidative currents are due to mostly Ga stripping. A stoichiometry of $\mathbf{Cu_{1.2}In_{0.9}Ga_{0.1}Se_{1.9}}$ was obtained in the as-deposited sample as shown by the electron probe micro analysis data shown at the bottom left corner of Figure 7 and Table 9. Cu content in the deposit was drastically reduced to 29 atomic % when compared to 41 atomic % obtained in the quaternary CIGS program with longer Cu deposition time. The glancing angle X-ray diffraction in Figure 8 of the as-deposited of the CIGS sample with ($\mathbf{Cu_{1.2}In_{0.9}Ga_{0.1}Se_{1.9}}$) stoichiometry shows the chalcopyrite peaks (112), (204) and (116) at the positions expected for CIGS as previously reported in the literature [33]. The resulting deposit appeared homogeneous when observed under the optical microscope.

In the second superlattice experiment made of **2InSe/2GaSe/1CuSe** cycles, we then attempted to increase the amount of Ga in the CIGS deposit by increasing the number of GaSe cycles from 1 to 2 cycles, while maintaining the sequence of the binary compounds in the superlattice CIGS similar to the superlattice described in the previous paragraph. Figure 9 shows a section of the current and potential time traces of the obtained **2InSe/2GaSe/1CuSe** CIGS sample with Se, In, Ga and Cu deposited at -0.6 V, -0.7 V, -0.8 V and 0.14 V respectively, where once again the sequence and deposition currents of all the elements of the period of the superlattice are evident. Moreover, the only time oxidative currents are present is when the potential for Cu deposition is applied. The second superlattice deposit resulted in a stoichiometry of $\mathbf{Cu_{1.2}In_{0.8}Ga_{0.2}Se_{2.1}}$ as confirmed by the electron probe micro analysis data shown at the bottom left corner of Figure 9 and in Table 9 where Ga atomic % slightly increases, but not by much when compared to the first superlattice experiment. Cu and In contents in the deposit are more or less consisted to the amount in the first superlattice sample. The glancing angle X-ray diffraction pattern in Figure 10 of the as-deposited of the **2InSe/2GaSe/1CuSe** CIGS sample shows once again the expected CIGS crystal planes peaks (112), (204) and (116) corresponding to the chalcopyrite lattice structure. The (111) diffraction appears to have a shoulder, which could be due to the presence of Cu_2Se(111) Bragg's diffraction peak as the EPMA seems to suggest a deposit slightly rich in Cu and Se. Once again, the resulting deposit appeared homogeneous when observed under the optical microscope.

In the third superlattice ALD program, the sequence of the binary InSe and GaSe were switched within the period, with 2 GaSe cycles being deposited first, followed by 2 InSe cycles and then 1 CuSe cycle was deposited. The number of the cycles within the period in this experiment was similar to the second superlattice experiment presented in the previous paragraph. Figure 11 represents a section of the current and potential time traces of a superlattice consisting of 20 periods of **2GaSe/2InSe/1CuSe** cycles on Au on glass substrate with Se, Ga, In and Cu deposited at -0.55 V, -0.8 V, -0.7 V and 0.14 V respectively. Both the sequence and deposition currents of the constituent elements of CIGS are once again evident in Figure 11. As was the case in the previous superlattice programs, the only evident oxidative currents only occurred when Cu deposition potential was applied, which could mostly be attributed to bulk In stripping. The resulting superlattice appeared homogeneous when observed under the optical microscope. This ALD program resulted in the best CIGS grown so far using the electrochemical ALD as a stoichiometry of **$CuIn_{0.7}Ga_{0.3}Se_2$** was confirmed by its electron probe micro analysis data summarized in Table 9. Growing GaSe prior to InSe and as a superlattice resulted in a higher Ga content (~ 7 atomic %) in the deposited film as Ga, on top of being bound to Se, was buried by two compound layers of InSe. In addition, not much of In (~18 atomic %) was also lost during Cu deposition time which was kept at 5 s. Figure 12 shows the glancing angle X-ray diffraction pattern of the as grown **2GaSe/2InSe/1CuSe** superlattice sample obtained where once again (112), (204) and (116) Bragg's diffraction peaks corresponding to chalcopyrite structure are visible.

Conclusion

This article discussed and presented various CIGS experiments carried out using two major growth routes via the electrochemical atomic layer deposition. Encouraging results were obtained when CIGS samples were grown as a superlattice. The best stoichiometric CIGS (**$CuIn_{0.7}Ga_{0.3}Se_2$**) deposit was obtained in the superlattice CIGS program when GaSe cycles of the superlattice preceded InSe cycles which preceded CuSe cycles. The film appeared homogeneously distributed when observed under the optical microscope as it was confirmed by EPMA results. The crystal structure studies revealed that superlattice based CIGS samples were chalcopyrite in nature. Additional studies are being carried out for the determination of the optical and electronic properties of the best CIGS samples, while their morphological studies by scanning tunneling microscope are also pending.

Acknowledgements

Support from the National Science Foundation is gratefully acknowledged.

References

1. Kemell, M., M. Ritala, and M. Leskela, *Thin film deposition methods for CulnSe(2) solar cells.* Critical Reviews in Solid State and Materials Sciences, 2005. **30**(1): p. 1-31.
2. Liu, Z., A. Masuda, and M. Kondo, *Investigation on the crystal growth process of spherical Si single crystals by melting.* Journal of Crystal Growth, 2009. **311**(16): p. 4116-4122.
3. Illiberi, A., et al., *Novel approach to thin film polycrystalline silicon on glass.* Materials Letters, 2009. **63**(21): p. 1817-1819.
4. Strobel, C., et al., *Productivity potential of an inline deposition system for amorphous and microcrystalline silicon solar cells.* Solar Energy Materials and Solar Cells, 2009. **93**(9): p. 1598-1607.
5. Bang, J.H. and P.V. Kamat, *Quantum Dot Sensitized Solar Cells. A Tale of Two Semiconductor Nanocrystals: CdSe and CdTe.* Acs Nano, 2009. **3**(6): p. 1467-1476.
6. Josell, D., et al., *Three Dimensionally Structured CdTe Thin-Film Photovoltaic Devices with Self-Aligned Back-Contacts: Electrodeposition on Interdigitated Electrodes.* Journal of the Electrochemical Society, 2009. **156**(8): p. H654-H660.
7. Sieber, B., C.M. Ruiz, and V. Bermudez. *Evaluation of diffusion-recombination parameters in electrodeposited CuIn(S, Se)(2) solar cells by means of electron beam induced current experiments and modelling*. 2009.
8. Yoon, S., et al. *Nanoparticle-based approach for the formation of CIS solar cells*. 2009.
9. Naghavi, N., et al., *Towards better understanding of high efficiency Cd-free CIGS solar cells using atomic layer deposited indium sulfide buffer layers.* Materials Research

Society Symposium Proceedings, 2003. **763**(Compound Semiconductor Photovoltaics): p. 465-470.

10. Nakada, T., et al., *Novel device structure for Cu(In,Ga)Se2 thin film solar cells using transparent conducting oxide back and front contacts.* Solar Energy, 2004. **77**(6): p. 739-747.

11. Nakada, T., et al., *High-efficiency Cu(In,Ga)Se2 thin-film solar cells with a CBD-ZnS buffer layer.* Solar Energy Materials and Solar Cells, 2001. **67**(1-4): p. 255-260.

12. Bhattacharya, R.N., et al., *High efficiency thin-film CuIn1-xGaxSe2 photovoltaic cells using a Cd1-xZnxS buffer layer.* Applied Physics Letters, 2006. **89**(25).

13. Sato, S., et al. *Degradation modeling of InGaP/GaAs/Ge triple-junction solar cells irradiated with various-energy protons*. 2009: Elsevier Science Bv.

14. Ramanathan, K., et al., *Properties of 19.2% efficiency ZnO/CdS/CuInGaSe2 thin-film solar cells.* Progress in Photovoltaics, 2003. **11**(4): p. 225-230.

15. Contreras, M.A., et al., *Diode characteristics in state-of-the-art ZnO/CdS/Cu(In1-xGax)Se2 solar cells.* Progress in Photovoltaics, 2005. **13**(3): p. 209-216.

16. Dharmadasa, I.M., *Fermi level pinning and effects on CuInGaSe2-based thin-film solar cells.* Semiconductor Science and Technology, 2009. **24**(5).

17. Ingrid, R., et al., *Short Communication: Accelerated Publication 19·9%-efficient ZnO/CdS/CuInGaSe2 solar cell with 81·2% fill factor.* Progress in Photovoltaics: Research and Applications, 2008. **16**(3): p. 235-239.

18. Ahmed, E., et al., *Significance of substrate temperature on the properties of flash evaporated CuIn0.75Ga0.25Se2 thin films.* Thin Solid Films, 1998. **335**(1-2): p. 54-58.

19. Liao, D. and A. Rockett, *Epitaxial growth of Cu(In, Ga)Se2 on GaAs(110).* Journal of Applied Physics, 2002. **91**(4): p. 1978-1983.

20. Islam, M.M., et al., *Effect of Se/(Ga plus In) ratio on MBE grown Cu(In,Ga)Se2 thin film solar cell.* Journal of Crystal Growth, 2009. **311**(7): p. 2212-2214.

21. Shirakata, S., et al., *Properties of Cu(In,Ga)Se2 thin films prepared by chemical spray pyrolysis.* Japanese Journal of Applied Physics Part 1-Regular Papers Short Notes & Review Papers, 1999. **38**(9A): p. 4997-5002.

22. Bhattacharya, R.N., et al. *CuIn1-xGaxSe2-based photovoltaic cells from electrodeposited and chemical bath deposited precursors*. 1998.

23. Ao, J.P., et al., *Properties of one-step electrodeposited Cu(In1-x9 Ga-x)Se-2 thin films.* Acta Physico-Chimica Sinica, 2008. **24**(6): p. 1073-1079.

24. Ao, J.P., et al., *Comparison of the compositions and structures of electrodeposited Cu-poor and Cu-rich Cu(In1-xGax)Se-2 films before and after selenization.* Acta Physica Sinica, 2009. **58**(3): p. 1870-1878.

25. Bhattacharya, R.N., et al., *CuIn1-xGaxSe2-based photovoltaic cells from electrodeposited and chemical bath deposited precursors.* Solar Energy Materials and Solar Cells, 1998. **55**(1-2): p. 83-94.

26. Bhattacharya, R.N., et al., *The performance of CuIn1-xGaxSe2-based photovoltaic cells prepared from low-cost precursor films.* Solar Energy Materials and Solar Cells, 2000. **63**(4): p. 367-374.

27. Calixto, M.E., et al. *Cu(In,Ga)Se-2 based photovoltaic structure by electrodeposition and processing*. 1998.

28. Fahoume, M., et al. *One, step electrodeposition of Cu(Ga,in)Se-2 thin films from aqueous solution*. 2005.

29. Fernandez, A.M. and R.N. Bhattacharya, *Electrodeposition of CuIn1-xGaxSe2 precursor films: optimization of film composition and morphology.* Thin Solid Films, 2005. **474**(1-2): p. 10-13.

30. Kampmann, A., et al., *Large area electrodeposition of Cu(In,Ga)Se-2.* Thin Solid Films, 2000. **361**: p. 309-313.

31. Fu, Y.P., R.W. You, and K.K. Lew, *Electrochemical Properties of Solid-Liquid Interface of CuIn1-xGaxSe2 Prepared by Electrodeposition with Various Gallium Concentrations.* Journal of the Electrochemical Society, 2009. **156**(9): p. E133-E138.

32. Sebastian, P.J., et al., *A 10% Cu(In,Ga)Se-2 based photovoltaic structure formed by electrodeposition and subsequent thermal processing.* Journal of the Electrochemical Society, 1998. **145**(10): p. 3613-3615.

33. Dejene, F.B., *The structural and material properties of CuInSe2 and Cu(In,Ga)Se2 prepared by selenization of stacks of metal and compound precursors by Se vapor for solar cell applications.* Solar Energy Materials and Solar Cells, 2009. **93**(5): p. 577-582.

34. Adzic, R.R., in *Advances in Electrochemistry and Electrochemical Engineering*, H. Gerishcher and C.W. Tobias, Editors. 1984, Wiley-Interscience: New York. p. 159.

35. Adzic, R.R., et al., *Electrocatalysis by foreign metal monolayers: oxidation of formic acid on platinum.* JEC, 1975. **65**: p. 587-601.

36. Kolb, D.M., *Physical and Electrochemical Properties of Metal Monolayers on Metallic Substrates*, in *Advances in Electrochemistry and Electrochemical Engineering*, H. Gerischer and C.W. Tobias, Editors. 1978, John Wiley: New York. p. 125.

37. Kolb, D.M. and H. Gerisher, *Further aspects concerning the correlation between underpotential depsoition and work function defferences.* SS, 1975. **51**: p. 323.

38. Kolb, D.M., Przasnys.M, and Gerische.H, *Underpotential Deposition of Metals and Work Function Differences.* Journal of Electroanalytical Chemistry, 1974. **54**(1): p. 25-38.

39. Banga, D., et al., *Optimization of PbSe Nanofilms formation by Electrochemical Atomic Layer Deposition (ALD).* ECS Transactions, 2009. **19**(3): p. 245-272.

40. Banga, D.O., et al., *Formation of PbTe nanofilms by electrochemical atomic layer deposition (ALD).* Electrochimica Acta, 2008. **53**(23): p. 6988-6994.

41. Venkatasamy, V., et al., *Optimization studies of CdTe nanofilm formation by electrochemical atomic layer epitaxy (EC-ALE).* J. Appl. Electrochem., 2006. **36**: p. 1223.

42. Zhu, W., et al., *Electrochemical atom-by-atom growth of highly uniform thin sheets of thermoelectric bismuth telluride via the route of ECALE.* Journal of Electroanalytical Chemistry, 2008. **614**(1-2): p. 41-48.

43. Vaidyanathan, R., et al., *Preliminary studies in the electrodeposition of PbSe/PbTe superlattice thin films via electrochemical atomic layer deposition (ALD).* Langmuir, 2006. **22**(25): p. 10590-10595.

44. Zhu, W., et al., *Electrochemical aspects and structure characterization of VA-VIA compound semiconductor Bi2Te3/Sb2Te3 superlattice thin films via electrochemical atomic layer epitaxy.* Langmuir, 2008. **24**(11): p. 5919-5924.

45. Vasiljevic, N., et al., *High resolution electrochemical STM: New structural results for underpotentially deposited Cu on Au(111) in acid sulfate solution.* Journal of Electroanalytical Chemistry, 2008. **613**(2): p. 118-124.

46. Huang, B.M., T.E. Lister, and J.L. Stickney, *Se adlattices formed on Au (100), studies by LEED, AES, STM and electrochemistry.* Surface Science, 1997. **392**(1-3): p. 27.

47. Lister, T.E., et al., *Electrochemical formation of Se atomic layers on Au(100).* J. Vac. Sci. Technol. B, 1995. **13**: p. 1268.

48. Lister, T.E. and J.L. Stickney, *Atomic level studies of selenium electrodeposition on gold (111) and gold (110).* Journal of Physical Chemistry, 1996. **100**(50): p. 19568-19576.

49. Lister, T.E., et al., *Electrochemical Formation of Se Atomic Layers On Au(100).* Journal of Vacuum Science & Technology B, 1995. **13**(3): p. 1268.

50. Villegas, I. and J.L. Stickney, *Preliminary studies of gallium arsenide deposition on gold (100), (110), and (111) surfaces by electrochemical atomic layer epitaxy.* Journal of the Electrochemical Society, 1992. **139**(3): p. 686-94.

51. Kim, J.Y., Y.G. Kim, and J.L. Stickney, *Cu nanofilm formation by electrochemical atomic layer deposition (ALD) in the presence of chloride ions.* Journal of Electroanalytical Chemistry, 2008. **621**(2): p. 205-213.

52. Herrero, E., L.J. Buller, and H.D. Abruna, *Underpotential Deposition at Single Crystal Electrodes Surfaces of Au, Pt, Ag and other Materials.* Chemical Reviews, 2001. **101**: p. 1897-1930.

53. Lay, M.D. and J.L. Stickney, *EC-STM Studies of Te and CdTe Atomic Layer Formation from a Basic Te Solution.* Journal of the Electrochemical Society, 2004. **151**(6): p. C431-C435.

Table 9: Electron Probe Microanalysis (EPMA) Data of the various CIGS ALD programs formed on Au on glass. Electrode area: 4 cm^2

Sample	**Quaternary CIGS**	**2InSe/1GaSe/1 CuSe**	**2InSe/2GaSe/1 CuSe**	**2GaSe/2InSe/1 CuSe**
Cu Atomic %	41	29	27	25
In Atomic %	11	22	20	18
Ga Atomic %	7	3	4	7
Se Atomic %	41	46	49	50
Period Number	34	25	20	20
Stoichiometry	$Cu_{2.3}In_{0.6}Ga_{0.4}Se_{2.3}$	$Cu_{1.2}In_{0.9}Ga_{0.1}Se_{1.9}$.	$Cu_{1.2}In_{0.8}Ga_{0.2}Se_{2.1}$.	$CuIn_{0.7}Ga_{0.3}Se_2$

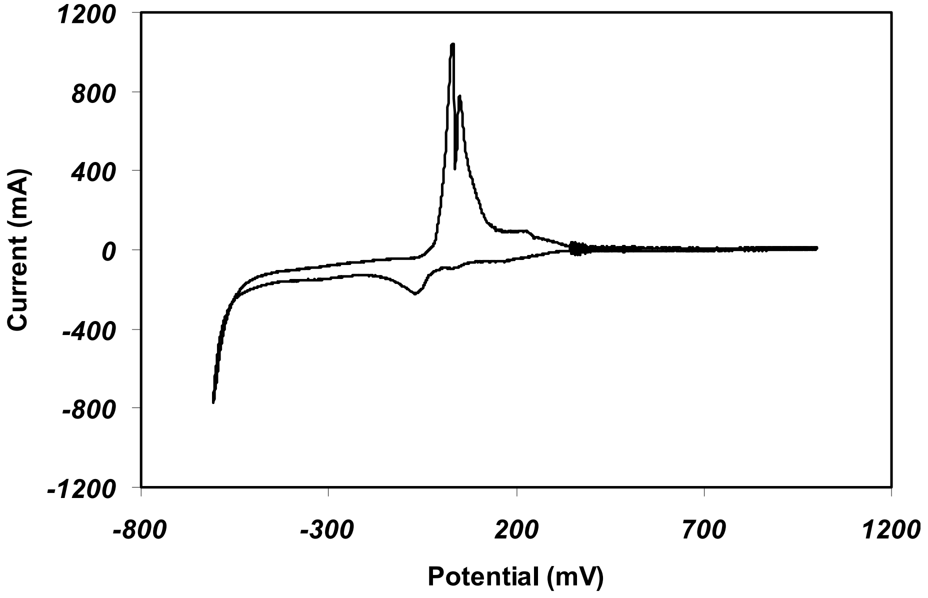

Figure 7.1: Cyclic voltammogram of Au electrode in 0.5 mM $Cu(SO_4)_2$, pH 4.5, (electrode area: 4 cm^2, scan rate: 10 mV s^{-1}).

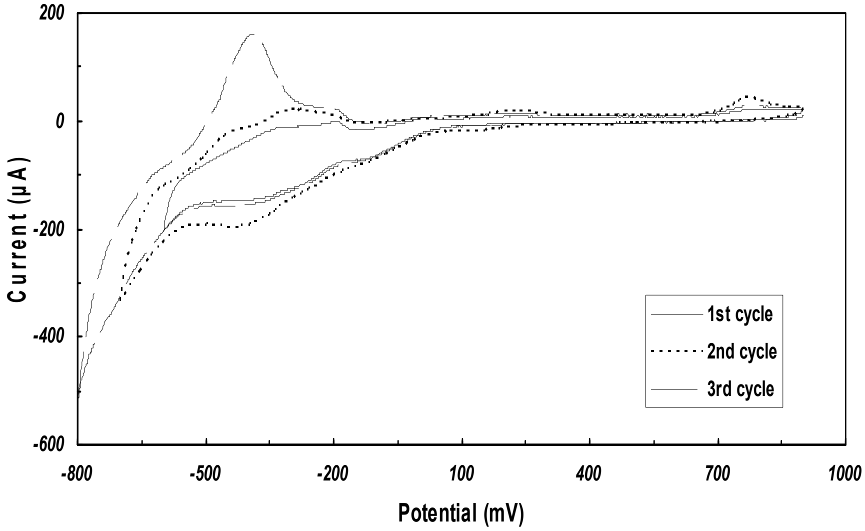

Figure 7.2: Cyclic voltammogram of Au electrode in 0.5 mM $In_2(SO_4)_3.xH_2O$, pH 3, (electrode area: 4 cm^2, scan rate: 10 mV s^{-1}).

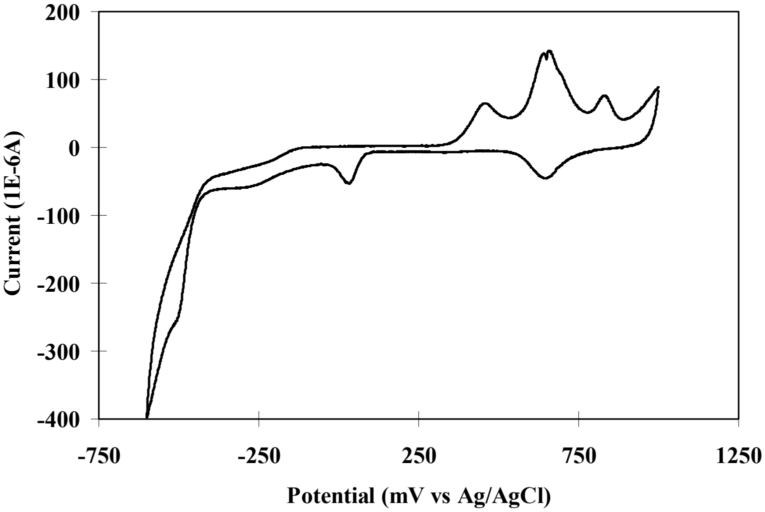

Figure 7.3: Cyclic voltammogram of Au electrode in 0.5 mM $HSeO_3^+$, pH 5, (electrode area: 4 cm^2, scan rate: 10 mV s^{-1}).

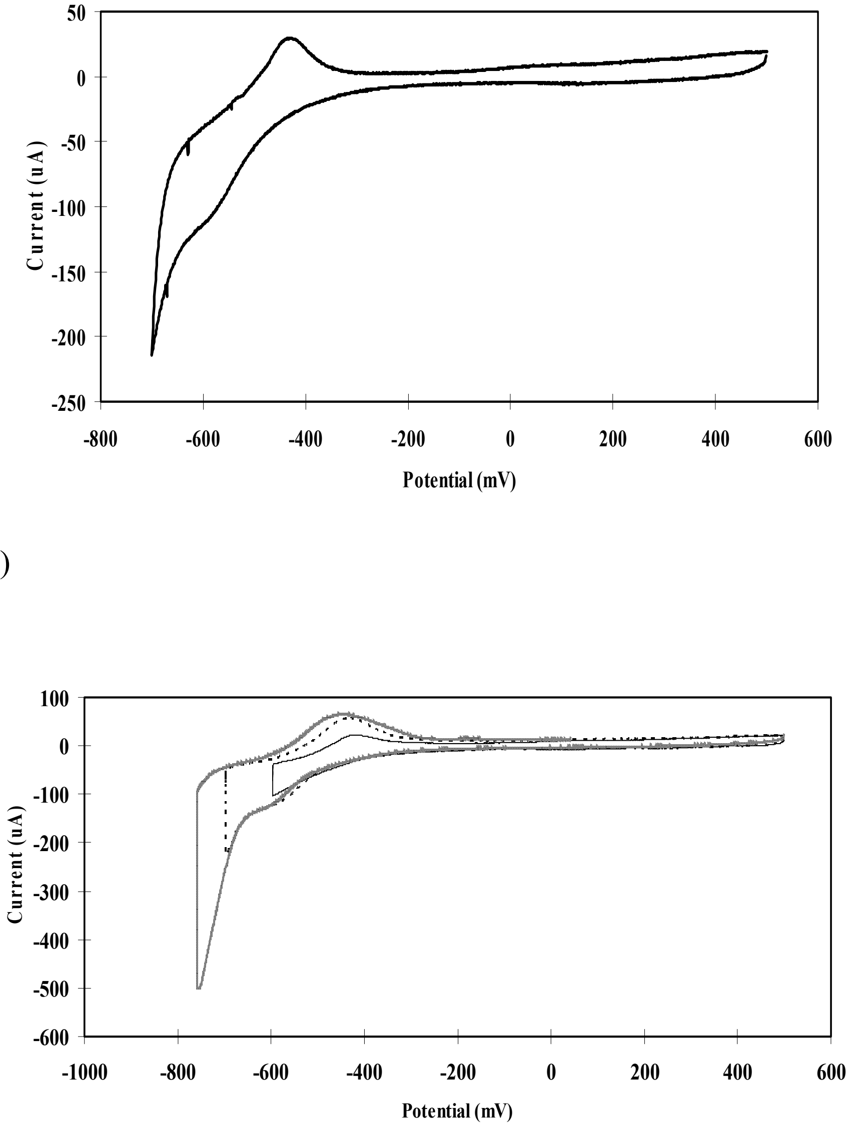

a)

(b)

Figure 7.4: Cyclic voltammograms (a) of Au electrode in 1 mM $Ga_2(SO_4)_3$ and (b) when held for 2 minutes to successive decreasing potentials, pH 3, (electrode area: 4 cm^2, scan rate: 10 mV s^{-1}).

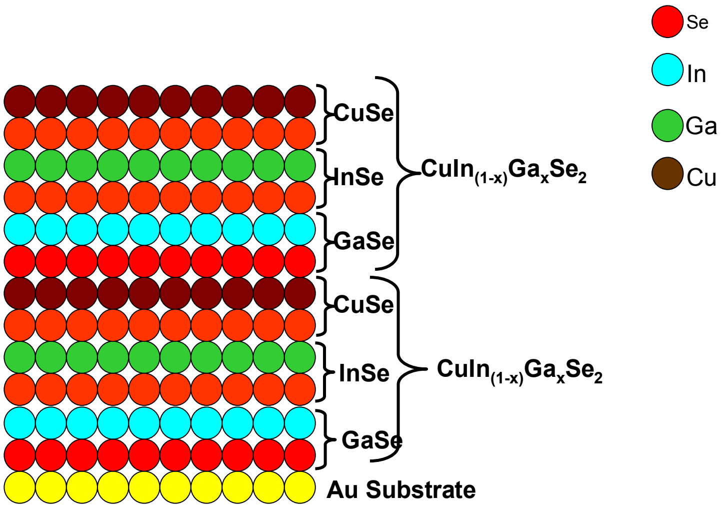

Figure 7.5: A cartoon of CIGS sequence grown as a quaternary Ga, In, Cu and Se.

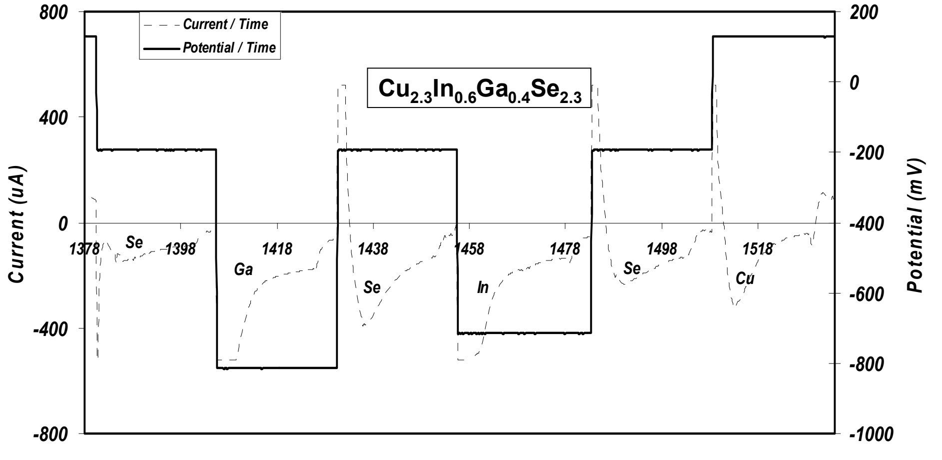

EPMA Atomic %
Cu: 41
In: 11
Ga: 7
Se: 41

Figure 7.6: A section of current and potential time traces and the resulting EPMA data of the quaternary CIGS with Se, Ga, In and Cu deposited at -0.18 V, -0.8 V, -0.7 V and 0.14 V respectively. Electrode area: 4 cm^2.

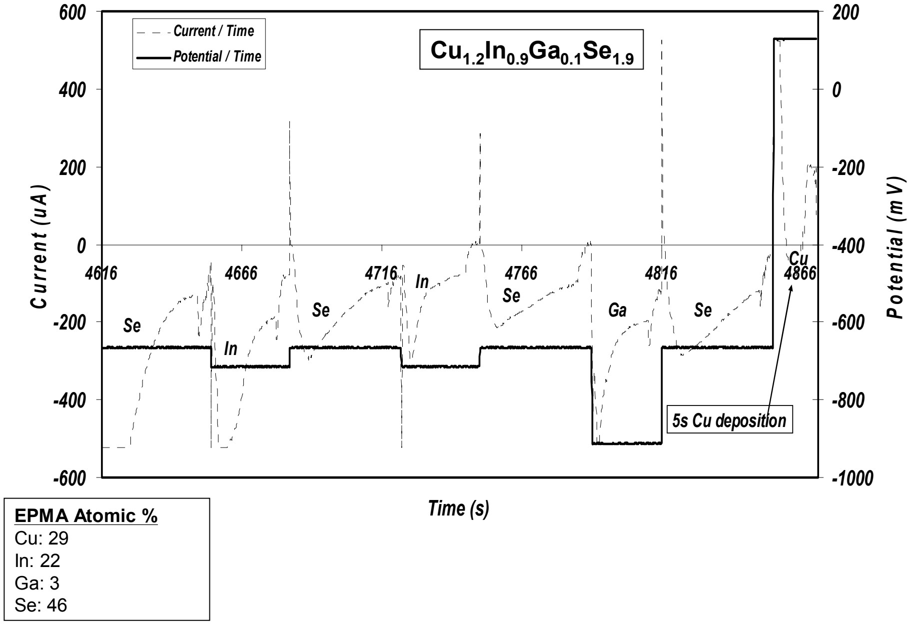

EPMA Atomic %
Cu: 29
In: 22
Ga: 3
Se: 46

Figure 7.7: A section of current and potential time traces and the resulting EPMA data of a 25 ALD period **2InSe/1GaSe/1CuSe** CIGS superlattice grown on Au on glass electrode with Se, In, Ga and Cu deposited at -0.6 V, -0.7 V, -0.9 V and 0.14 V respectively. Cu deposition time was reduced from 15 s to 5 s whereas Se deposition time was increased from 15 s to 30 s. Electrode area: 4 cm^2.

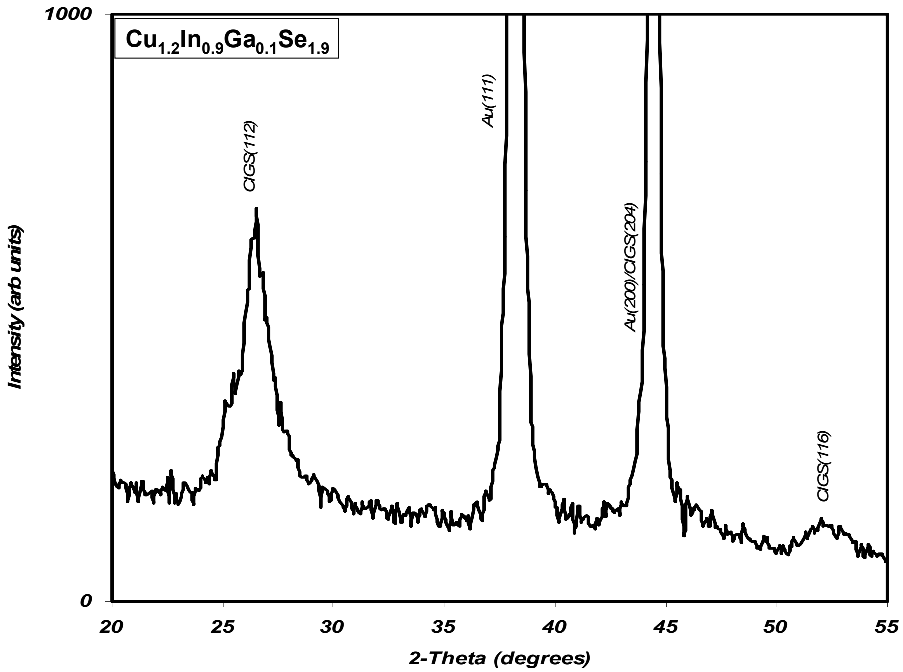

Figure 7.8: X-ray diffraction pattern of a 25 ALD period **2InSe/1GaSe/1CuSe** CIGS superlattice grown on Au on glass electrode with Se, In, Ga and Cu deposited at -0.6 V, -0.7 V, -0.9 V and 0.14 V respectively. Angle of incidence is 0.1°, Cu Kα source. Electrode area: 4 cm^2.

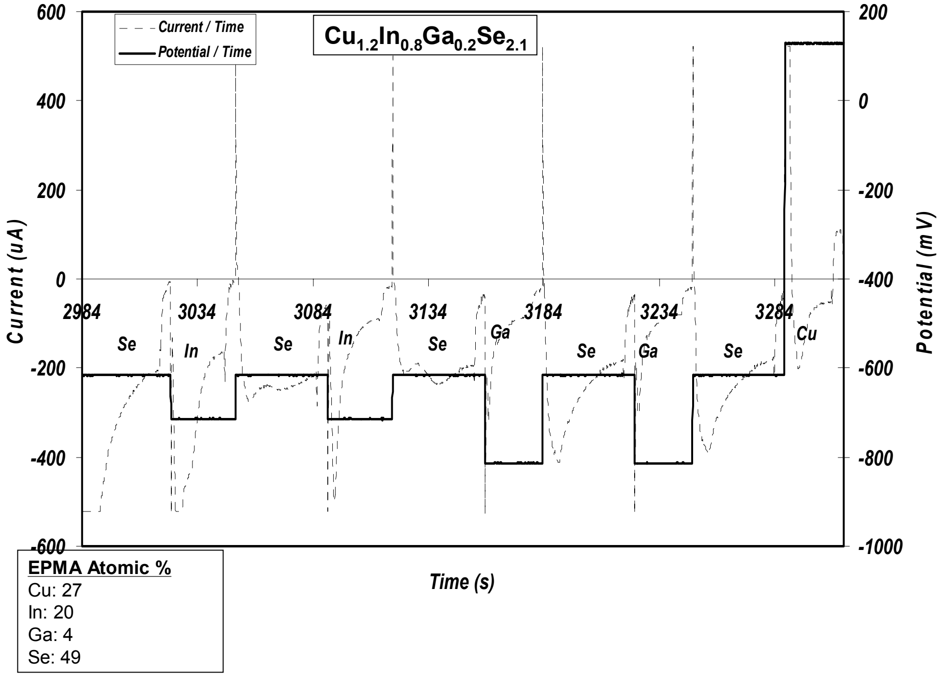

Figure 7.9: A section of current and potential time traces and the resulting EPMA data of a 20 ALD period **2InSe/2GaSe/1CuSe** CIGS superlattice grown on Au on glass electrode with Se, In, Ga and Cu deposited at -0.6 V, -0.7 V, -0.8 V and 0.14 V respectively. Cu deposition time was reduced from 15 s to 5 s whereas Se deposition time was increased from 15 s to 30 s. Electrode area: 4 cm^2.

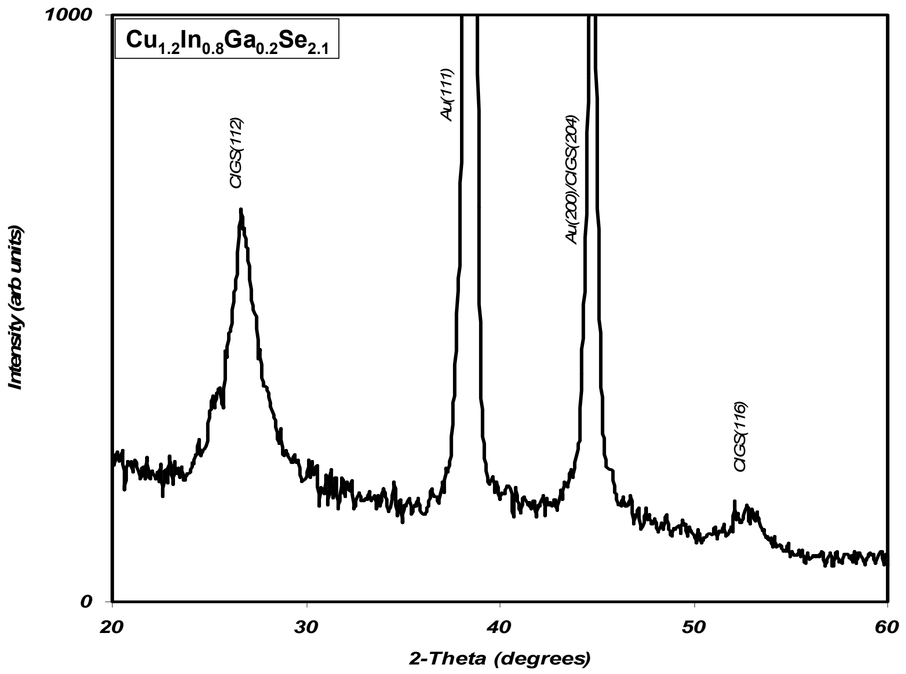

Figure 7.10: X-ray diffraction pattern of a 20 ALD period **2InSe/2GaSe/1CuSe** CIGS superlattice grown on Au on glass electrode with Se, In, Ga and Cu deposited at -0.6 V, -0.7 V, -0.8 V and 0.14 V respectively. Angle of incidence is 0.1°, Cu Kα source. Electrode area: 4 cm^2.

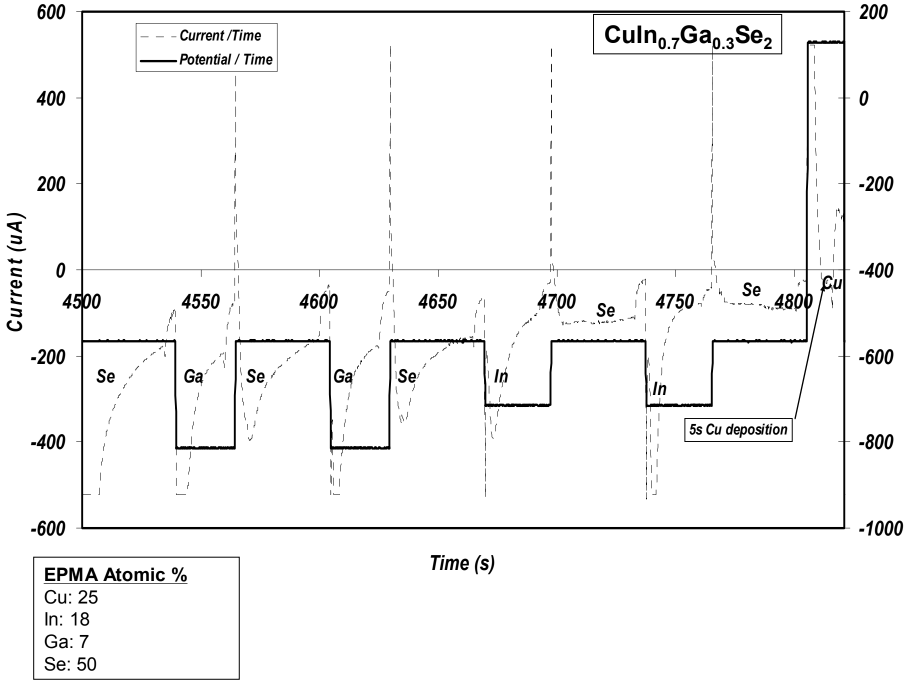

EPMA Atomic %
Cu: 25
In: 18
Ga: 7
Se: 50

Figure 7.11: A section of current and potential time traces of a 20 ALD period **2GaSe/2InSe/1CuSe** CIGS superlattice grown on Au on glass electrode with Se, Ga, In and Cu deposited at -0.55 V, -0.8 V, -0.7 V and 0.14 V respectively. Cu deposition time was reduced from 15 s to 5 s whereas Se deposition time was increased from 15 s to 30 s. Electrode area: 4 cm^2.

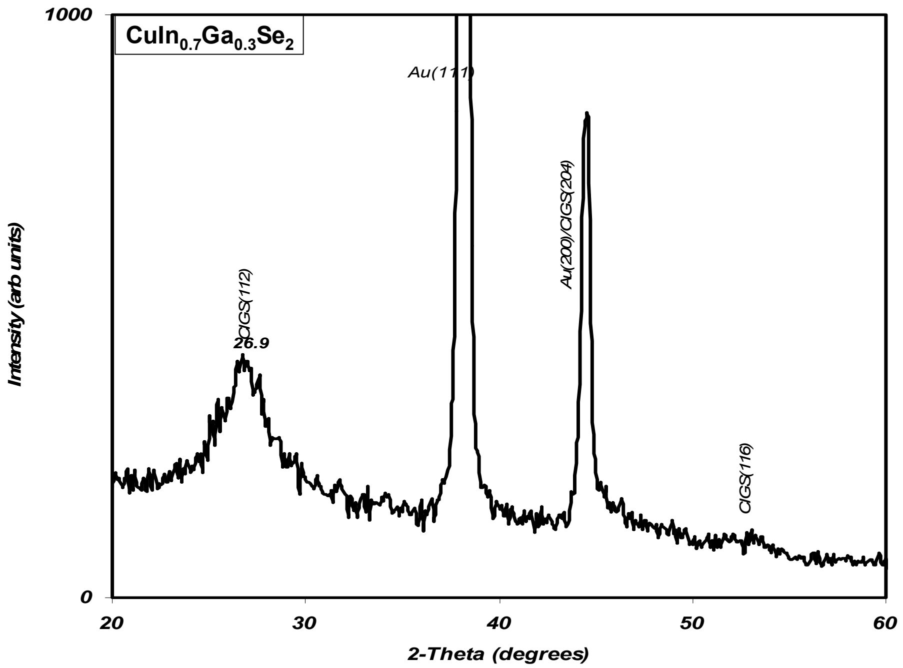

Figure 7.12: X-ray diffraction pattern of a 20 ALD period **2GaSe/2InSe/1CuSe** CIGS superlattice grown on Au on glass electrode with Se, Ga, In and Cu deposited at -0.55 V, -0.8 V, -0.7 V and 0.14 V respectively. Angle of incidence is 0.1°, Cu Kα source. Electrode area: 4 cm^2.

CHAPTER 8

CONCLUSIONS AND FUTURE STUDIES

The formation IV-VI compounds PbSe, PbTe and their subsequent superlattices using EC-ALD were demonstrated in this dissertation. Chapter 2 presented about PbSe thin film formation using various EC-ALD cycle methods of which the one containing the ramps of both Se and Pb for the first 20 cycles resulted in the successful growth of smooth epitaxial PbSe films on both Au on glass and Au on mica substrates after the inspection under the microscope. Coulometry and charges confirmed coverage of near or below a ML/cycle. Quantum confinement effects were visible in the samples grown at 300 cycles or less as observed from the absorption spectra. EPMA results confirmed that the deposits were homogeneous and stoichiometric. XRD revealed the films had a rocksalt structure and a preferential (200) orientation in deposits on both Au on glass and Au on mica substrates. STM images of PbSe samples showed clusters of improved crystallinity and similar roughness to the ones seen on Au on glass. In chapter 3, smooth epitaxial PbTe deposits were grown as confirmed by optical microscopy and visual inspection of the deposits. EPMA results confirmed that the deposit was homogeneous and stoichiometric as expected from the current time traces. XRD revealed the films had a preferential (200) orientation. Strong quantum confinement effects were also observed in the PbTe deposits grown with 100 cycles or less, as evident from the absorption spectra. Two different types of PbSe/PbTe superlattices consisting of equal and unequal numbers of cycles were presented in chapter 4. The coverage of based on the coulometry was found to average one monolayer in both cases due to the optimization of the potential range chosen for the electrochemical ALD program. EPMA characterization determined both deposits to be stoichiometric and the ratio of PbSe and PbTe in the superlattices followed the relative numbers of the cycles. The presence of the satellite peaks was visible in the XRD patterns of both superlattices. In addition, adjusting the number of cycles within a period resulted in changes in the position of the satellite peaks around the (111) peak. STM indicated that the as-deposited superlattice was essentially conformal with Au on glass substrate and evidence of epitaxial growth was observed in the image of the superlattice deposit as attested by the presence of steps.

In chapter 5, CdTe thin film grown prior to growing PbTe/CdTe was stoichiometric and homogeneous as confirmed by EPMA. The deposit exhibited a predominantly (111) orientation in XRD and a bandgap of around 1.45 eV. In PbTe/CdTe superlattice, the presence of the satellite peaks was visible in the XRD pattern of the deposit and EPMA characterization determined the superlattice to be stoichiometric.

Chapter 6 presented the electrodeposition of Cu_2Se, InSe and $CuInSe_2$ thin films. Nearly stoichiometric $Cu_{2.1}Se$ and $InSe_{1.1}$ were obtained as confirmed by EPMA data of their deposits. Expected peaks were obtained in their XRD patterns. The nearly stoichiometric ($\mathbf{Cu_{1.1}InSe_{1.9}}$) CIS sample, as confirmed by EPMA results, was obtained from the 25P/3InSe/1CuSe superlattice program where Cu deposition time was reduced to 3 s, while steady potentials were applied for the constituent elements of CIS. The film appeared homogeneously distributed when observed under the optical microscope as it was confirmed by EPMA results. The crystal structure studies revealed that the stoichiometric CIS sample was chalcopyrite in nature. AFM indicated the images of the Au substrate and the CIS sample to be conformal.

Chapter 7 discussed various CIGS experiments carried out using two major growth routes via the electrochemical atomic layer deposition. Encouraging results were obtained when CIGS samples were grown as a superlattice. The best stoichiometric CIGS (**$CuIn_{0.7}Ga_{0.3}Se_2$**) deposit was obtained in the superlattice CIGS program when GaSe cycles of the superlattice preceded InSe cycles which preceded CuSe cycles. The film appeared homogeneously distributed when observed under the optical microscope as it was confirmed by EPMA results. XRD characterization revealed that superlattice based CIGS samples were chalcopyrite in nature.

For future studies, the need for additional characterization techniques that may well be used to determine optical, electrical and photoelectrochemical properties of CIS and CIGS samples is obvious. In addition, the effects of annealing time and temperature on the composition, crystal structure and efficiency of EC-ALD grown CIS and CIGS samples could also be explored.